

**THERMAL AND ECONOMICAL ANALYSIS OF
HDH SYSTEMS DRIVEN BY SOLAR THERMAL
ENERGY WITH A STORAGE OPTION**

BY

MOHAMED IFRAS ZUBAIR

A Thesis Presented to the
DEANSHIP OF GRADUATE STUDIES

KING FAHD UNIVERSITY OF PETROLEUM & MINERALS

DHAHRAN, SAUDI ARABIA

In Partial Fulfillment of the
Requirements for the Degree of

MASTER OF SCIENCE

In

MECHANICAL ENGINEERING

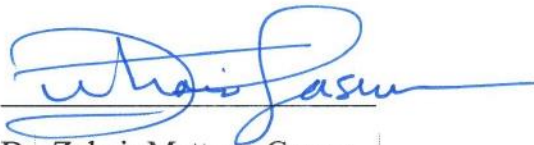
DECEMBER 2015

KING FAHD UNIVERSITY OF PETROLEUM & MINERALS

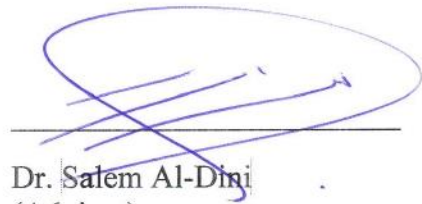
DHAHRAN- 31261, SAUDI ARABIA

DEANSHIP OF GRADUATE STUDIES

This thesis, written by **Mohamed Ifras Zubair** under the direction his thesis advisor and approved by his thesis committee, has been presented and accepted by the Dean of Graduate Studies, in partial fulfillment of the requirements for the degree of **MASTER OF SCIENCE IN MECHANICAL ENGINEERING.**



Dr. Zuhair Mattoug Gasem
Department Chairman



Dr. Saleem Al-Dini
(Advisor)



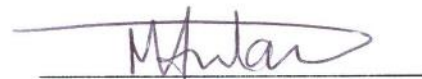
Dr. Salam A. Zummo
Dean of Graduate Studies



Dr. Fahad Al-Sulaiman
(Member)

Date

28/12/15



Dr. Mohamed A. Antar
(Member)

© Mohamed Ifras Zubair

2015

Dedication

This thesis is dedicated to my parents, siblings and my wife. Without your constant support and patience, this would have been impossible. I appreciate everything you all have done to make this process easier on me. Thank you!

ACKNOWLEDGMENTS

I express my deepest gratitude to my advisor and my thesis committee, Dr. Salem Al-Dini, Dr. Fahad Al-Sulaiman and Dr. Mohamed A Antar whose guidance, excitement, and knowledge were invaluable to the success of this thesis.

The support provided by King Fahd University of Petroleum and Minerals for this research is highly acknowledged.

My greatest thanks go to my family, wife, and friends who in spite of hardships have always been an abundant source of love and encouragement.

TABLE OF CONTENTS

ACKNOWLEDGMENTS	iii
LIST OF TABLES.....	vi
LIST OF FIGURES	vii
LIST OF ABBREVIATIONS.....	ix
NOMENCLATURE	x
GREEK SYMBOLS	xiii
ABSTRACT.....	xiv
ملخص الرسالة.....	xvi
CHAPTER 1 INTRODUCTION	1
1.1 Background.....	1
1.2 Objectives	5
CHAPTER 2 LITERATURE REVIEW	6
CHAPTER 3 RESEARCH METHODOLOGY	21
3.1 System Description	21
3.2 Modeling Assumptions	23
3.3 Mathematical Modeling	25
3.3.1 Evacuated Tube Collector (ETC).....	25
3.3.2 Humidification Dehumidification System (HDH).....	33
3.3.3 Thermal Storage.....	35
3.4 Methodology	37
3.5 Validation.....	38
3.5.1 Evacuated Tube Collector.....	38
3.5.2 Humidification Dehumidification Desalination System	42
CHAPTER 4 RESULTS & DISCUSSION	49
4.1 Optimization	49
4.2 Base Case	55
4.2.1 Base Case Results	58

4.3 Complete System with Thermal Storage.....	66
4.4 Cost Analysis	86
4.5 Multiple Location Analysis.....	89
CHAPTER 5 CONCLUSIONS	111
REFERENCES	114
APPENDIX.....	117
VITAE	121

LIST OF TABLES

Table 1: Excerpt of the table from APPENDIX A.....	39
Table 2: Validation data for the evacuated tube model at an irradiation of 800 W/m ²	42
Table 3: Validation of the HDH model by comparison with the results obtained by Sharqawy et al. [26]	43
Table 4: The values of the variables used to assess the effect of relative humidity of air by Narayan et al.[28].....	43
Table 5: GOR vs. MR calculation for T _{max} 60°C.....	51
Table 6: Productivity and Operational Hours for four storage cases.	72
Table 7: Cost per liter of water produced.	87
Table 8: List of costs incurred.	87
Table 9: Operating hours and daily total fresh water product (KACARE).....	92
Table 10: Operating hours and daily total fresh water product (KAU).	93
Table 11: Operating hours and daily total fresh water product (KFUPM).	93
Table 12: Operating hours and daily total fresh water product (Qassim).	94
Table 13: Operating hours and daily total fresh water product (Sharurah).....	94
Table 14: Operating hours and daily total fresh water product (Tabuk).....	95
Table 15: Annual Productivity for all locations and all cases.....	96
Table 16: Maximum Tank Temperatures for KACARE.	97
Table 17: Maximum Tank Temperatures for KAU.	98
Table 18: Maximum Tank Temperatures for KFUPM.	98
Table 19: Maximum Tank Temperatures for Qassim.	99
Table 20: Maximum Tank Temperatures for Sharurah.	99
Table 21: Maximum Tank Temperatures for Tabuk.....	100

LIST OF FIGURES

Figure 1: Proposed Design.....	22
Figure 2: Thermal circuit of an evacuated tube collector.	27
Figure 3: Useful heat gained and available heat input vs. time.	40
Figure 4: GOR vs. Relative Humidity Validation with Narayan et al. [28].....	44
Figure 5: Plot of GOR vs MR for the validation of water heated HDH cycle [26].	46
Figure 6: GOR vs. MR Optimization results.	52
Figure 7: Dependence of the amount of freshwater produced daily on the collector area.....	54
Figure 8: Base case system configuration.....	57
Figure 9: Fresh water Product vs. Time of Day.....	59
Figure 10: Accumulated Total Freshwater product vs. Incident Solar Radiation (June).	61
Figure 11: Daily Averaged Productivity for each month of the year.....	63
Figure 12: Daily Averaged GOR of every month.....	65
Figure 13: Freshwater Product vs. No. of Hours (March).	70
Figure 14: Freshwater Product vs. No. of Hours (June).	71
Figure 15: Freshwater Product vs. No. of Hours (September).....	72
Figure 16: Freshwater Product vs. No. of Hours (December).	73
Figure 17: Total useful energy collected for the averaged day of each month.	75
Figure 18: Tank temperature variation within 24 hours (March).	77
Figure 19: Tank temperature variation within 24 hours (June).....	78
Figure 20: Tank temperature variation within 24 hours (September).....	79
Figure 21: Tank temperature variation within 24 hours (December).	80
Figure 22: GOR vs. Hour of operation (24 hour case).....	82
Figure 23: GOR vs. Hour of operation (Ideal flow case).....	83
Figure 24: GOR vs. Hour of operation (Average flow case).	84

Figure 25: GOR vs. Hour of operation (maximum flow case). 85

Figure 26: Heat input throughout the year at multiple locations. 90

Figure 27: Storage Tank Temperature variation for the 24 hour case. 103

Figure 28: Storage Tank Temperature variation for the Ideal Flow case..... 105

Figure 29: Storage Tank Temperature variation for the Average Flow case..... 107

Figure 30: Storage Tank Temperature variation for the Max Flow case. 109

LIST OF ABBREVIATIONS

EES	:	Engineering Equation Solver
ETC	:	Evacuated Tube Collector
GOR	:	Gained Output Ratio
HDH	:	Humidification Dehumidification
KACARE	:	King Abdullah City for Atomic and Renewable Energy
KAU	:	King Abdulaziz University
KFUPM	:	King Fahd University of Petroleum and Minerals
MED	:	Multiple Effect Distillation
MSF	:	Multi-stage Flash Distillation
MVC	:	Mechanical Vapor Compression
RO	:	Reverse Osmosis
SEC	:	Single Effect Vapor Compression

NOMENCLATURE

A_{cond}	Surface area of the condenser [m ²]
A_{evap}	Surface area of the evaporator [m ²]
A_{ma}	Surface area of the manifold [m ²]
A_r	Area of the receiver [m ²]
C_p	Heat capacitance of the working fluid [kJ/kg K]
C_{pw}	Specific heat capacitance of water [kJ/kg K]
$D_{i,cond}$	Inner diameter of the condenser [m]
$D_{i,evap}$	Inner diameter of the evaporator [m]
$D_{i,fin}$	Inner diameter of the fin [m]
$D_{i,ma}$	Inner diameter of the manifold [m]
$D_{o,cond}$	Outer diameter of the condenser [m]
$D_{o,evap}$	Outer diameter of the evaporator [m]
$D_{o,fin}$	Outer diameter of the fin [m]
$D_{o,ma}$	Outer diameter of the manifold [m]
F'	Collector efficiency factor
F_R	Collector heat removal factor
g	Gravitational acceleration
h_{a1}	Enthalpy of air at exit of the dehumidifier or the inlet of the humidifier [kJ/kg]
h_{a2}	Enthalpy of air at the exit of the humidifier or the inlet of the dehumidifier [kJ/kg]
h_{cond}	Heat transfer coefficient of the condenser [kJ/kg]
h_{fg}	Enthalpy of latent heat [kJ/kg]

h_{fg}	Enthalpy of latent heat of vaporization of water [kJ/kg]
h_{fw}	Enthalpy of freshwater leaving the dehumidifier [kJ/kg]
h_{hp}	Heat transfer coefficient of the heat pipe
h_{w1}	Enthalpy of the water entering the dehumidifier [kJ/kg]
h_{w2}	Enthalpy of water at the exit of the dehumidifier [kJ/kg]
h_{w4}	Enthalpy of brine at the exit of the humidifier [kJ/kg]
I	Incident radiation on the horizontal [MJ/m ²]
I_b	Fraction of beam radiation in a given hour [MJ/m ²]
I_d	Fraction of diffused radiation in a given hour [MJ/m ²]
I_T	Total radiation available to the collector [MJ/m ²]
k_{cond}	Conductivity of the condenser [W/m K]
k_{evap}	Evaporator conductivity [W/m K]
k_{fin}	Conductivity of the fin [W/m K]
k_l	Conductivity of the working fluid [W/m K]
k_{ma}	Conductivity of the manifold [W/m K]
k_v	Conductivity of vapor in the condenser [W/m K]
L_{cond}	Length of the condenser [m]
L_{evap}	Length of the evaporator [m]
L_{ma}	Manifold length [m]
m	Mass capacity of the storage tank [kg]
\dot{m}	Mass flow rate of the working fluid [kg/s]
\dot{m}_a	Mass flow rate of air [kg/s]
\dot{m}_b	Mass flow rate of brine [kg/s]
\dot{m}_{fw}	Mass flow rate of fresh water [kg/s]

m_w	Mass flow rate of sea water [kg/s]
Q	Energy input by the water heater [W]
Q_u	Useful heat gained by the collector [W]
R_b	Geometric factor for beam radiation
$R_{cond,w}$	Condenser wall thermal resistance [W/K]
R_d	Geometric factor for diffused radiation
R_{gr}	Geometric factor for ground reflected radiation
R_{hp}	Evaporator (heat pipe) thermal resistance [W/K]
$R_{loss,rad}$	Radiation thermal resistance [W/K]
R_{ma}	Manifold resistance [W/K]
T_a	Ambient temperature [K]
T_a'	Ambient temperature of the storage tank surrounding [K]
T_f	Temperature of the working fluid [K]
T_i	Fluid inlet temperature [K]
T_k	Temperature at the condenser wall [K]
T_{Lr}	Load range temperature [K]
T_o	Outlet temperature [K]
T_p	Plate temperature [K]
T_s^+	Temperature of storage at the end of the time period [K]
T_{w2}	Temperature of water before the heater [K]
T_{w3}	Water temperature at the exit of the water heater [K]
U_L	Overall loss coefficient [W/m ² K]
U_{ma}	Manifold loss coefficient [W/m ² K]

GREEK SYMBOLS

$(UA)_s$	Storage tank loss coefficient-area product [kJ/hr K]
$(\tau\alpha)_b$	Transmittance-absorptance product for beam radiation
$(\tau\alpha)_d$	Transmittance-absorptance product for diffused radiation
$(\tau\alpha)_{gr}$	Transmittance-absorptance product for ground reflected radiation
μ_l	Viscosity of the working fluid [m^2/s]
Δt	Length of the time period for which the calculations are carried out
ε	Emissivity of the absorber coating
ε_L	Load heat exchanger effectiveness
θ	Angle of incidence
ρ_{gr}	Ground reflectance
ρ_l	Density of the liquid within the evaporator [kg/m^3]
ρ_v	Density of vapor in the condenser [kg/m^3]
σ	Steffan Boltzmann constant
ω_1	Absolute humidity of air at the exit of the dehumidifier and the inlet of the humidifier [kg/m^3]
ω_2	Absolute humidity of air at the exit of the humidifier and the inlet of the dehumidifier [kg/m^3]

ABSTRACT

Full Name : Mohamed Ifras Zubair
Thesis Title : Thermal and economical analysis of HDH systems driven by solar thermal energy with a storage option.
Major Field : Thermofluid Sciences
Date of Degree : December 2015

This study is motivated by the common known issue of many solar energy related thermal systems, where operation is restricted for the duration of day light hours and the unpredictability in weather. Desalination systems linked with solar thermal energy applications often have limited operational hours and are significantly affected by widely varying solar intensity.

As means to improve solar desalination systems, this study analyzes an HDH system integrated with evacuated tube collectors as water heaters. The design was first studied to optimize and analyze the system performance. Then a similar system integrated with a thermal storage tanks was studied. Two separate tanks were considered, in which one tank was for the hot water while the second one was for the cold water. This provides the ability to control the outlet temperature of the storage component. Furthermore, the study assessed the effect of the location on the system performance for both cases, with and without the thermal energy storage systems. Six different locations were selected: Riyadh, Jeddah, Dhahran, Qassim, Sharurah, and Tabuk.

The system integrated with the storage tank was studied under four different flow rates, where the tank's inlet and outlet flow rates were assumed to be equal. The storage tank flow was varied for four cases as follows: (i) 24 hour operation; (ii) ideal flow; (iii) average flow; and (iv) maximum flow. The tank flow rates were, 0.0343 kg/s, 0.0385 kg/s, 0.064 kg/s and 0.1065 kg/s, respectively.

The effect of the flow rate was studied to evaluate the number of operating hours and the rate of freshwater production. A higher flow rate presented a higher productivity of freshwater but a significantly lower operating time, whereas lower flow rates presented longer operational times, with a lower rate of freshwater productivity. The maximum productivity reported for Dhahran was 9.346 liters an hour under the maximum flow rate case and a minimum of 3.01 liters per hour related to the 24 hour case. The longest operating time reported was 24 hours, and the shortest was 10 hours.

Moreover, the performance and cost of the system for both cases was evaluated for six different locations in Saudi Arabia. It was found that an increased freshwater productivity and operational time for locations that had longer day light hours and a higher solar intensity. Further it was found that the system integrated with a storage option produced significantly larger quantities of freshwater as compared to the direct solar HDH system. The cost analysis concluded that, with an expected system life of 20 years the cost per liter of freshwater produced would vary from \$0.018 to \$0.024.

ملخص الرسالة

الاسم الكامل: محمد ايفراس زبير

عنوان الرسالة: التحليل الحراري والاقتصادي لنظم تحلية المياه بالترطيب والتجفيف مدارة بالطاقة الشمسية مع

استخدام تخزين حراري

التخصص: علوم سريان الموائع الحرارية

تاريخ الدرجة العلمية: ديسمبر ٢٠١٥

تكمن مشكلات تجميع الطاقة الشمسية وتحويلها إلى طاقة حرارية في محدودية ساعات ضوء النهار (أو الطاقة الشمسية) وتقلبات الجو . وترتبط نظم تحلية المياه بالطاقة الشمسية بمشكلة محدودية ساعات التشغيل والتغير في شدة الطاقة الشمسية.

ولتحسين ظروف تشغيل طرق التحلية بالترطيب والتجفيف واستخدام مجمعات الأنابيب المفرغة للطاقة الشمسية كمسخنات للماء تم عمل تحليل رياضي لهذا النظام أولا ، وأتبع ذلك استخدام نظام التخزين الحراري باستخدام الماء كمائع تخزين في وعائي تخزين منفصلين أحدهما للماء الساخن والآخر للماء البارد ، وهذا يوفر القدرة على التحكم في درجة حرارة الماء الخارج من نظام التخزين .

وقد تمت دراسة نظام التحلية بالطاقة الشمسية متكاملًا مع نظام التسخين الحراري باستخدام أربعة سريانات وبفرض تساوي معدل سريان الدخول والخروج من أوعية التخزين الحراري . وتم تغيير السريان إلى أوعية التخزين خلال أربع وعشرين ساعة بحيث يكون السريان الأدنى 0.0343 كج/ثانية ، والسريان المثالي 0.0385 كج/ثانية ، والسريان المتوسط 0.064 كج/ثانية ، والسريان الأقصى 0.1065 كج/ثانية .

وتمت دراسة تأثير تغير السريانات على ساعات التشغيل ومعدل إنتاج مياه التحلية. وقد أعطى السريان المرتفع إنتاجًا أكبر للمياه المحلاة ، ولكن ساعات الإنتاج قلت كثيرا ، بينما أعطى السريان المنخفض ساعات تشغيل أطول

ولكن إنتاجاً أقل لمياه التحلية لكل ساعة. وقد تبين أن أقصى إنتاج في مدينة الظهران هو 9.346 لتر/ساعة عند أقصى سريان لماء التخزين ، وأقل إنتاج كان 3.01 لتر/ساعة عند أقل سريان خلال الأربع والعشرين ساعة .

وقد تمت دراسة تأثير الموقع بداخل المملكة على إنتاج مياه التحلية وتبين أن هذا النظام سيعطي إنتاجاً أكثر وساعات تشغيل أكثر إذا كان الموقع يتميز بساعات ضوء أكبر خلال النهار ، كما تبين أن ربط نظام التحلية بالطاقة الشمسية مع التخزين الحراري سيعطي إنتاجاً أكثر من مياه التحلية مقارنة بعدم وجود نظام التخزين ، أي باستخدام الطاقة الشمسية للتحلية بالترطيب والتجفيف بدون تخزين .

ويكمن الفرق عند استخدام التخزين الحراري وبدونه في إضافة وعائي التخزين وزيادة سعة كل من جهازي الترطيب والتجفيف . وقد بينت الدراسة الاقتصادية عن فرص العمر المتوقع لنظام التحلية بالطاقة الشمسية بعشرين عاماً ، وأن ثمن إنتاج لتر المياه المحلاة يتراوح بين \$0.018 و \$0.024 دولار أمريكي.

CHAPTER 1

INTRODUCTION

Water is an essential component for the existence of life forms. The majority of the earth's surface (nearly 70%) is filled with water, nonetheless close to 97% is salt water. Although it is believed that the small percentage of fresh water available is suitable to support life forms on earth, the consumable water is not evenly scattered all through the planet, and in some parts of the globe it is scarce. The main source of producing fresh water from oceans is solar energy. Thermal energy is absorbed by the earth's surface which in turn provides sufficient energy to evaporate sea water. Water vapor raises forming clouds at different elevations. This is a natural way of obtaining fresh water as rain [1].

1.1 Background

The world as we know currently has around 40% of its population facing water scarcity. This percentage is expected to rise up to the 60s, mainly due to the exponential growth of the population in the world. The usage of impure water is also a common source for most diseases, and also a considerable amount of deaths throughout the world [1].

The integrated effects of the continuously increasing population in the world, changes in people's lifestyles and the limited natural resources for pure consumable water, rapidly develops a need for desalination and water recycling. One of the main solutions

considered, is desalination of sea water. This is a commonly used method for supplying fresh water to dry zones throughout the world, mainly due to the fact that almost 70% of the people living in the world, live nearby seas or oceans situated within 70km. Desalination is considered to be the most feasible and economical solution for the fresh water shortage throughout the world [1].

Two major contributors for the stress on the demand for water are the growth rate of the population and the increase in demand per capita. A third stress factor would be the climatic change. Climatic change accelerates along with industrialization and population growth. Membrane based systems is a rising market in countries such as, Algeria, Australia and Spain, where as thermal processes are still widely in use throughout the middle-east, in countries such as Saudi Arabia, UAE, Bahrain, Kuwait etc., where 34.8% of all thermal desalination processes in the world are in Saudi Arabia. The use of thermal desalination systems in Saudi Arabia are a viable and suitable option, considering the geographical location and weather conditions [2].

Commonly known regions facing scarcity of fresh water resources are dry regions, where solar energy is bounteous. Considering the biggest disadvantage and advantage of dry regions throughout the world, a common solution widely in use is desalination with solar energy technology. This caters the need for fresh water through the purification of saline water, with the use of the abundantly available solar energy in dry regions [3].

Desalination is derived from the root word desalt, that stands for the removal of salt [4]. Industrial desalination plants are mostly common in dry zones across the world, where

the Middle East and North Africa are the largest consumers of desalination techniques [5]. According to data published by Global water Intelligence there has been a 57% capacity increase in desalination plants.

At the end of 2008, desalination plants across the world had a capacity of 47.6 million m^3/d , whereas currently it stands at 78.4 million m^3/d . Communities living inland areas have a tendency to use groundwater, which has an increasing tendency to go brackish over time, whereas communities in coastal areas are attending to sea water as a source for their fresh water requirements. This is shown in the market growth for desalination, where about 40% of the desalination capacity treats brackish less saline water, whereas 60% of the desalination capacity treats seawater.

History indicates industrial desalination plants were mainly built in areas where no substitute was present for public water supply, such as the Gulf region. The blend of low cost membrane desalination and the exponential increase in fresh water scarcity has motivated industrial desalination plants to move to other regions throughout the world. One of the largest desalination plants soon to be operational is the Magtaa plant in Algeria, where the outputs are estimated to be over 500,000+ m^3/day . The world's largest thermal desalination plant as of 2014 is the Ras Al Khair project in Saudi Arabia, where a combined technology of both thermal and membrane is to be used with a production rate of 1,025,000 m^3/day . Desalination is currently in practice among 150 countries in the world, through Europe, the Middle East and North Africa [6].

A publisher of Global Water Intelligence, Christopher Gasson mentioned that, at present nearly 1% of the world's population is dependent on desalinated water, and by 2025 14% of the world is to encounter scarcity of water according to the UN. Therefore he pointed out that unless there's a radical improvement in water conservation, the water desalination industry has very high potential. Furthermore he pointed out that sea water desalination is the only other alternative renewable source of fresh water production [6].

Further, Patricia A. Burke, Secretary General for the International Desalination Association (IDA), mentioned that the growth in desalination is nonlinear, where other factors such as the availability of financing, and the global oil prices are a few of the major factors affecting the slow growth, however growth accelerators such as pollution of traditional water resources, industrial development, population growth and climate change are still partaking with a heavy impact. The desalination industry has continuously provided solutions for low cost desalination through the development of lower energy consuming technologies, implementing techniques that provide greater efficiencies and further adopting methods to boost environmental quality [6].

The thesis discusses the operation of a standard Solar HDH desalination system and then proposes a unique thermal storage system to be integrated to a system operating with evacuated tube water heaters linked with an HDH desalination system. Investigating the effects of solar radiation, ambient temperature and geographical locations on the operational time and the freshwater production rate of the complete system integrated with thermal storage. The investigative part of the report is mainly broken down into four

sections, where first a general HDH system that uses evacuated tube collectors as water heater is presented, then the addition of thermal storage and optimization for specified operational hours, furthermore a feasibility study is performed along with a cost analysis, lastly presenting the comparison study of operating the system for different locations in Saudi Arabia.

1.2 Objectives

The overall objectives of this study are to conduct thermodynamic and cost analyses for solar driven HDH system with and without thermal storage option. The specific objectives of this study are as follows:

- Comparison study between:
 - Direct Solar HDH system,
 - 9-12 hour operational solar HDH system,
 - 14-16 hour operational solar HDH system,
 - 24 hour operational solar HDH system;
- Cost analysis and feasibility study of the system proposed;
- Location dependence performance of the HDH systems;
- Possible applications in rural areas and areas with fresh water scarcity; and
- Unique storage system with capabilities of constant temperature output and operational time control.

CHAPTER 2

LITERATURE REVIEW

The main two variations of industrialized desalination systems are within the method of separation, where the two widely used choices are membranes or thermal processes. These separation methods further subdivide into two, where thermal separation is subdivided as either evaporation and condensation or freezing and melting of water ice crystals. The evaporation and condensation technique is the most commonly used technique, and are mostly integrated with other thermal processes such as power generation. Commonly used evaporation processes are many, such as solar stills, humidification dehumidification (HDH), multi stage flash desalination (MSF), the multiple effect evaporation (MEE) and single effect vapor compression (SEC). Solar stills and HDH processes are quite different to others mentioned previously mainly due to the ability of operating at low temperatures due to the concentration difference of water vapor in the air stream [1].

Membrane technologies are thought to imitate functions of biological membranes such as lungs, skin, kidneys etc. Membrane technology adopts separation mechanisms from artificial membranes, Reverse Osmosis and Electro-dialysis. Reverse Osmosis permeates fresh water through semi-permeable membranes at high pressure, where the remainder is a highly concentrated brine solution. With electro dialysis electrically charged salt ions separate through the use of selective ion exchange membranes that leaves behind low

salinity water. Electro-dialysis however has very limited industrial applications [1]. Due to the absence of phase change unlike thermal desalination technologies, membrane technologies consume far less energy.

Due to low specific energy consumption compared to thermal technologies, membrane technologies are at present the leading technology in desalination, specifically reverse osmosis, conversely these technologies require highly skilled operating personnel for maintenance and have comparatively high maintenance and operating costs. Furthermore they are also less compatible with raw water turbidity, and due to its sensitivity to feed water quality it also requires pretreatment of the feed water [5].

The fundamentals of a thermal desalination process, is the vaporization of saline water and the collection of fresh water through vapor collection. The main concern with thermal desalination systems is the need for large sum of energy to cater for the phase change from liquid to vapor.

The demand for fresh water for consuming and domestic needs, for agricultural and livestock production, energy generation, and commercial and industrial applications are growing exponentially, along with economic development and population [2].

Close to 50% of the world's entire desalination market uses thermal desalination processes, where the remainder is mostly under the reverse osmosis (RO) process. The thermal desalination processes consist of multi-stage flash (MSF), multiple-effect distillation (MED), mechanical vapor compression (MVC), humidification dehumidification, solar stills, freezing etc. [7].

Solar still in comparison to many other thermal desalination techniques have a considerably lower gained-output-ratio (GOR), and thereby requires a greater total area of the solar collector. These also integrate the functions of evaporation, condensation, solar collection and water heating, which generally results in the lower GOR [8].

However HDH systems and Solar Stills are common in two ways, that they evaporate water at temperatures lower than the boiling temperature and that the main driving force for evaporation is the concentration difference of water vapor in the air stream. Solar stills have a long history from as far back as the 1800's where single stage stills were operated in batch mode on board ships [1]. In a solar still the saline water is placed within a blackened basin that's placed in an air tight transparent structure, where the water evaporates due to solar radiation absorption, where the condensed vapor falls along the sloped structure while losing its latent heat of condensation to the environment. These condensed droplets are then collected as pure water. A well-known rule of thumb with solar still is to aim for a goal of achieving around 3-5 liters of fresh water per day and per m^2 of the area of the solar still [2]. Solar stills are known to use a small scale hydrological cycle. The efficiency depends on general meteorological limitations of which some are the sky clearness, solar radiation, ambient temperature. Wind velocity etc. the output of a solar still is also affected by many other factors such as, vapor leakage, brine depth, cover slope, thermal insulation, and shape material [9].

The humidification dehumidification desalination process often known as HDH among engineers is a commonly known process considered to be favorable for small scale

desalination plants. The primary advantages of using a HDH process is its capability to operate at low temperatures, the possible integration of renewable and sustainable energy sources and the use of low-level technical features. The biggest advantage however is that HDH process' use separate independent components for each thermal process, which also allows the flexibility of designing each component independently, this in turn provides flexibility with thermodynamic cycles for condensing vapor and evaporating water into air [8]. HDH processes in comparison to solar stills have a much greater gained-output-ratio (GOR) which therefore reduces the total solar collector area for a given fresh water demand. HDH processes are considered to be more appropriate in terms of the limited technical support required and the capital investment as it involves reasonably priced and simple mechanisms that are operational under a wide range of raw water quality minus the need for complicated maintenance procedures [10].

A conventional HDH desalination process includes components such as, an evaporator, a condenser and a heat supply system with a combination with/without thermal storage. The HDH process includes bringing warm saturated air into direct contact with warm saline water, where a desired level of humidity is reached followed by the extraction of vapor from the humid air, through the use of a condenser [5].

General classification of HDH systems depends on the heating fluid (air/water) and if the fluid streams flow through an open or closed loop system. Various experimentations have been carried out with the use of combinations of air and water heaters, the use of water storage tanks, steam generators etc. thermodynamic analysis of an HDH system is

commonly based on energy and mass balances of each individual component within a system. Many existing literature on HDH desalination technologies focused on. Multi-stage air heated cycle, mechanical compression driven cycles, HDH with common heat transfer wall, HDH with thermodynamic balancing, hybrid systems combined with reverse osmosis etc.

Four different HDH system layouts were assessed by Ettouney [11]. The common parameter among the different layouts considered was the air humidifier that was used to increase the ambient air humidity to saturation at a desired temperature. The key alteration among the separate layouts was the dehumidification process. One of the layouts had a condenser to reduce the temperature of the humidified air and also to condense the fresh water vapor.

The other layouts considered included, membrane air drying, desiccant air drying and vapor compression. Various equations were presented that had been developed for the desiccant and the condenser layouts. The primary drawback stressed upon was the presence of bulk air along with water vapor, which was found to be the reason for the drastically reduced efficiency.

A study on photovoltaic driven HDH system by Wang et al. [12] considered the main factors affecting evaporation and condensation in the system. The study mentioned that the rate of evaporation of water and condensation of the mass flow rate increased along with the increase in evaporative raw water. It was also found that lower the cooling water temperature the higher the condensation rate. Further it was found that the forced

convection method had a higher yield of fresh water in comparison to natural convection. The highest recorded freshwater yield was $0.873 \text{ kg/m}^2\text{-day}$ with an evaporative temperature of 64.3°C .

One of the first methods established for the production of consumable water through salt water used solar energy technology. Solar thermal energy was used to vaporize water, which separated fresh water from brine. Considering the environmental impact, no carbon dioxide is released to the environment and the effects from water pollution and air pollution are minimal. However the disposal of brine may significantly harm the environment and lead to ecological degrading. A few of the methods currently in use to dispose of brine are, transporting the brine to a saline water body, evaporation by solar means, or injecting the brine into an existing zone of highly saline ground water.

Various collector types used for solar heating include [13]:

- Solar Ponds
- Flat Plate Collectors
- Evacuated Tube Collectors
- Compound Parabolic Collector
- Linear Fresnel Reflector
- Parabolic Trough Collector
- Cylindrical Trough Collector
- Parabolic Dish Reflector
- Heliostat Field Collector.

Solar energy varies with time and is known as a time-dependent energy source, storage of solar energy is a necessity for most solar process systems. The major constituents of such a system are:

- Solar collector
- Storage units
- Conversion devices
- Loads
- Auxiliary energy supplies
- Control systems

Generally the performance of each of these elements is inter-related. The vast impact of temperature on the collector performance, in turn affect all other components within a solar process system. The available solar radiation at a given time, the various loads expected within the system, the type of auxiliary energy and the method in which it is used, economic feasibility, the rate of solar energy required in terms of substituting

conventional energy used, and the degree of reliability required are some of the main factors that the optimum capacity of the storage depends on [3].

Investigating modeling of evacuated tube collectors, Budihardjo and Morisson presented a model using TRNSYS, where a study was conducted in order to evaluate the performance of water in glass evacuated tube solar water heater. The evacuated tube collector consisting of 30 tubes was compared to a two panel flat plate collector, where it was concluded that the flat plate system had slightly better performance under operating conditions for Sydney, Australia [14].

In a study of various absorber tubes in evacuated tube collectors conducted by Kim and Seo [15] it was proven that the performance of the collector varies depending on the type and arrangement of the absorber tubes. It was shown that a U tube welded onto a copper absorber plate attained the best results.

Ng et al. [16] analyzed an evacuated tube collector that uses a heat pipe design similar to the one used in this report. They evaluated the thermal losses such as radiation heat losses between the absorber and the ambient environment, losses at the manifold and thermal resistance losses within the collector. The model presented was validated with comparison to experimental data, where the theoretical values were slightly higher than the experimental useful heat gain by about 4%.

Heat pipes mainly consist of an evaporator, condenser and working fluid. Generally they have a very high thermal conductivity. The process within a heat pipe work as follows, the evaporator absorbs heat there by evaporating the working fluid, where the fluid

absorbs heat equivalent to its latent heat of vaporization, the evaporated fluid is then condensed by a cooling fluid that carries away the heat gained within the manifold. The flow of the fluid depends on the design of the heat pipe. An evacuated tube collector using heat pipes consists of a row of heat pipes within evacuated glass tubes similar to the collector discussed in this study. Having an indirect contact between the heat pipe and the condenser provides an advantage of being able to operate the collector system even while maintenance for some of the tubes are carried out, for example having to replace one of the tubes in the collector while it still operates, this also reduces leakage problems within the collector system [17].

Investigating the use of multiple collectors such as a heat pipe evacuated tube collector and a parabolic trough solar collector with solar stills it was found that freshwater production rates could be increased by around 40%, where the cost of the clean water produced was found to be around \$0.045/L [18].

In a study conducted by Yildirim C, and Solmus I. [19] on HDH desalination system using air heater and water heaters, it was perceived that water heated HDH desalination had a significant effect on producing freshwater, reason being that water has a higher heat capacitance in comparison to air. Therefore for systems using flat plate solar collectors for air and water heating, water heated systems have a higher significance on the effects of producing freshwater.

The storage of solar energy or the products of solar processes may be stored as either Electrical, chemical, mechanical or thermal energy. The main concern within this study is

the storage of thermal energy. Thermal energy storage can be sub categorized in to three constituents as Sensible Heat Storage, Latent Heat Storage and Thermo-Chemical heat storage [3].

In a common solar energy system, the thermal storage component would usually store the excess energy during the day, where then it may be regenerated according to the demand for thermal energy (night time, or cloudy days or under unfavorable weather conditions).

The main characteristics of energy storage systems are [5]:

- The time during which energy may be stored
- The volumetric energy capacity for the same amount of energy (smaller the storage the better)
- Energy may be added or withdrawn conveniently from the system.

Heat storage capacity an order of magnitude larger than Sensible Storage may be achieved through Thermo-Chemical Storage. This method relies on a completely reversible process, where the energy absorption and release relies on breaking and reforming molecular bonds as a completely reversible endothermic chemical process. The extent of conversion, the endothermic heat of reaction and the amount of storage material are factors that the amount of heat stored depends on. This method has a major advantage in long-term storage and minimal losses. Depending on the reaction, Thermo-chemical storage is believed to have the capability of storing up to 1MWh/m^3 and also are more flexible, although they are far more sophisticated than other thermal storage methods and are currently in the development stage [5].

Latent heat storage also known as phase change material storage, whereas the name suggests the storage depends on the phase change of materials from solid to liquid, liquid to gas etc. The phase change process is an isothermal process, where there is no temperature change on the storage materials. The phase changes should take place with constrained super heating and super cooling and should also add and remove heat while containing the storage material. This method of storage may operate a small range of temperature, have high storage capacities and have relatively low mass and volume [3].

Sensible heat storage, presents a direct relationship between the heat energy stored and the storage material. The quantity of the stored heat depends on:

- Specific heat of the medium
- The temperature change
- The amount of storage material

Widely used sensible heat storage systems use oil, water or air as the heat transfer fluid whereas iron, ceramic bricks, earth, water or stones are used as the storage medium. The considerably high heat capacitance of water makes it logical to be used as a storage medium for applications that require heating and cooling although the low density of water brings forth a need for large quantities. Water storage tanks are highly recommended for 24hour operation of humidification dehumidification desalination plants. Storage materials such as rocks or ceramics have the capability of maintaining large temperature difference, however they have a relatively low heat capacitance [20].

Shabaneh et al. [21] have presented a paper which disclosed a theoretical investigation on the performance of a solar air-heated desalination system using HDH technique based on a closed water, open air cycle. The assumed location for the system was Dhahran, Saudi Arabia. The proposed system included a tilted two-pass solar air heater, a storage tank, a dehumidifier and a humidifier. A simulation had been presented that had been developed using energy and mass balances. The results presented showed that the tilted solar air heater gives 7% higher performance, where the humidifier performance was shown to have a significant effect on system productivity.

Summers et al. [22] pointed out that within the context of HDH desalination air heating provides significant performance increases. It was also pointed out that a constant heating temperature and constant heat output are important for the cycle performance. The use of phase change materials (PCM) was shown to provide consistent air outlet temperatures through day and night. In the proposed design the PCM was placed just below the

absorber plate. Through the use of a two dimensional transient finite element model it was shown that 8cm PCM layer below the absorber plate was adequate to provide a steady outlet temperature near to the PCM melting temperature, where the collector was found to have a 35% time averaged collector efficiency.

The technology of thermal storage with phase change is considered as the most mature technology in thermal storage. A few of the reasons for it to be considered as one of the most useful thermal storage options is due to the constant temperature in storing and releasing heat, high density in heat storage, and ease of control. Proposed experiment uses a plate-fin thermal storage device. The heat storage and release performance of the storage device is affected by the flow rate and the inlet temperature. The desalination plant considered comprises of a solar unit that provides the thermal energy, a storage device as fore mentioned and a desalination module that uses a plate-fin desalination unit. During the day time if the temperature of the collector outlet exceeds the maximum allowed temperature of the control valve some of the liquid flows into the thermal storage unit. The phase change material (PCM) within the storage unit stores large amounts of energy during melting and releases large amounts of energy while solidifying [23].

Muller-Holst et al. [24] examined decentralized desalination systems, where it was found that constant performance may be achieved for over five years without the need for broad maintenance. In an attempt to further improve the efficiency through economic solutions, it was pointed out that there is a need for thermal storage to be integrated with the desalination system. It further mentioned that, for the whole system to be economical the desalination system had to be operational for 24 hours. The possible cost reduction was found to be more than half through the implementation of storage. Fresh water production costs were shown to drop by 20% through the use of better evaporation surfaces and thinner flat plate heat exchangers, and further reduction was shown to be possible through the implementation of a storage unit.

Miyatake et al. [25] introduced a hybrid spray flash system combined with latent heat storage in order to develop an energy saving desalination system that stored thermal energy from solar heat, waste heat, and the surplus steam of a power station, where the stored energy was used not only for air conditioning and power generation but also fresh water production. Experimental results on heat storage through the use of phase change materials had been presented, along with high efficiency rates of the hybrid system of around 95%.

It may be observed through the literature review, that humidification dehumidification systems using renewable energy along with thermal storage options, have received relatively less attention. The importance of thermal storage systems to be combined with solar thermal desalination systems occurs mainly due to the variation in heat input with the time dependent solar irradiation.

This study introduces a unique energy storage system that uses hot and cold storage tanks as two separate storage entities to provide a constant heat addition for the HDH system in order to smooth out the energy input through renewable sources, where the heat gained through collectors usually vary along the day introducing various issues with thermal stresses and irregular water production rates. The design proposed in this study introduces a water heated HDH system that uses evacuated tube collectors for thermal energy collection, along with thermal storage as explained previously. The humidifier and dehumidifier units used within the system use packed beds that provide a highest efficiency of about 85% for the components for evaporation and condensation. Detailed thermodynamic analysis has been carried out to evaluate the performance of the proposed system, where the preliminary performance measures were carried out for Dhahran, Saudi Arabia.

CHAPTER 3

RESEARCH METHODOLOGY

This chapter introduces the proposed model followed by a detailed description of mathematical modeling along with the assumptions made in modeling the proposed system.

3.1 System Description

Figure 1 presents the proposed design for a Closed Air Open Water (CAOW) HDH system, integrated with an Evacuated Tube Water Heater as well as a thermal storage system. The choice of having a closed loop air system was due to the generally humid air present within the environment in Dhahran, Saudi Arabia. The thermal storage system is to provide 24hour functional capability to the system along with a constant production rate of fresh water, by providing saline water to the humidifier at a set constant temperature. The fluid used within the collector part of the design may be of a special sought in order to improve thermal energy collection and prevent boiling or freezing etc.

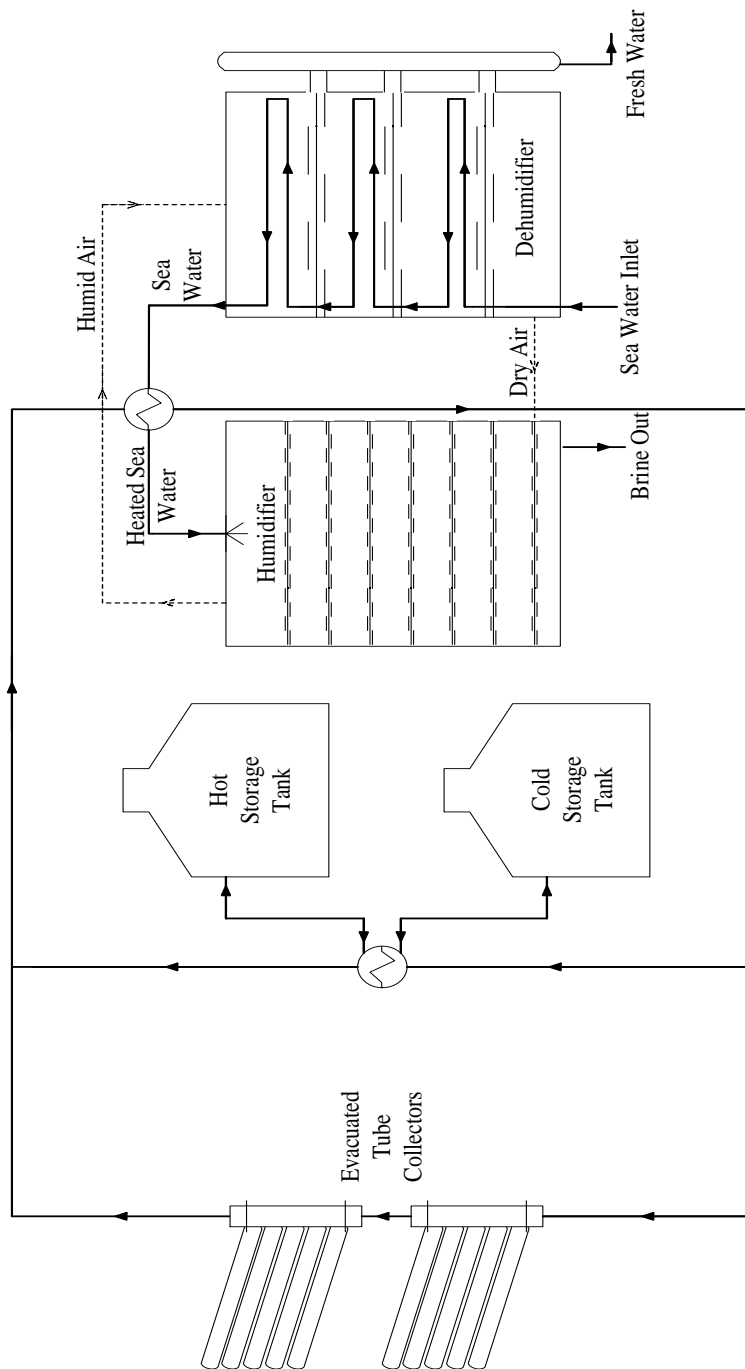


Figure 1: Proposed Design.

3.2 Modeling Assumptions

- The complete cycle is considered under steady state conditions, and assumed to be operating at atmospheric pressure.
- Insolation data are obtained as hourly data
- The performance is considered to be time dependent
- No leakage of water or air within the complete system
- The complete system is well insulated
- The energy balances consider incompressible flow and neglects pressure differences
- Assumption specifically for the collector, are as follows:
 - The temperature of the collector receiver area is uniform at all times
 - The temperature gradients across the plate thickness and along the perimeter are negligible.
 - The temperature gradient along the longitudinal direction is negligible due to constant temperature during phase change within the evaporator.
 - Thermal resistance due to contact between the receiver area and the evaporator section, and the manifold and the condenser, are negligible.
 - The joint between the evaporator heat pipe and the condenser is adiabatic.

- Assumptions specifically for the HDH desalination system, are as follows:
 - Heat loss from any of the components considered within the system is neglected.
 - The fan power for air circulation is negligible in comparison to thermal energy.
 - The freshwater leaving the dehumidifier is at the average temperature between the dew-point temperature of the inlet air and the dry-bulb temperature of the exit air in the dehumidifier.
 - The relative humidity of air at the exits of the humidifier and the dehumidifier is 0.9.
 - The effectiveness of both the humidifier and the dehumidifier is 0.85.
 - The minimum temperature of the sea water inlet is constant at 25 °C.
 - The maximum water temperature range considered is between 50-80 °C.

3.3 Mathematical Modeling

A mathematical model describing a system consisting of three different parts is considered in this study, where the solar collector, the humidification dehumidification cycle, and the thermal storage systems have been considered as the three main sections.

3.3.1 Evacuated Tube Collector (ETC)

Absorbed radiation (S) is given by the following equation [3]:

$$S = I_b R_b (\tau\alpha)_b + I_d (\tau\alpha)_d \left(\frac{1+\cos\theta}{2} \right) + \rho_{gr} I (\tau\alpha)_{gr} \left(\frac{1-\cos\theta}{2} \right) \quad (3.1)$$

where; I_b is the fraction of beam radiation in a given hour

R_b is the geometric factor for beam radiation

$(\tau\alpha)_b$ is the transmittance-absorptance product for beam radiation

I_d is the fraction of diffused radiation in a given hour

R_d is the geometric factor for diffused radiation

$(\tau\alpha)_d$ is the transmittance-absorptance product for diffused radiation

θ is the angle of incidence

ρ_{gr} is the ground reflectance

I is the incident radiation on the horizontal surface

R_{gr} is the geometric factor for ground reflected radiation

$(\tau\alpha)_{gr}$ is the transmittance-absorptance product for ground reflected radiation

The thermal circuit of an evacuated tube collector is shown in Figure 2 which has been used as a reference for modeling heat transfer equations. S represents the radiation absorbed by the receiver of the ETC, of which a relatively small portion is lost through radiation shown as $Q_{loss,rad}$ in the Figure. Q_u is the useful heat gain of the thermal collector which is obtained from the difference between the heat pipe gain (Q_{hp}) and the $Q_{loss,ma}$ known as the manifold heat loss.

$R_{loss,rad}$, the radiation thermal resistance is given by the following equation[17]:

$$R_{loss,rad} = \frac{(T_p - T_a)}{\varepsilon\sigma(T_p^4 - T_a^4)A_r} \quad (3.2)$$

where, T_p is the plate temperature

T_a is the ambient temperature

ε is the emissivity of the absorber coating

σ is the Steffan Boltzmann constant

A_r is the area of the receiver

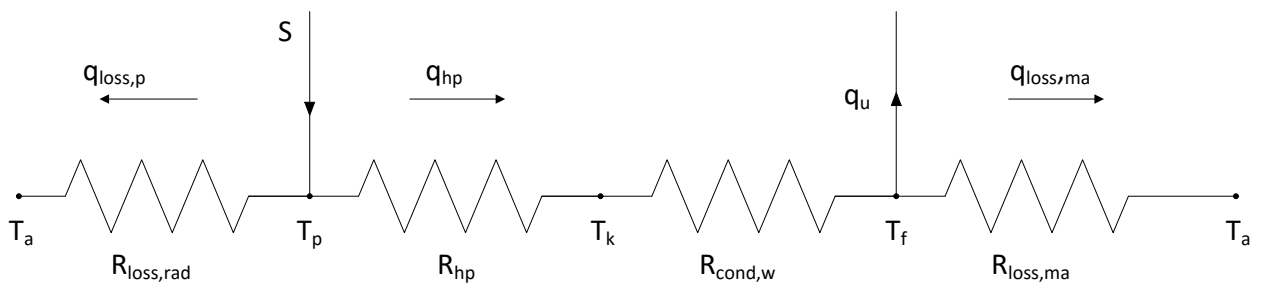


Figure 2: Thermal circuit of an evacuated tube collector.

R_{hp} , the evaporator (heat pipe) thermal resistance is given by the following equation [17]:

$$R_{hp} = \frac{\ln\left(\frac{D_{o,fin}}{D_{i,fin}}\right)}{2\pi k_{fin} L_{evap}} + \frac{\ln\left(\frac{D_{o,evap}}{D_{i,evap}}\right)}{2\pi k_{evap} L_{evap}} + \frac{1}{h_{hp} A_{evap}} \quad (3.3)$$

where,

$$h_{hp} = 0.555 \left(\frac{g \rho_l (\rho_l - \rho_v) k_l^3 h_{fg}}{\mu_l (T_p - T_k) D_{evap}} \right)^{\frac{1}{4}} \quad (3.4)$$

$D_{o,fin}$ is the outer diameter of the fin

$D_{i,fin}$ is the inner diameter of the fin

$D_{o,evap}$ is the outer diameter of the evaporator

$D_{i,evap}$ is the inner diameter of the evaporator

k_{fin} is the conductivity of the fin

L_{evap} is the length of the evaporator

k_{evap} is the evaporator conductivity

A_{evap} is the surface area of the evaporator

h_{hp} is the heat transfer coefficient of the heat pipe

g is the gravitational acceleration

ρ_l is the density of the liquid within the evaporator

ρ_v is the density of vapor in the condenser

k_l is the conductivity of the working fluid

h_{fg} is the enthalpy of latent heat

μ_l is the viscosity of the working fluid

T_k is the temperature at the condenser wall

$R_{cond,w}$, the condenser wall thermal resistance is given by the following equation[17]:

$$R_{cond,w} = \frac{1}{h_{cond}A_{cond}} + \frac{\ln(D_{o,cond}/D_{i,cond})}{2\pi k_{cond}L_{cond}} + \frac{\ln(D_{o,ma}/D_{i,ma})}{2\pi k_{ma}L_{ma}} \quad (3.5)$$

where,

$$h_{cond} = 0.555 \left(\frac{g\rho_l(\rho_l - \rho_v)k_v^3 h_{fg}}{\mu_l(T_p - T_k)D_{cond}} \right)^{\frac{1}{4}} \quad (3.6)$$

$D_{o,ma}$ is the outer diameter of the manifold

$D_{i,ma}$ is the inner diameter of the manifold

k_{ma} is the conductivity of the manifold

L_{ma} is the manifold length

$D_{o,cond}$ is the outer diameter of the condenser

$D_{i,cond}$ is the inner diameter of the condenser

k_{cond} is the conductivity of the condenser

L_{cond} is the length of the condenser

A_{cond} is the surface area of the condenser

h_{cond} is the heat transfer coefficient of the condenser

k_v is the conductivity of vapor in the condenser

R_{ma} , the manifold resistance is given by the following equation [17]:

$$R_{ma} = \frac{1}{U_{ma}A_{ma}} \quad (3.7)$$

where, U_{ma} is the manifold loss coefficient

A_{ma} is the surface area of the manifold

Therefore the heat transfer balance is then given by the following equation [17]:

$$Q_{in} = Q_{loss,rad} + Q_{hp} = Q_{loss,rad} + Q_u + Q_{loss,ma} \quad (3.8)$$

from which the following equation is obtained [17]:

$$SA_r = \frac{T_p - T_a}{R_{rad}} + Q_u + \frac{T_f - T_a}{R_{loss,ma}} \quad (3.9)$$

Where, T_f is the temperature of the working fluid

For simplification of the equations, the terms R_{cr} and R_{hr} are introduced, which are as follows:

$$R_{cr} = \frac{R_{cond,w}}{R_{rad}}, R_{hr} = \frac{R_{hp}}{R_{rad}} \quad (3.10)$$

Q_{hp} can be represented by the following equation [17]:

$$Q_{hp} = \frac{T_p - T_f}{R_{hp} + R_{cond,w}} = Q_u + Q_{loss,ma} = Q_u + \frac{T_f - T_a}{R_{loss,ma}} \quad (3.11)$$

Through the use of energy balances, Q_u is defined as follows [17]:

$$Q_u = \frac{SA_r}{1 + R_{hr} + R_{cr}} - \frac{T_f - T_a}{1 + R_{hr} + R_{cr}} \left(\frac{1}{R_{rad}} + \frac{1}{R_{loss,ma}} (1 + R_{hr} + R_{cr}) \right) \quad (3.12)$$

The equation above may be rewritten, where Q_u is defined as follows [3]:

$$Q_u = F' A_r [S - U_L (T_f - T_a)] \quad (3.13)$$

F' is the collector efficiency factor

U_L is the overall loss coefficient

where, [17]

$$F' = \frac{1}{1 + R_{hr} + R_{cr}} \quad (3.14)$$

and

$$U_L = \frac{1}{R_{rad} A_r} + \frac{1}{R_{loss,ma} A_r F'} \quad (3.15)$$

F_R known as the collector heat removal factor is given by the following equation [3]:

$$F_R = \frac{\dot{m} C_p}{A_r U_L} \left[1 - \exp \left(- \frac{U_L A_r F'}{\dot{m} C_p} \right) \right] \quad (3.16)$$

Q_u (collector) can then be rewritten as follows [3]:

$$Q_u = A_r F_R [S - U_L (T_i - T_a)] \quad (3.17)$$

where, T_i is the fluid inlet temperature

Q_u (working fluid) is defined as follows [17]:

$$Q_u = \dot{m} C_p (T_f - T_o) \quad (3.18)$$

where, m is the mass flow rate of the working fluid

C_p is the heat capacitance of the working fluid

T_o is the outlet temperature

The ratio of useful energy to the absorbed solar radiation is known as the efficiency of the collector, which is given by the following equation [17]:

$$\eta = Q_u / A_r I_T = F_R (\tau \alpha) - F_R U_L (T_i - T_a) / I_T \quad (3.19)$$

where, I_T is the total radiation available to the collector

3.3.2 Humidification Dehumidification System (HDH)

Energy balance equations were evaluated for the humidifier, dehumidifier and the solar water heater as follows [26]:

Humidifier

$$\dot{m}_w h_{w3} + \dot{m}_a h_{a1} = \dot{m}_b h_{w4} + \dot{m}_b h_{a2} \quad (3.20)$$

where, m_w is the mass flow rate of sea water

h_{w2} is the enthalpy of seawater at the exit of the dehumidifier

m_a is the mass flow rate of air

h_{a1} is the enthalpy of air at exit of the dehumidifier or the inlet of the humidifier

m_b is the mass flow rate brine

h_{w4} is the enthalpy of brine at the exit of the humidifier

h_{a2} is the enthalpy of air at the exit of the humidifier or the inlet of the dehumidifier

Dehumidifier

$$\dot{m}_w (h_{w2} - h_{w1}) + \dot{m}_{fw} h_{fw} = \dot{m}_a (h_{a2} - h_{a1}) \quad (3.21)$$

where, h_{w1} is the enthalpy of the seawater entering the dehumidifier

m_{fw} is the mass flow rate of fresh water

h_{fw} is the enthalpy of freshwater leaving the dehumidifier

Solar Water Heater

$$Q = \dot{m}_w c_{pw} (T_{w3} - T_{w2}) \quad (3.22)$$

where, Q is the energy input by the seawater heater

c_{pw} is the specific heat capacity of seawater

T_{w3} is the water temperature at the exit of the seawater heater

T_{w2} is the temperature of seawater before the heater

The effectiveness of the humidifier and the dehumidifier is given by the following equation:

$$\eta = \frac{\Delta\dot{H}}{\Delta\dot{H}_{max}} \quad (3.23)$$

The mass flow rate of fresh water is defined by the humidity ratios of the outlet and inlet of the humidifier, as shown below:

$$\dot{m}_{fw} = \dot{m}_a (\omega_2 - \omega_1) \quad (3.24)$$

where, ω_2 is the absolute humidity of air at the exit of the humidifier and the inlet of the dehumidifier

ω_1 is the absolute humidity of air at the exit of the dehumidifier and the inlet of the humidifier

The flow rate of brine is then found by subtracting the flow rate of fresh water by the flow rate of water entering the system:

$$\dot{m}_b = \dot{m}_w - \dot{m}_{fw} \quad (3.25)$$

The performance of an HDH system, known as the gained output ratio (GOR) is defined as follows:

$$GOR = \frac{\dot{m}_{fw} h_{fg}}{Q_u} \quad (3.26)$$

where, h_{fg} is the enthalpy of latent heat of vaporization of water

The recovery ratio, defined as the ratio between fresh water and the raw water input is given by the following equation:

$$RR = \frac{\dot{m}_{fw}}{\dot{m}_{sw}} \quad (3.27)$$

3.3.3 Thermal Storage

The thermal storage consists of two units, a hot storage and a cold storage, where the hot storage tank is considered as an un-stratified water storage unit, where all the collected heat by the solar collector is stored in. When the heat demanded by the HDH system is to be supplied a control system is implemented, where the hot storage temperature is measured and water from the cold storage is mixed together at the heat exchanger to provide the required temperature to the water line between the humidifier and the dehumidifier.

Hot Storage:

$$T_s^+ = T_s + \frac{\Delta t}{(mC_p)_s} \left\{ A_c F_R [S - U_L(T_s - T_a)]^+ - (UA)_s(T_s - T_a') - \varepsilon_L (\dot{m}C_p)_{min} (T_s - T_{Lr}) \right\} \quad (3.28)$$

where, T_s^+ is the temperature of storage at the end of the time period

Δt is the length of the time period for which the calculations are carried out

m is the mass capacity of the storage tank

$(UA)_s$ is the storage tank loss coefficient-area product

T_a' is the ambient temperature of the storage tank surrounding

ε_L is the load heat exchanger effectiveness

T_{Lr} is the load range temperature

The afore mentioned equations are implemented to simulate the design presented, through the use of Engineering Equation Solver, commonly known as EES, which is a computer program that solves equations simultaneously.

3.4 Methodology

- Modeling and validation for each section as previously shown :
 - HDH Desalination
 - Evacuated Tube Solar Collector
 - Thermal Storage System
- Complete combined system model
- Identify best operating conditions (Optimization)
- Daily, monthly and annual calculations (for Dhahran Saudi Arabia)
- Result Comparison for several other locations in Saudi Arabia (Location Dependent Performance)
- Comparison Study between a typical HDH system, 12 hour operational system and a 24 hour operational system.
- Cost Analysis for the complete system shown above. (Economical Analysis)

The research performed for this study used the steps described above, where first was modeling the three main components individually and then combining them, followed by optimization. The complete system model was then evaluated first with a Direct Solar HDH system and later adding a thermal storage option. Simulations were then carried out in detail for Dhahran, to study the complete system with storage and further simulations were also run for other locations in Saudi Arabia. A cost analysis was also performed, to find the cost per liter of fresh water produced.

3.5 Validation

The mathematical models described in the previously were implemented using the engineering equation solver (EES) software. The software uses a numerical iterative procedure to solve the set of equations. Convergence is reached when the residuals of the relevant equations are smaller than 10^{-6} or if the change in variables is less than 10^{-9} . The meteorological data required are mainly the hourly incident solar irradiation on a horizontal surface (MJ/m^2) and ambient temperatures (K). The data obtained, as well as the calculations were carried out for Dhahran, Saudi Arabia.

3.5.1 Evacuated Tube Collector

Initially the mathematical models were evaluated individually for the HDH system and the evacuated tube solar collector. The HDH system was modeled as a closed air open water system (CAOW) with water heating, whereas the collector was modeled as a water heater. Initial calculations were performed in order to verify the mathematical models.

An excerpt from Appendix A is shown below in Table 1 that presents the collectors with the highest output capacity and the lowest collector area. The pricing of these collectors were based on an average cost of \$500 per square meter of a collector. Thereby it was possible to determine the best value collector with the highest productivity. The calculations were carried out using RetScreen which gives the expected annual output and also calculates the price using the collector data available in its database. Commonly known manufacturers of solar collectors and manufacturers with more than one collector

type to offer were included in this process. The best performing collector is the Apricus AP-30 evacuated tube collector shown at the top of the Table. This collector has the highest capacity with respect to the gross area and the estimated cost is very nearly the same as the real purchase price later found to be \$1930 [27]. Thus this option proves itself to be an even better value for the capital spent. The complete list of collectors and manufacturers considered can be found in Appendix A.

Table 1: Excerpt of the table from APPENDIX A.

Evacuated Tube Manufacturer	Model	Gross area per collector (m ²)	Capacity (kW)	Cost per unit	capacity per dollar	Capacity/Gross Area
Apricus	Arpicus AP-30	4.05	2.66	\$1,900	0.0014	0.65679
Calpak	16 VTN	2.86	1.83	\$1,430	0.00128	0.63986
Ritter Solar	CPC 30 Star Azzurro	3.30	2.11	\$1,651	0.00128	0.639394
Calpak	6 VTN	1.06	0.67	\$530	0.00126	0.632075
Oventrop	OV 5-8 AS/AB	2.03	1.28	\$1,014	0.00126	0.630542
Ritter Solar	CPC 14 Star azzurro	2.61	1.63	\$1,305	0.00125	0.624521
Beijing Sunda Solar Energy Technology	Seido 10-20 AS/AB	3.39	2.11	\$1,697	0.00124	0.622419

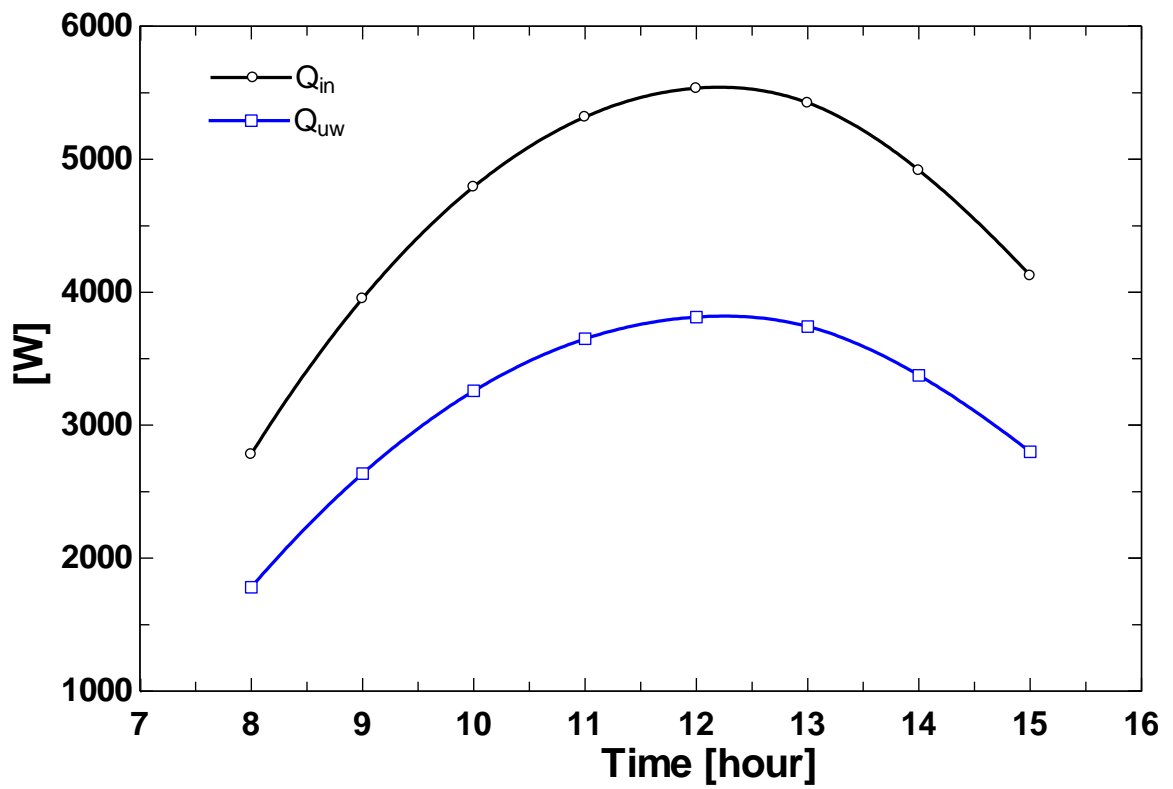


Figure 3: Useful heat gained and available heat input vs. time.

Figure 3 shows the useful heat gained (Q_{uw}) calculated from the input of the available radiation on a horizontal surface on 11th of June. The calculation depends on several variables such as the transmittance absorptance product, the tilt angle, the time of day, the day and the month of the year, the collector cover characteristics etc. As expected the heat gained is lower than the available heat input (Q_{in}), and the curve for Q_{uw} follows the same trend as that of Q_{in} at the same instance of time. Therefore the results indicate that the absorbed radiation values calculated by the model are valid, based on a qualitative perspective.

As means to the main parameter used to validating the code for the evacuated tube collector, is the efficiency of the collector. Table 2 shows a comparison between the calculated collector efficiencies and the manufacturer's technical information sheet illustrating the measured efficiencies at a certain operating temperature. The comparison is for temperatures from 40°C to 80°C, which would be well within the expected temperature limits of this system. The calculated values are within a tolerance of 0.01-0.02 of the measured efficiencies. Thus, the mathematical model presented for the ETC provides considerably accurate efficiencies which agree well with the measured efficiencies, proving that the model can be used to simulate an Apricus AP-30 collector.

Table 2: Validation data for the evacuated tube model at an irradiation of 800 W/m².

$\Delta T = (T_{\text{mean}} - T_a)$	Calculated Efficiency	Measured Efficiency
40°C	0.62	0.64
50°C	0.59	0.6
60°C	0.57	0.58
70°C	0.53	0.54
80°C	0.5	0.51

3.5.2 Humidification Dehumidification Desalination System

Two independent published journal articles on closed water open water HDH desalination were used to validate the model presented for the HDH part of the system. Sharqawy et al. [26] presented a design example for a CAOW HDH desalination system, which used inputs such as the latent heat of vaporization, the gained output ratio, the recovery ratio along with the mass ratio as shown in Table 3 to calculate the required heat input and the relevant air and sea water flow rates. The Table also shows that the relevant values calculated by the HDH system model proposed here agree very well with the values reported, indicating the validity of the proposed model.

Table 3: Validation of the HDH model by comparison with the results obtained by Sharqawy et al. [26].

Constant Variables	Calculated Variables	Literature Values	Model Values
GOR = 1.93	Q_{in}	3.34 (kW)	3.37 (kW)
MR = 2.04	m_w	0.0899 (kg/s)	0.0907 (kg/s)
RR = 0.0306	m_a	0.0442 (kg/s)	0.0445 (kg/s)

The results obtained with the proposed model was also validated by comparing the results reported by Narayan et al. [28]. They evaluated the effect of relative humidity of air at the inlet and exit of the humidifier and dehumidifier has on the performance as measured by GOR of a CAOW HDH system (Figure 4). The values of the variables used to produce the graph in Figure 4 are shown in Table 4.

Table 4: The values of the variables used to assess the effect of relative humidity of air by Narayan et al.[28].

Variable Name	Value
Maximum Temperature	80 (°C)
Minimum Temperature	35 (°C)
Humidifier Effectiveness	90%
Dehumidifier Effectiveness	90%
Mass Ratio	5
mass flow of water	0.5 (kg/s)
mass flow of air	0.1 (kg/s)

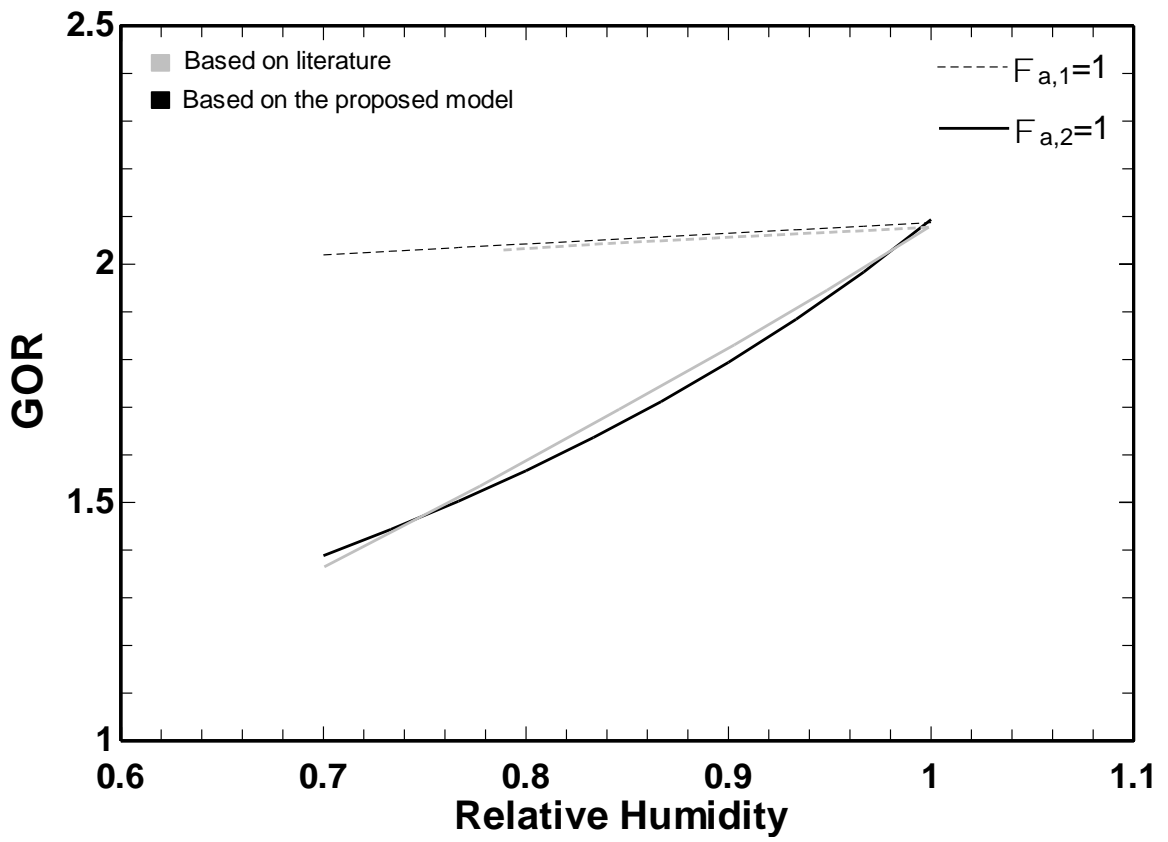


Figure 4: GOR vs. Relative Humidity Validation with Narayan et al. [28].

A plot of the effect of relative humidity on the performance of an HDH system computed using the EES code for the HDH desalination system is compared with a similar plot reported by Narayan et al. [28] the values of the maximum and minimum temperatures, humidifier and dehumidifier effectiveness, and the mass flow ratios used in the comparison are shown in Table 2. The humidity ratios of air at the exit and inlet of the humidifier are given as $\phi_{a,1}$ and $\phi_{a,2}$ respectively. Narayan et al. [28] reported that varying the relative humidity of air at the exit of the humidifier from 70% to 100% only causes a change of about 3% in GOR as shown by the grey dashed line in Figure 4. The black dashed line in the Figure refers to the results obtained through the EES code under similar conditions. The two curves agree very well, with the EES code also predicting a 3% change in GOR. Varying the relative humidity of air at the inlet of the humidifier has a much greater effect on the performance as measured by the GOR, depicted by the grey solid line, which changes by about 34%. Effect of relative humidity of air at the inlet of the humidifier on the performance calculated by the EES code, depicted by the black solid line, predicts a change of about 31% and agrees well with the results.

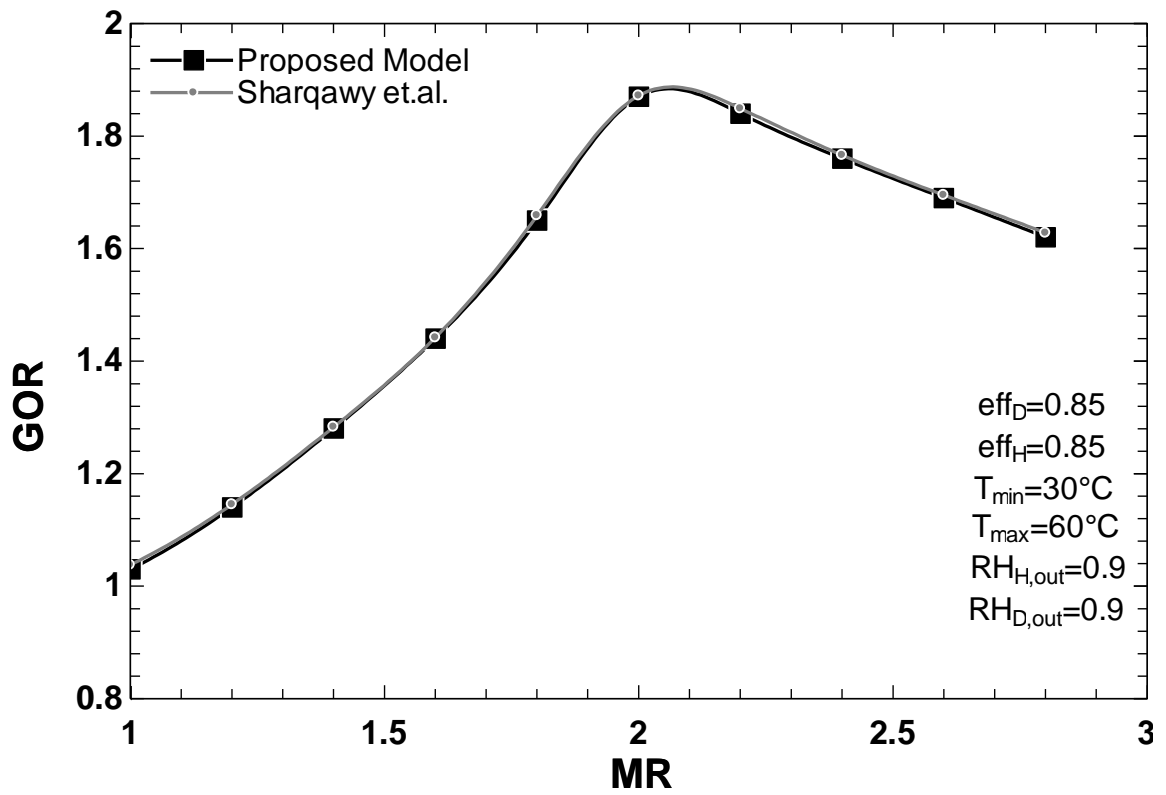


Figure 5: Plot of GOR vs MR for the validation of water heated HDH cycle [26].

Figure 5 shows a comparison of the plots of GOR vs. the mass flow rate ratio (MR) reported by Sharqawy et al. [26] and computed using the proposed model for the HDH system. Both were computed using similar values of the effectiveness of the humidifier and the dehumidifier, the minimum and maximum temperature of the sea water and the relative humidity of air at the inlet and exit of the humidifier.

The lines fit over each other proving the calculations to be exact values, which are expected in the case of similar equations being used under the exact same operational parameters. The GOR is a maximum close to a MR of 2. The GOR increases until the maximum and then gradually decreases as the air flow in comparison to the sea water flow is inadequate to further increase the productivity of the HDH system. The effectiveness values for both the humidifier and the dehumidifier are considered to be 0.85 as proven to be the highest attainable rates in practical situations, and the relative humidity values of 0.9 are also considered to be the operating conditions in the system used in this study.

The evidence for the existence of an optimum mass flow rate ratio for given operating conditions, where GOR is maximized, is shown in the Figure. The optimum mass flow ratio suggests that adequate amount of water is sprayed within the humidifier to humidify the air to its required condition, for a humidifier with an effectiveness of 85%. Excess spray of water would suggest the unnecessary use of heat input to heat additional water, where as a flow too low would suggest almost dry air exiting the humidifier. This

comparison study is further used to optimize the HDH system for the complete system presented in this study.

In summary the results presented in this section indicate that the modeled evacuated tube collector and the HDH system provides accurate and acceptable results. Thus the proposed model is suitable for simulating the operation of a water heated CAOW humidification dehumidification desalination system.

CHAPTER 4

RESULTS & DISCUSSION

The effects of solar radiation, ambient temperature and geographical location on the operational time and the rate of freshwater production by the complete system integrated with thermal storage. Detailed analysis on choosing the best performing collector is also presented. The results are discussed in four sections, divided as follows: (i) a general HDH system that uses evacuated tube collectors as water heater; (ii) the addition of thermal storage and optimization for specified operational hours, (iii) a feasibility study is performed along with a cost analysis, and (iv) comparison study of operating the system at different locations is presented.

4.1 Optimization

The HDH system was optimized by itself so that it can be used with direct solar heating along with a storage option. The seawater temperature at the inlet and the cold water tank in the storage system is assumed to be constant at 25°C. Figure 6 shows a plot of GOR vs. MR calculated using the HDH model to determine the optimum mass flow ratio and the highest expected GOR at temperature of the water at the inlet of the humidifier providing the best performance. Seawater attains its maximum temperature before entering the humidifier and HDH systems are known to operate at low temperatures, which is one of its major advantages. Thus in this study maximum temperature is varied

between 60 and 80°C. Figure 6 indicates that a higher freshwater output may be attained with a maximum temperature of 60°C. The lower maximum temperature is also advantageous in helping reduce scale formation within the heat exchanger or the water heater. The results of specific calculations performed for each point on the 60°C line in the Figure is shown in Table 5. The results in the Table show that a MR of 1.8 provides the highest value of GOR (1.6). This MR value is the optimum value which provides the highest productivity with the least amount of heat input. Thus the MR for seawater and the air within the HDH system was set at 1.8 for all cases discussed in this report.

Table 5: GOR vs. MR calculation for T_{max} 60°C.

MR	Product	T_{max}	m_w	Q	m_{fw}	GOR
1	4	60	0.03892	2.616	0.001111	1.001
1.2	4	60	0.03672	2.301	0.001111	1.138
1.4	4	60	0.03457	1.994	0.001111	1.314
1.6	4	60	0.03248	1.697	0.001111	1.543
1.8	4	60	0.03191	1.635	0.001111	1.602
2	4	60	0.03235	1.723	0.001111	1.52
2.2	4	60	0.0328	1.81	0.001111	1.447
2.4	4	60	0.03326	1.895	0.001111	1.383
2.6	4	60	0.03372	1.978	0.001111	1.325
2.8	4	60	0.03594	2.306	0.001111	1.136

The optimized HDH calculations were then used to determine the number of collectors required to achieve the calculated GOR and productivity of the system. In the system without a storage option, described later in this report, the flow rate of seawater in to the system is adjusted so that the collector outlet temperature is fixed at 60°C. The average available radiation was calculated from the data for Dhahran, Saudi Arabia, which was found to be 1.9 MJ/m². This value was then used as the available radiation to determine the required area of the collector to produce the value of Q shown in Table 5 using equations described in Chapter 3. The equations were used to model the evacuated tube collector to find the area of collector.

Calculations show that two AP-30 collectors are required to produce the required heat input for the system to produce an average of 4 liters of fresh water per hour at the specified GOR and the average solar radiation.

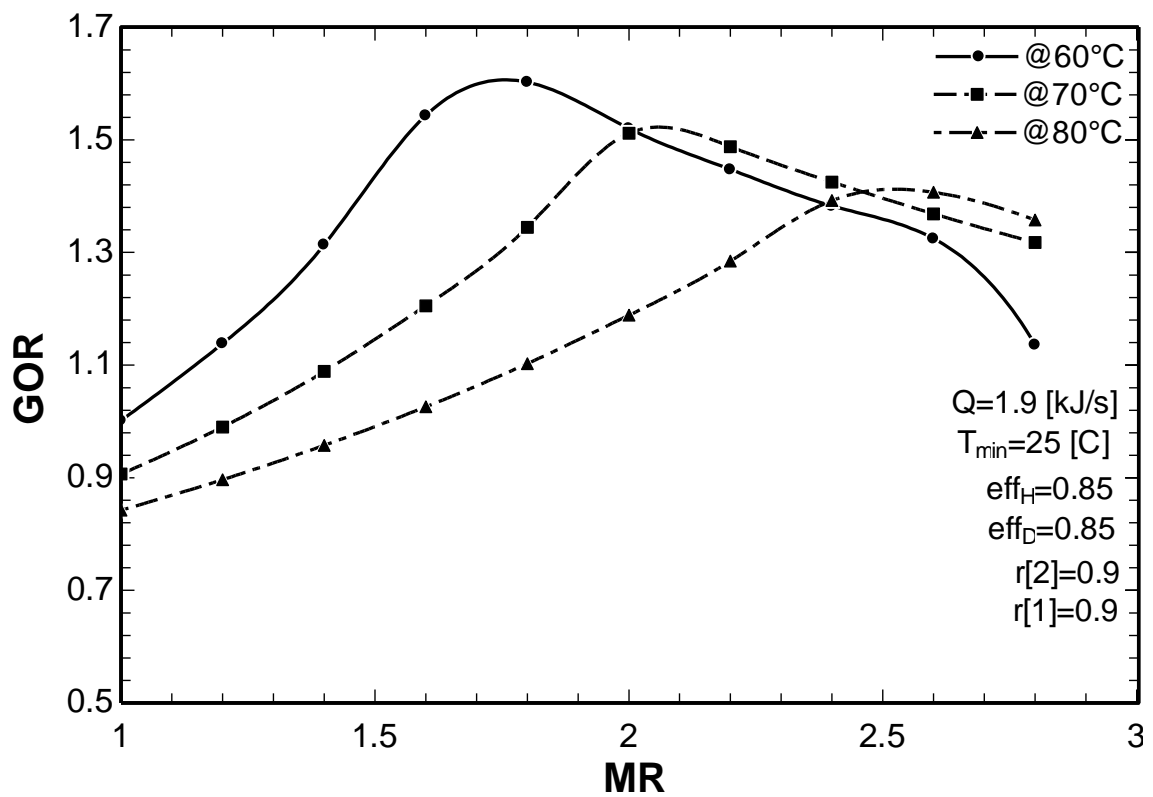


Figure 6: GOR vs. MR Optimization results.

A comparison study shown in Figure 7 the amount of fresh water produced linearly increases with the area of the collector (i.e. the number of tubes in the evacuated tube collector). Six different collector size variations with 10, 20 and 30 tubes and their combinations were used for the calculations.

In the calculations using two collectors, they were connected in series with the required number of total tubes to maintain the required flow rate through the system and to further increase the working fluid temperature. This arrangement allows a higher flow rate through the system which increases the productivity of the system as a whole. The Figure also shows the variation of the performance depending on time of the year for which the calculations are performed. The effects of the four seasons and the variation of irradiation are discussed later in the section of the base case.

The Figure clearly shows that a smaller collector operating under high irradiation is able to produce a similar output to that of a larger collector or combination of collectors under lower irradiation, as expected. For example, a 10 tube collector operating in June is able to produce a similar amount of freshwater to that of a 20 tube collector system operating in December or a 10 and 30 tube collector running in series in December produces a similar output to that of a 20 tube collector operating in June.

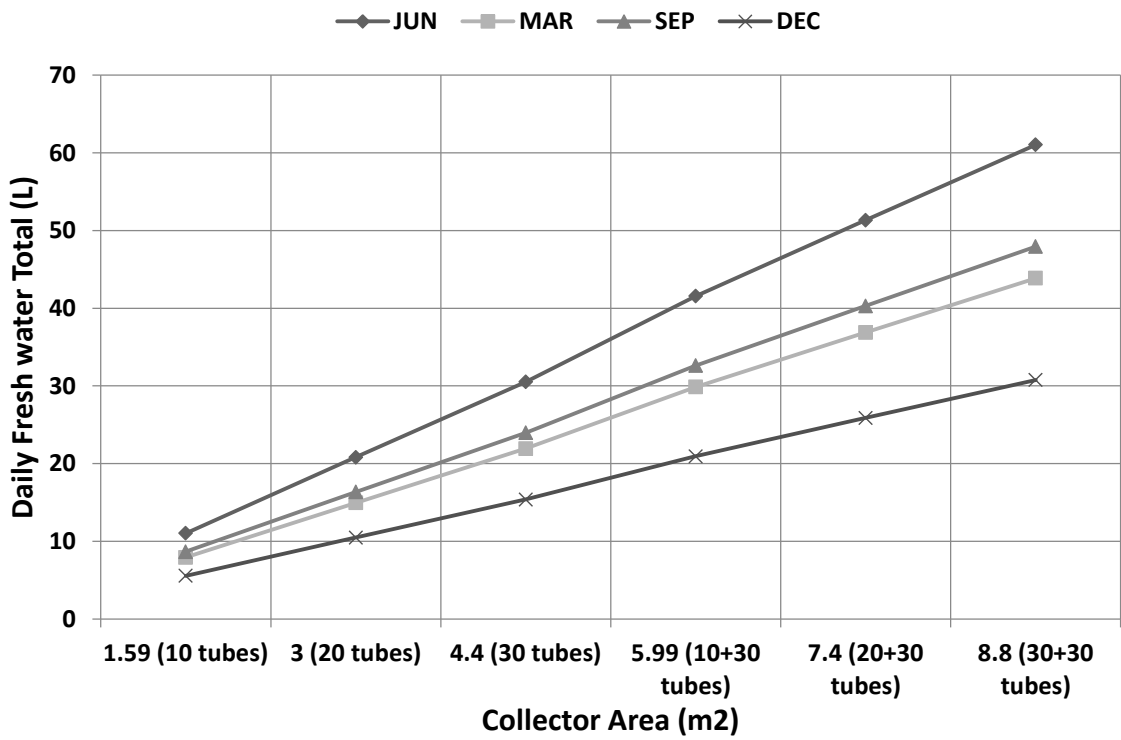


Figure 7: Dependence of the amount of freshwater produced daily on the collector area.

4.2 Base Case

A system where the evacuated tube collectors are used as a water heater for a direct solar HDH system was used as a base case to compare the effects of adding a storage system to conventional Solar HDH system. The configuration of this system is shown in Figure 8.

The Figure presents a water heated HDH system configuration, where the water flows in an open loop and the air flow is in a closed loop, similar to the proposed system configuration with storage, shown earlier in the report. Seawater enters the dehumidifier recovering a part of the energy from the moist air entering the dehumidifier meanwhile condensing it in order to extract the freshwater as droplets. The preheated water is further heated through the use of two Evacuated Tube Solar Collectors, where the heated water is then sprayed within the humidifier system over a series of packing material that helps increase the surface area for effective heat and mass transfer. A part of the water entering the humidifier is carried away with the air stream that has a counter flow, there by humidifying the air leaving the humidifier. The remaining water is extracted from the humidifier as brine.

At the exit of the humidifier the air is assumed to attain saturation. This air then flows into the dehumidifier repeating the process. The standard operating conditions for this system are equivalent to the ones specified earlier in this report. Where the inlet water temperature (25°C, minimum temperature), the maximum water temperature (60°C, collector outlet temperature), the relative humidity of air at the inlet and exit of the humidifier (0.9) and the effectiveness of the humidifier and the dehumidifier (0.85) unless specified in the Figure.

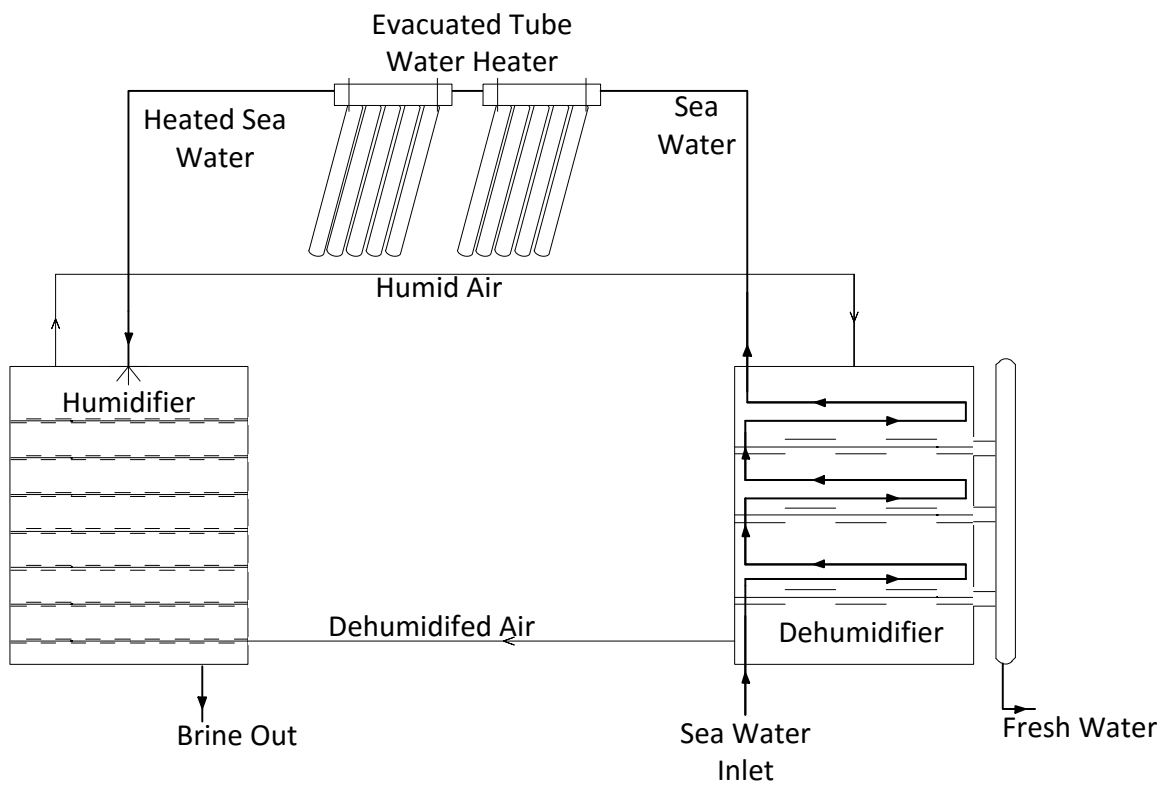


Figure 8: Base case system configuration.

4.2.1 Base Case Results

The main drawback of a Solar HDH system as discussed previously is the dependence on day light hours as discussed in the literature review. In this case, depending on the choice of location (Dhahran, Saudi Arabia) the number of hours chosen were 8am to 3pm, this was in order to maintain a constant number of operating hours, although some months of the year may have longer hours of sunlight. This allows the better analysis of the effects of other parameters such as the intensity of the sunlight and the ambient temperature. Figure 9 shows the results obtained from the combined system model consisting of the HDH system and the evacuated tube collectors used as a water heater. The four months chosen represent the four seasons of the year, where the weather conditions drastically differ. It should be noted that in case if the sea water inlet temperature or the systems T_{\min} was considered to vary accordingly for each of the months the difference in this temperature may well affect the production of freshwater. For example if in December the minimum water temperature was to reach around 15°C this would improve the condensation process within the dehumidifier, thereby improving the productivity of the system drastically.

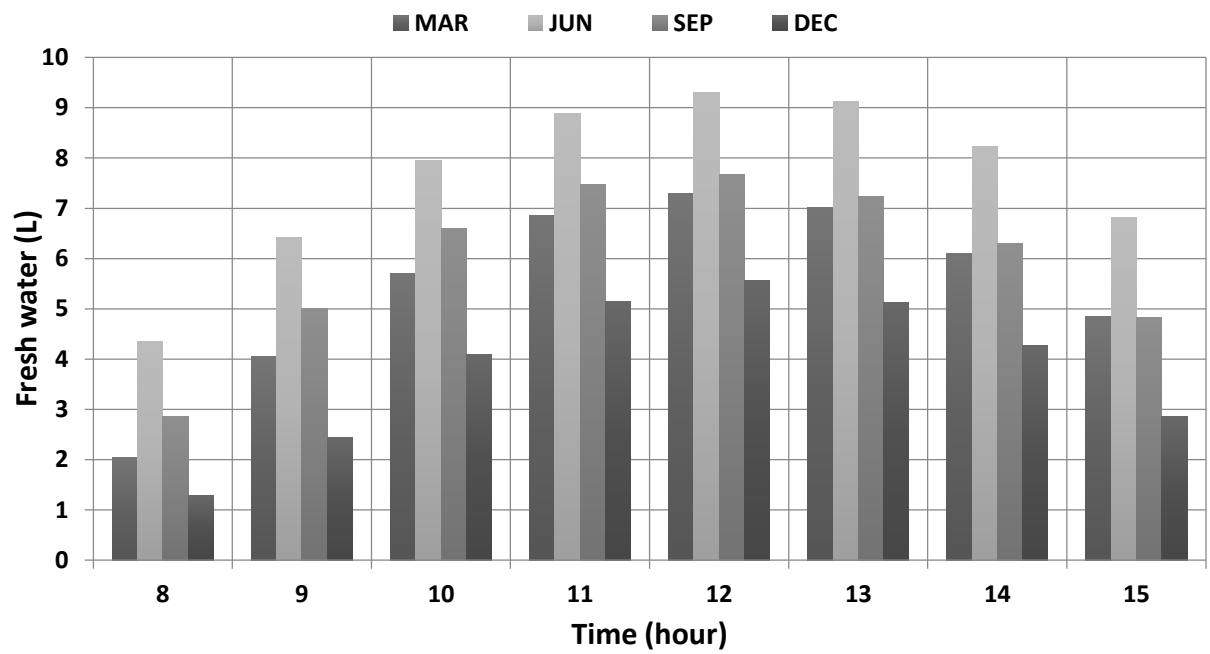


Figure 9: Fresh water Product vs. Time of Day.

The main parameters affecting the productivity would be the solar radiation and the ambient temperature, which may vary considerably through the span of a year. June is expected to have the highest radiation values as well as the ambient temperature, for all locations situated north of the equator. As it is in the summer time in this region, the highest values for irradiation and ambient temperatures are expected. March and September were selected to represent the seasons of autumn and winter, which have lower radiation levels and ambient temperatures. The lowest radiation levels and ambient temperatures are expected in winter and the month December was chosen for this season. Thus all the four seasons of a year are considered to measure the effect of weather on the system and its performance. The variation in the productivity of freshwater in the selected months closely followed the variation in the irradiation and ambient temperature values. As expected the month of June has the highest output of fresh water production followed by September and March with the lowest productivity in December. The effect of the time of day on the productivity is also shown in Figure 9, where the intensity of irradiation and the ambient temperatures gradually increase from morning until mid-day.

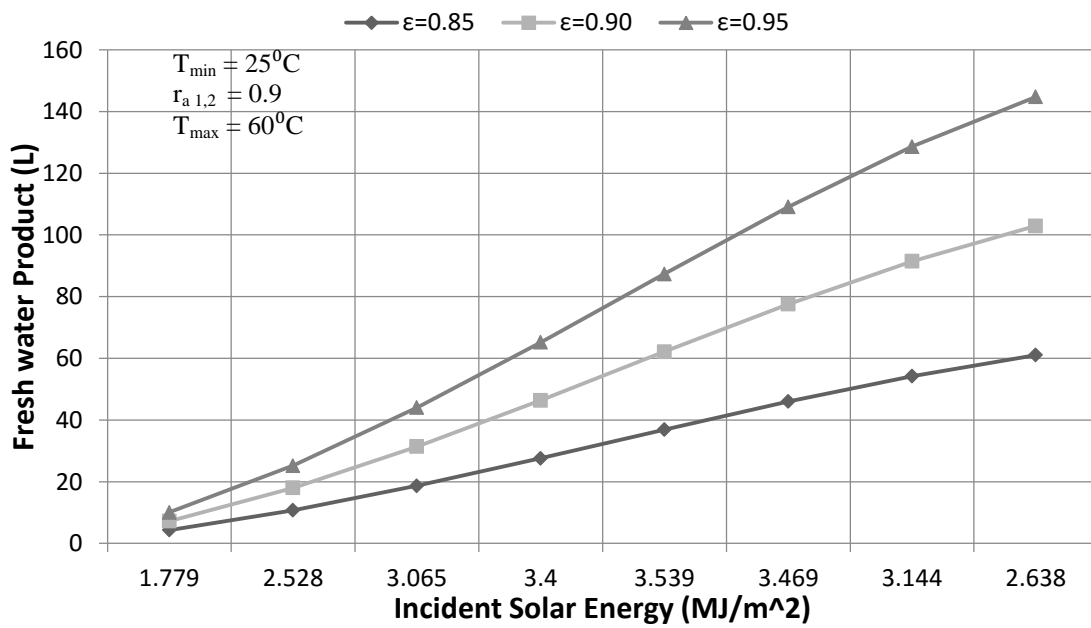


Figure 10: Accumulated Total Freshwater product vs. Incident Solar Radiation (June).

Figure 10 shows the operation of the system for the month of June indicating the accumulated freshwater output at each hour and the incident solar radiation at each hour. As the incident radiation level is directly related to the time of day, the first point at 8am and the last point at 3pm have considerably lower radiation levels, as compared to the radiation level of 3.539 MJ/m^2 at 12pm midday. The calculations assume similar operating conditions as mentioned earlier in this report except for the effectiveness of the humidifier and the dehumidifier. Increased productivity around midday is signaled by the increased slope of the line from the second data point onwards which decreases around the 7th data point. Figure 10 shows that the productivity doubles when the effectiveness is increased from 0.85 to 0.95. However such effectiveness is purely theoretical and is yet to be achieved practically. None-the less it proves that an increase of the effectiveness significantly increases fresh water production. Although such effectiveness may be achieved by using larger humidifiers and dehumidifiers with greater packing heights, cross sectional area etc., it is deemed impractical due to the exponential increase in the required capital investment, which cannot be justified by the significant increase in productivity. Two separate units would be cheaper to construct and will produce equal or more freshwater with a seemingly lower capital cost.

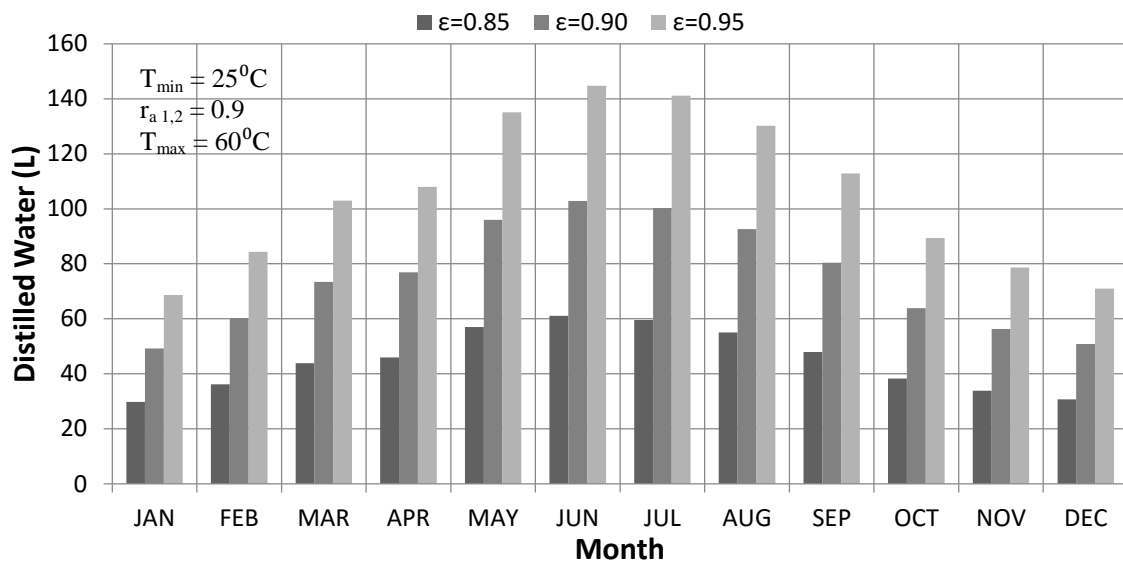


Figure 11: Daily Averaged Productivity for each month of the year.

The daily average amount of freshwater produced is represented by a bell shaped curve with respect to the month of the year, shown in Figure 11. Expected radiation values are lower towards the beginning and end of the year, where the day is quite short and the number of daylight hours is considerably lower in comparison towards the middle of the year. June is shown to have the highest recorded irradiation values, where the highest productivity is shown as well. It should be noted that the seawater inlet temperature is assumed to be a constant at 25°C, where the cold water effects are not considered. The daily averaged productivity follows the trend of the weather, where longer days are reported in summer and relatively shorter days in winter spring and autumn.

As expected the dependence of the daily averaged GOR on the month of the year shown in Figure 12 follows a similar trend. The gained output ratio is computed as an average per day on each average day of every month.

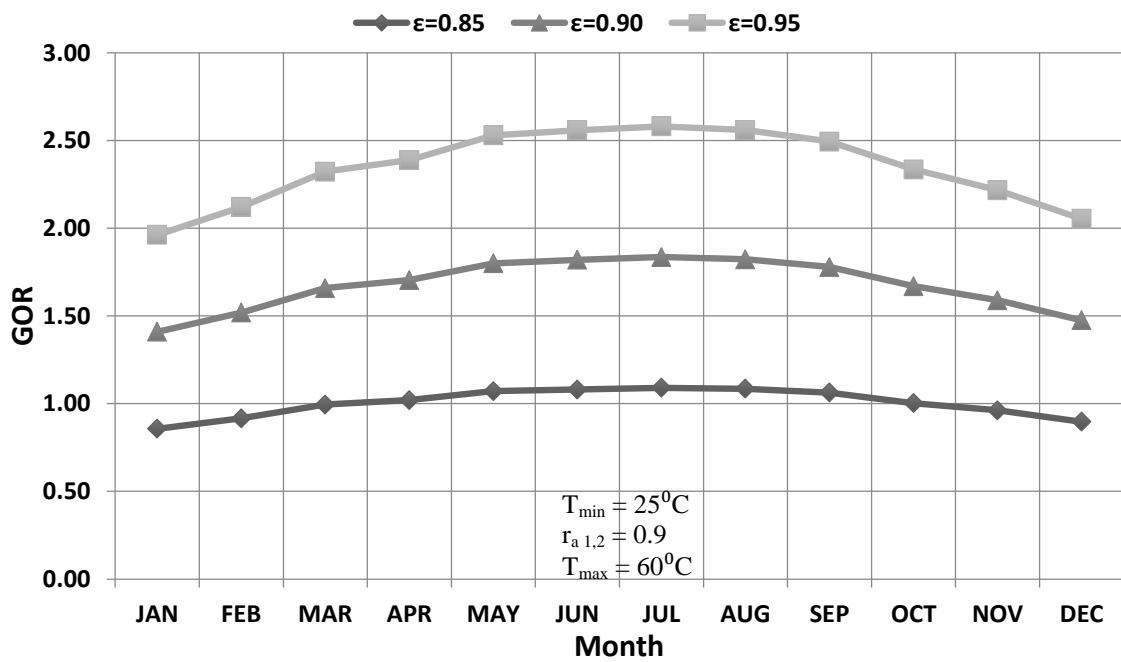


Figure 12: Daily Averaged GOR of every month.

4.3 Complete System with Thermal Storage

The schematic for the combined system with thermal storage is shown in Figure 1. The storage fluid considered within this study is water mainly due to its high thermal capacity and availability. It also reduces costs incurred to the system as a freely available source. The system description was presented earlier in this report under the proposed design. A standard storage capacity in common practice is (75L/m² collectors area), which is also used in this study, to calculate the size of storage required (660L/175 US gallons). The closest fitting tank by size, along with a built in heat exchanger is available by Apricus themselves, the added advantage of choosing the same manufacturer for the collectors and the storage tank is the cost reduction due package availabilities which drive down the total system cost, this will be further discussed under the cost analysis section in this report. It is also important to note that the number of collector or the collector size has not been altered. There by the collectors used in the base case and the complete system with thermal storage is the same.

The main objectives of the storage system are to attain continuous operation, constant productivity, greater productivity, possibly lower cost of freshwater etc. The main parameter that decides the operating hours for this system is found to be the flow rate of the storage fluid to and from the tank. A higher flow rate would add more heat with a shorter time but also remove heat equally as fast. It should be noted that the flow rate across the storage tank is assumed to be fixed in this study. The operating condition for the HDH system were that the system checks the hot storage tank temperature and if it is

above 60°C the HDH system is operational, where it would start the water flow pump and the blowers within the HDH system. This in turn also allows the tank start temperature to be fixed at 60°C as the system stop all flow there by rendering no heat losses except for standby heat losses from the tank. The tank specification shows that it has a thermal resistance of R16. It is possible to calculate the tank-area loss coefficient using this variable.

Furthermore, to check if the HDH system was required to be modified, a water flux condition mentioned by Sharqawy et.al [26] was used. This condition is used to find the humidifier cross-sectional area (CSA), where the water flux that is to flow over the packing material is assumed to have a value varying between 0.8-4.2 kg/s m². The higher value stands as the maximum possible where the lower value presents the minimum value. An average design value assumed for the water flux is 1.5 kg/s m². The relationship is given by the equation below:

$$Water\ Flux = \frac{Mass\ flow\ rate\ of\ water}{Cross-sectional\ Area} \quad (4.1)$$

The averaged mass flow rate of seawater in the base case was found to be 0.045 kg/s suggesting that a humidifier with a cross-sectional area of 0.03 m² is required. The maximum flow rate reached was on mid-day of June where the flow rate was found to be 0.075 kg/s. This flow rate was used as the maximum attainable flow for the storage equipped system there by providing a cross-sectional area (CSA) reduced to 0.018 m². Therefore it is evident that the storage combined system may use smaller humidifiers and

dehumidifiers. The smaller humidifier CSA was then used to calculate maximum, minimum flow rates for the storage tank as well as the ideal flow rate, a further calculation was done to maintain the average flow found from the base case. The minimum flow rate in the study was limited to the flow rate required to maintain 24 hour operation. The flow rate of the tank was calculated by finding the required heat input for the HDH system in order to maintain a seawater inlet flow rate of the values calculated.

Thereby four different cases were considered as follows:

- 24 hour operation – related to the minimum flow rate (0.024 [kg/s])
- Ideal Flow rate – 1.5 water flux (0.027 [kg/s])
- Average flow – average flow rate from the base case (0.045 [kg/s])
- Max flow rate – 4.2 water flux (0.075 [kg/s])

Simulations were carried out all throughout the year for the average day of each month, for each of the above mentioned cases. They were further used to calculate the product output, GOR hourly and daily averaged values and also to compute the number of operating hours with the production rate for each hour. As mentioned earlier in the report, the system with thermal storage is expected to have a constant production rate due to constant heat addition. Each of the cases was compared with the performance in mainly 4 months of the year as explained in the previous section of the report, where the change in weather and solar radiation was significant.

The freshwater production as mentioned previously is expected to be constant but the amount of water produced will change depending on the heat input from the thermal storage tank. Each case studied has a different freshwater output for each operating hour. However, this does not change with change in radiation or ambient temperature

significantly. It is although evident that the starting and ending hour of operation changes depending on the time of year. This is shown in Figures 13 through 16 which represent the four seasons of the year. The x-axis of these Figures shows the hour number starting from hour zero moving on until hour 24. Each case studied presents a different number of hours of operation. The productivity is clearly constant at operating hours. The variables affecting the number of hours of operation are mainly the storage tanks flow rate (heat input and output), available solar radiation and the HDH systems sea water flow rate which is controlled by the amount of heat added via the storage tank. The numbers of hours of operation, in the four months extracted from the Figures are shown in Table 6 along with the amount of water produced at each hour and the total productivity on an average day of each of the months.

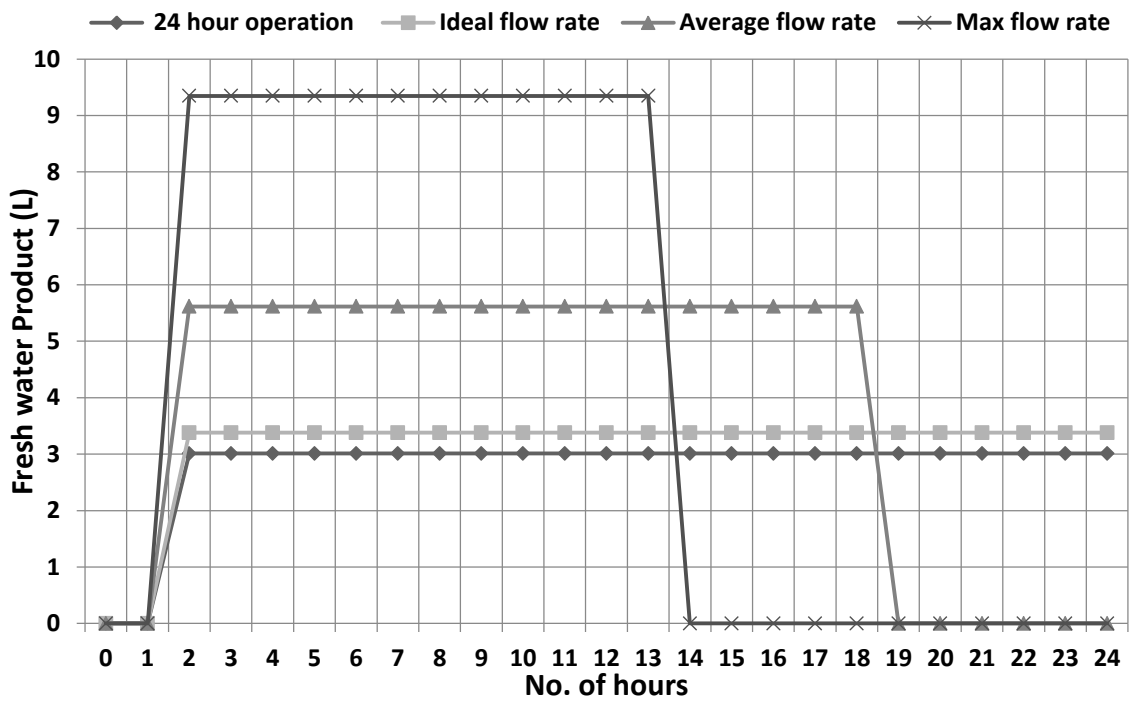


Figure 13: Freshwater Product vs. No. of Hours (March).

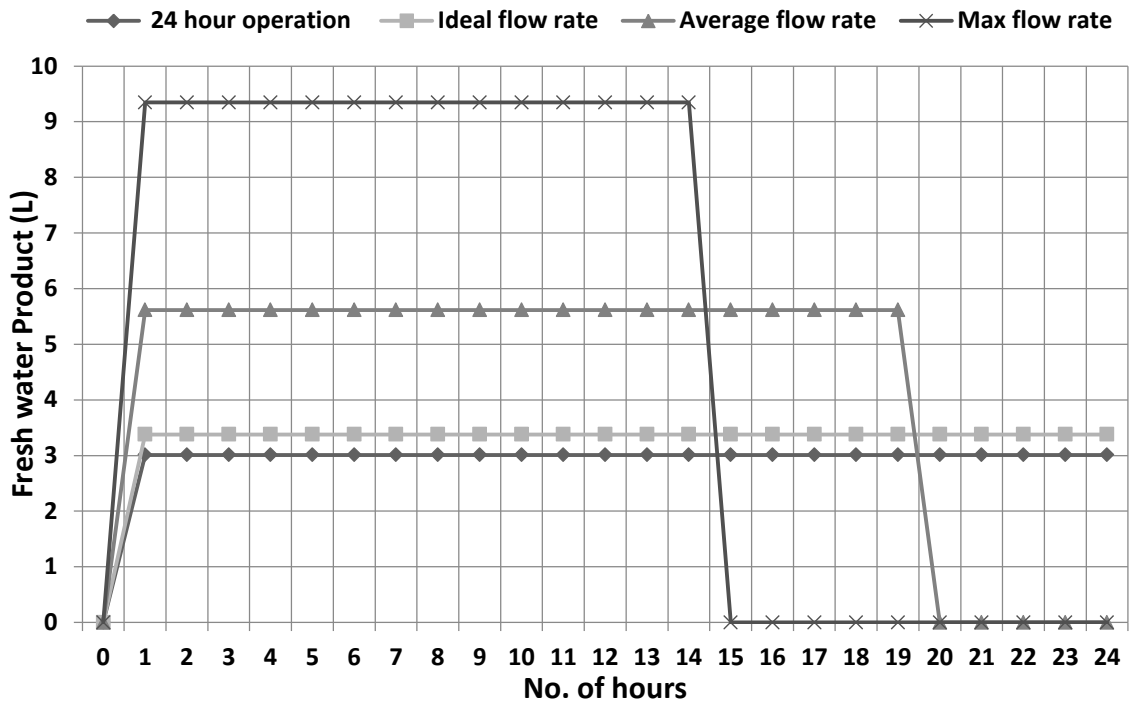


Figure 14: Freshwater Product vs. No. of Hours (June).

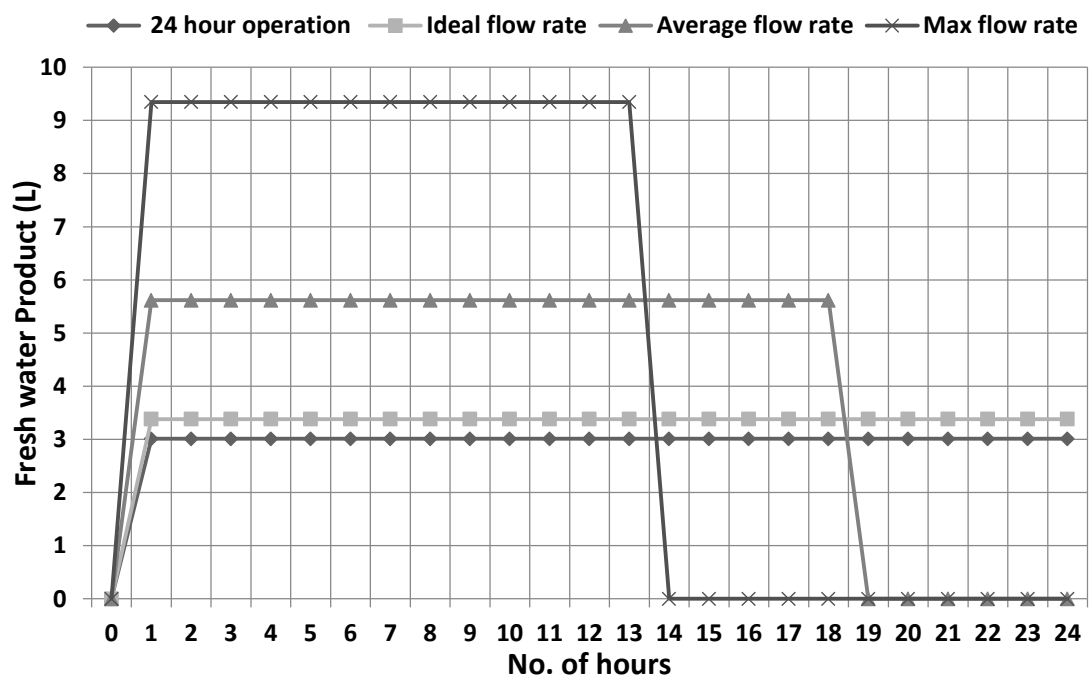


Figure 15: Freshwater Product vs. No. of Hours (September).

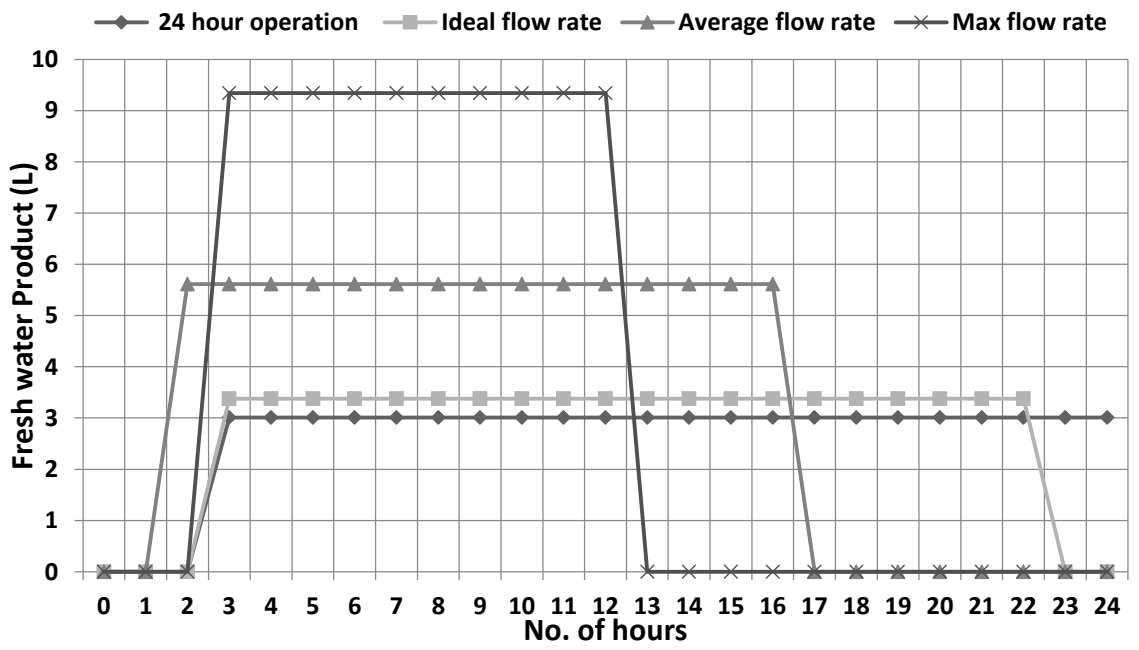


Figure 16: Freshwater Product vs. No. of Hours (December).

Table 6: Productivity and Operational Hours for four storage cases.

Case	Fresh water (liters per hour)				No. of operating hours				Total fresh water productivity per day			
	Mar	Jun	Sep	Dec	Mar	Jun	Sep	Dec	Mar	Jun	Sep	Dec
24 hour	3.0	3.0	3.0	3.0	23	24	24	22	69.2	72.2	72.2	66.2
Ideal Flow	3.4	3.4	3.4	3.4	23	24	24	20	77.7	81.1	81.1	67.6
Average Flow	5.6	5.6	5.6	5.6	17	19	18	15	95.5	106.7	101.1	84.2
Maximum Flow	9.3	9.3	9.3	9.3	12	14	13	10	112.2	130.8	121.5	93.5

The total averaged useful heat energy gained with each case on the average day of the month of the year is shown in Figure 17. With high flow rates within the collector and tank loop it is evident that more energy is gathered and stored. This change is significantly greater in high intensity irradiation months where the change is considerably smaller in months with lower solar radiation. This provides reason as to why having a higher flow rate within the storage tank loop increases the freshwater productivity considerably, since more energy is stored and also released at any given operating time. The useful heat collected is a maximum in June in all cases, where the highest value is reported through the case where the maximum flow is in operation. The recorded value for the total heat gained for the average day in June was 94MJ. Similarly due to reasons discussed previously the lowest useful heat total was recorded in December for all cases where the minimum value was at 33MJ where this value was almost constant in all cases considered. The change in the collected energy varies accordingly with the 4 seasons and the variation of available solar radiation.

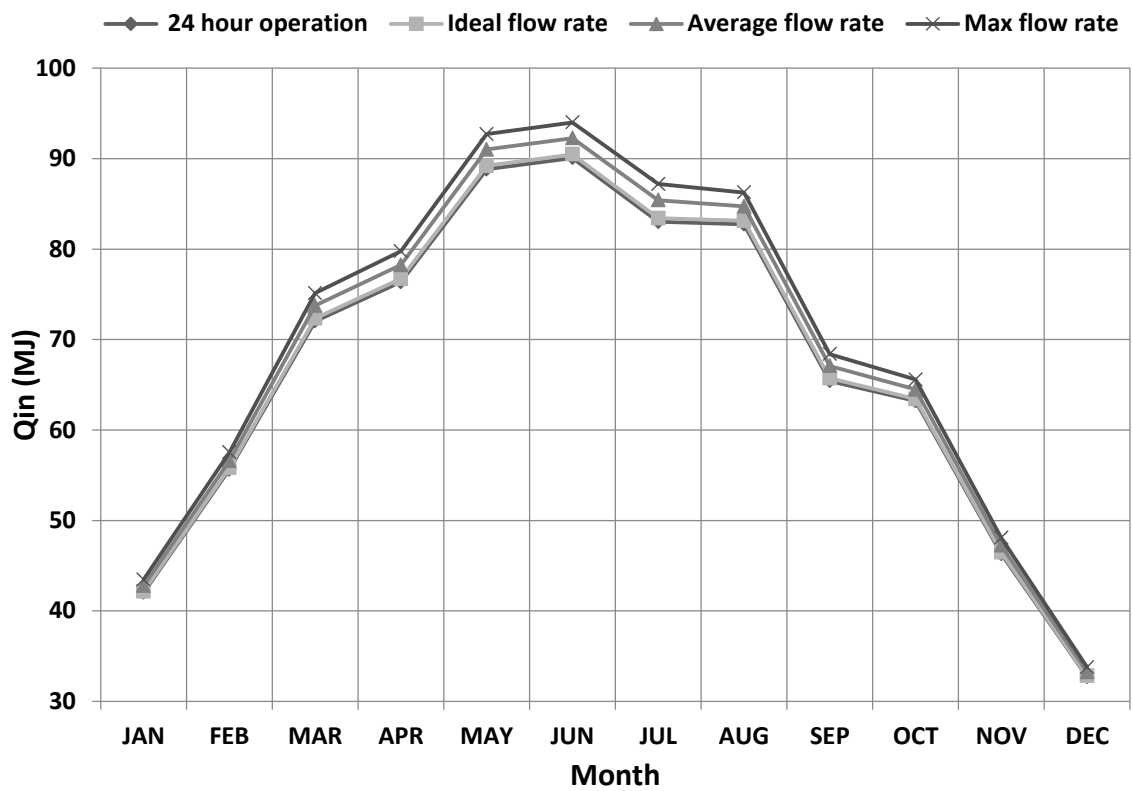


Figure 17: Total useful energy collected for the averaged day of each month.

The variance of tank temperature in each of these cases was also studied. Additionally this was also carried out for the four seasonal months, as shown in Figures 18 through 21. The curves in these Figures show that the temperature change is non-linear and has a bell shape as expected. The tank temperature starts at 333°K and gradually increases as heat is added until the added heat is either equal to or less than the heat removed from the tank. The highest temperature gradients are shown in the summer month and then March and September followed by the lowest in December as previously discussed in this report, due to solar radiation changes. The lower flow rates reach higher temperatures as heat removal is slower and higher flow rates reach lower temperatures as heat removal is faster. This is also due to the change in heat addition being comparatively smaller when compared to the change in heat removal. The maximum tank temperature (356.7°K) is reached in June in the case of the lowest sea water flow rate in the 24 hour operational system due to reasons previously conferred. The maximum temperatures for March, September and December were, 353.2°K, 351.5°K and 344.1°K respectively, where all recorded temperatures were from the same 24 hour operational case.

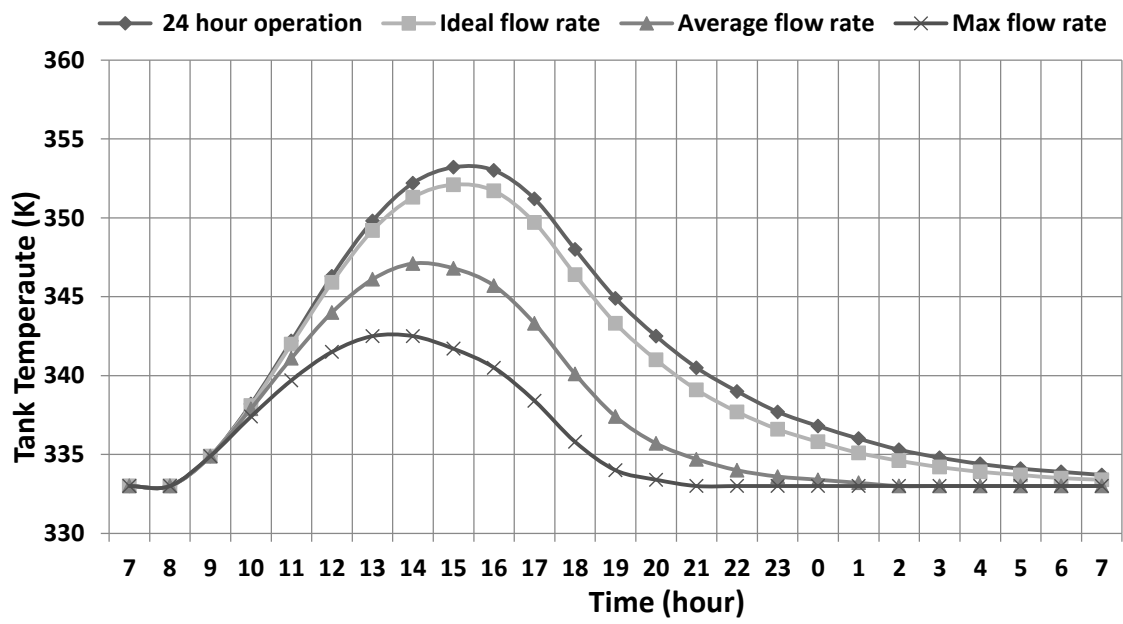


Figure 18: Tank temperature variation within 24 hours (March).

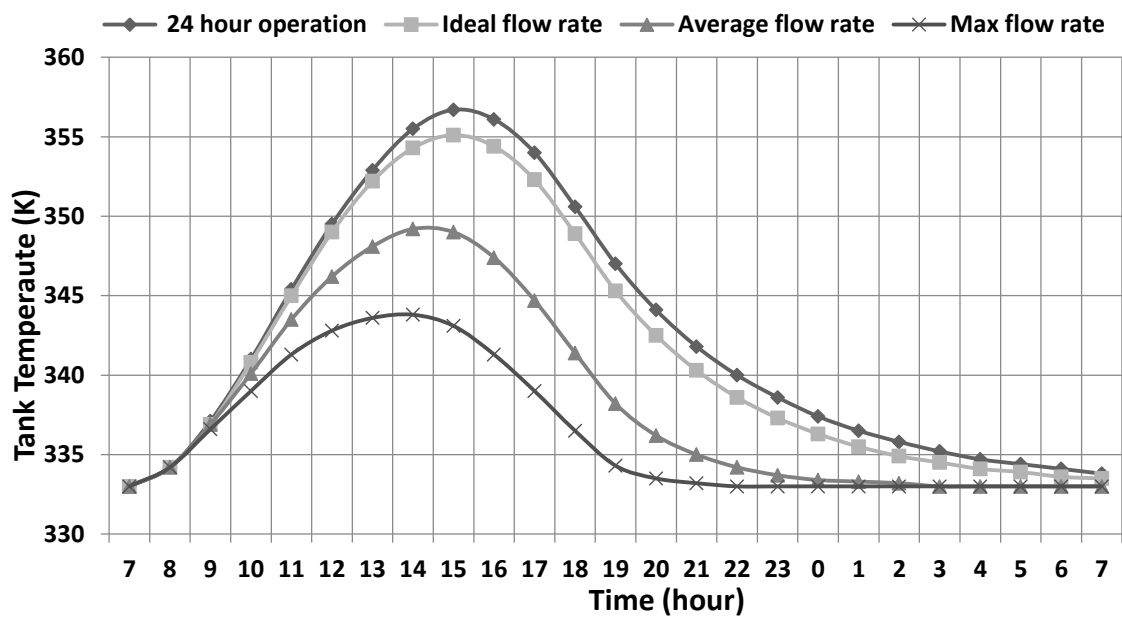


Figure 19: Tank temperature variation within 24 hours (June).

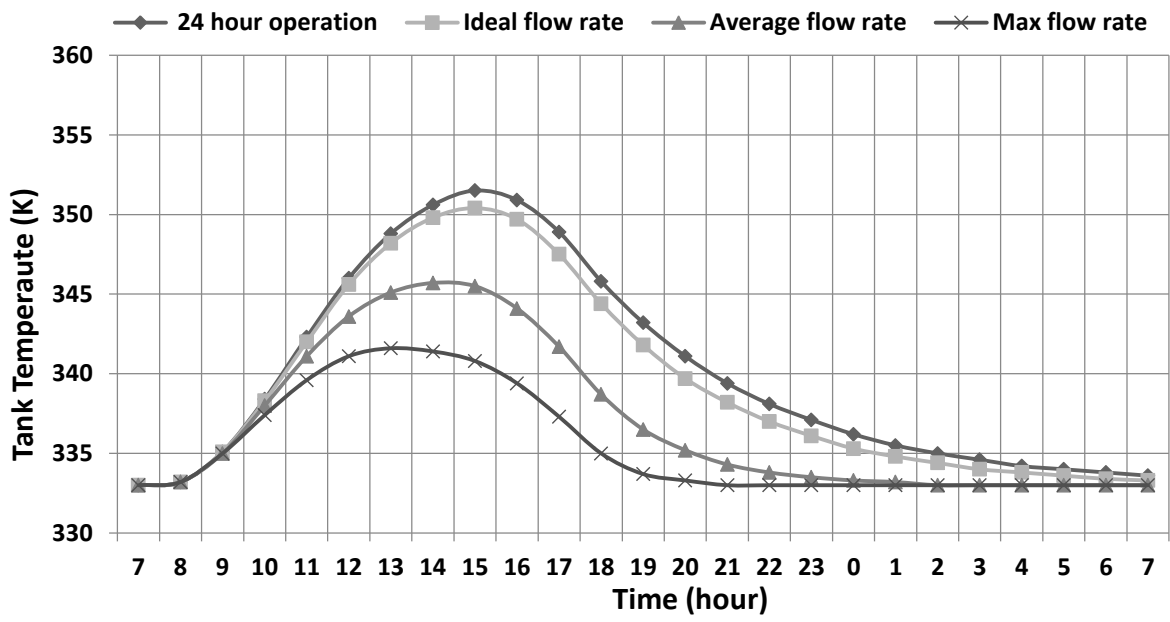


Figure 20: Tank temperature variation within 24 hours (September).

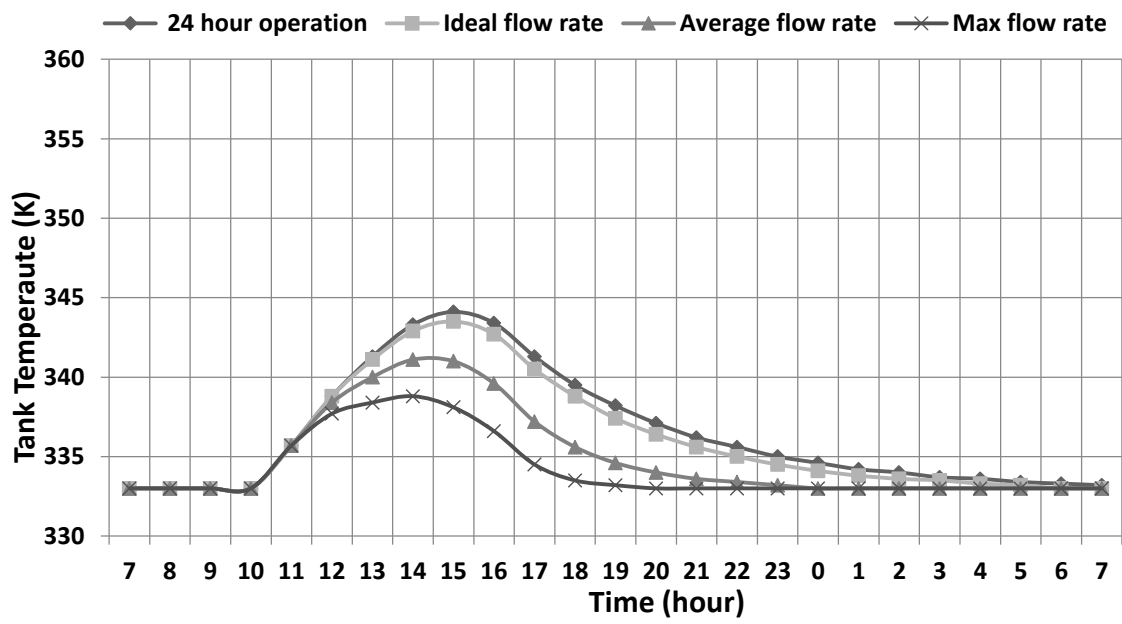


Figure 21: Tank temperature variation within 24 hours (December).

The gained output ratio is expected to be a constant in all cases and be a value closer to that of the calculation carried out under optimization. This GOR was 1.6 a value close to it (1.596) is achieved in all cases studied under the storage system. The constant GOR is due to the constant heat addition via the storage tank and the HDH systems heat recovery process discussed earlier within this report. The heating process is only required to heat the seawater exiting the dehumidifier at about 325°K to 333°C before it flows into the humidifier. This requires less energy in comparison to varying temperatures faced in the Base Case due to significantly varying flow rates. This also gives reason as to why a smaller HDH system with a thermal storage option is able to produce more freshwater as compared to the base case as shown in the section under productivity vs. number of operating hours. GOR reaches zero when the tank reaches 333°K since the HDH system component of the system is shutdown. This also provides a clear view of the operating hours for each case discussed, where the data is presented for the main 4 months reported throughout this study, shown in Figures 22 through 25. The longest operating hours simulated were 24 hours where the shortest was around 12 hours for the cases discussed. The reported hours of operations were from the minimum and maximum flow cases respectively.

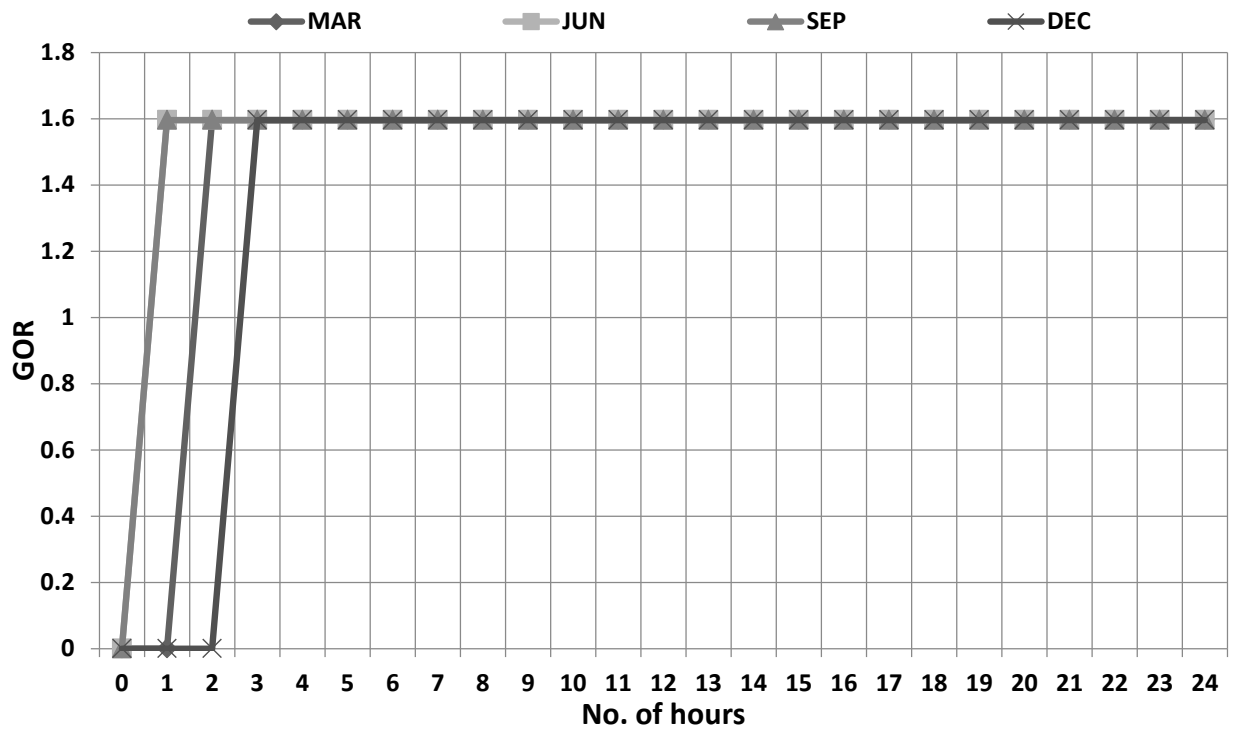


Figure 22: GOR vs. Hour of operation (24 hour case).

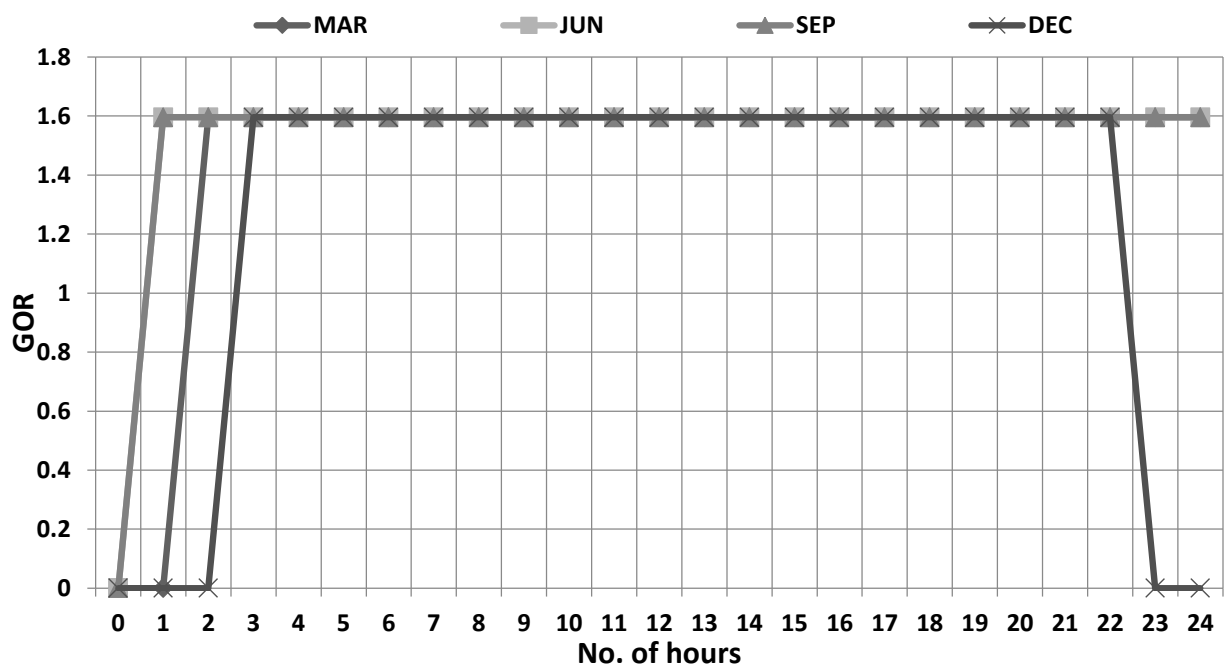


Figure 23: GOR vs. Hour of operation (Ideal flow case).

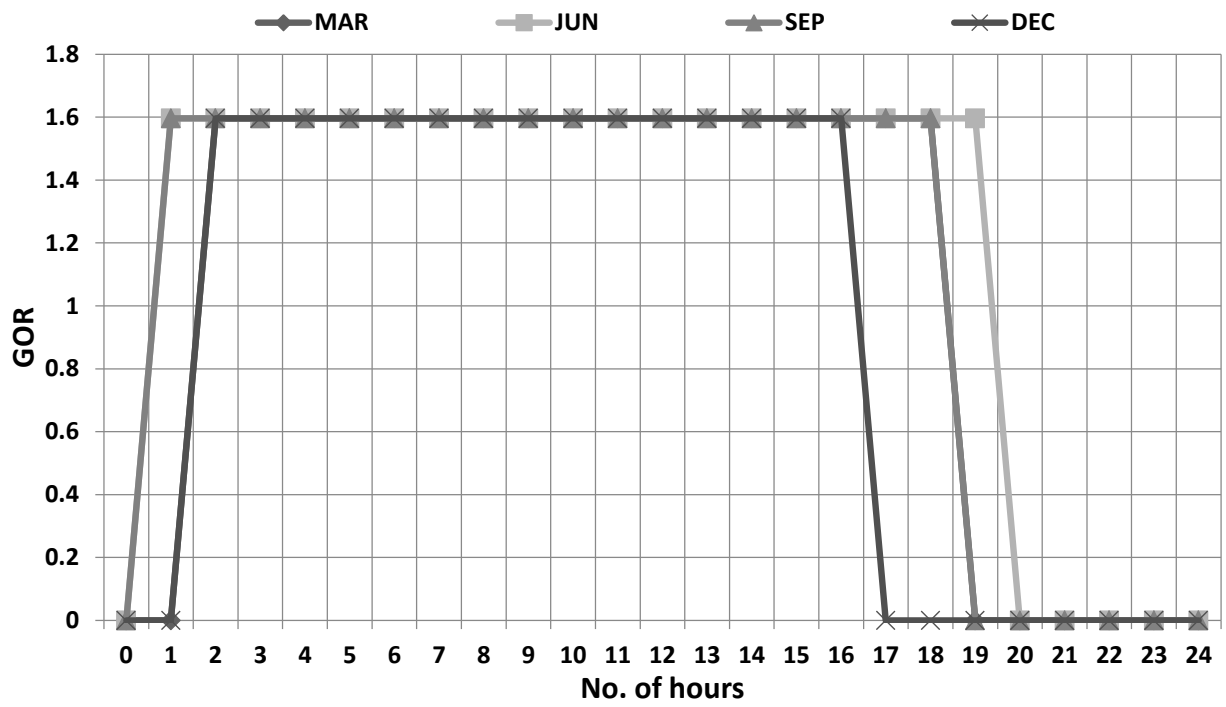


Figure 24: GOR vs. Hour of operation (Average flow case).

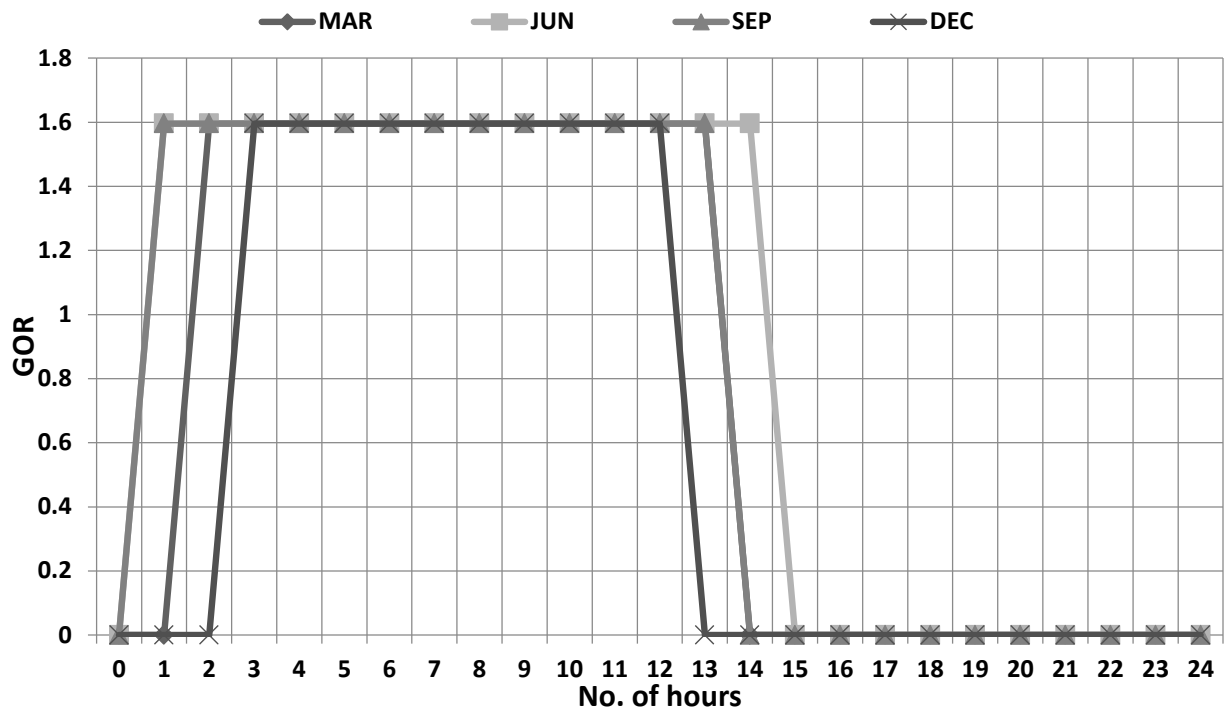


Figure 25: GOR vs. Hour of operation (maximum flow case).

4.4 Cost Analysis

The main objective of the cost analysis for the proposed system was to study the feasibility of the system in terms of the capital cost and the cost of water produced. The capital cost of a typical desalination plant includes items such as the cost of land, supply well, equipment costs such as piping, tanks, pumps etc. and building costs if indoor space is required. The costs may also include shipping, construction, services etc.

Considering the current system, land costs may be ignored assuming outdoor location and operating in a rural deserted area. The main costs to be considered would be the equipment costs. As the required technical knowhow in setting up a small plant according to the proposed design is low, no additional service or construction costs have to be incurred. This system is also expected to have no operational costs or maintenance requirements and the electricity consumption is negligible, which may be acquired without running costs, through photovoltaic technology. Thus running costs are not expected either, and only the capital cost would be of significance. This system may also be assumed to be operational for 20 years without maintenance. Therefore, the cost of freshwater produced may be calculated via the equation shown below:

$$\frac{\text{Total Capital Cost}}{\text{Annual Freshwater Produced} \times \text{System Lifetime}} = \text{cost of freshwater} \left(\frac{\$}{\text{liter}} \right) \quad (4.2)$$

The results obtained for each of these cases studied under the proposed design is shown in Table 7. The list of capital costs incurred is shown in Table 8. it should be noted that the cost of purchasing a packaged solar system with a storage tank is around \$4,000 cheaper than if each component was purchased individually.

Table 7: Cost per liter of water produced.

Case		Annual Output	Capital Cost		Cost per liter	Cost per m ³
Max flow rate	=	42,356	\$12,539.00	=	\$0.015	\$15
Average flow rate	=	35,375		=	\$0.018	\$18
Ideal flow rate	=	28,567		=	\$0.022	\$22
24 hour operation	=	25,730		=	\$0.024	\$24

Table 8: List of costs incurred.

Item	Unit Price	Quantity	Price
2xAP-30 + SOLX-120 Packaged system	\$8,461.00	1	\$8,461.00
AP-30 Mid-Angle Frame	\$219.00	2	\$438.00
Ducts	\$700.00	1	\$700.00
2 tanks	\$475.00	2	\$950.00
Packing	\$750.00	1	\$750.00
Dehumidifier	\$500.00	1	\$500.00
2 Blowers	\$250.00	2	\$500.00
Additional Pump	\$240.00	1	\$240.00
Total			\$12,539.00

Considering the cost of freshwater produced in cubic meters in comparison to the prices of freshwater in Saudi Arabia the cost of water is quite high. However, when cost of transporting water is considered to rural areas, or off grid system in decentralized areas the cost of water increases considerably as a result of transportation costs. Considering the proposed system being designed for such areas, the cost of water of water may still be justified. The cost of collectors and the storage tank as a packaged system with a heat

exchanger may seem quite expensive on first glance but, this cost may also be reasonable when considering the quality and performance of the products provided by Apricus which allowed a recommended system life 20 years without major maintenance requirements and operational costs. Cheaper collector systems may be considered in hopes of reducing the cost of fresh water but, the system life and performance may well be affected proving it unfeasible. The use of cheaper collector system may well also result in the need for operational costs and regular maintenance of the system which would deem problematic in rural areas where a technician's presence would be required.

4.5 Multiple Location Analysis

Further studying the performance and feasibility of the model presented, multiple locations in Saudi Arabia were selected in order to analyze the effects on the system, specifically on the system operational time and the total freshwater output. The main parameters that affect the system are expected to be the solar radiation intensity, the ambient temperature and the latitude of each location. It should be noted that the seawater inlet temperature is still presumed to be constant at 25°C as are all other system parameters such as the humidifier and dehumidifier effectiveness, and the relative humidity of air at the inlet and the exit of the humidifier. The four cases studied under the previous section are used to study the effects of various locations. As a first step the useful heat gained (Q_{in}) via the evacuated tube collectors is studied depending on six different locations. Each location corresponds to a certain region of Saudi Arabia. The chosen locations were as follows:

- Central Region – King Abdullah City for Atomic and Renewable Energy (KACARE)
Riyadh, Qassim
- Western Central Region – King Abdulaziz University (KAU) **Jeddah**
- Eastern Region – King Fahd University of Petroleum and Minerals (KFUPM) **Dhahran**
- Southern Region – **Sharurah**
- Western Internal Region – **Tabuk**

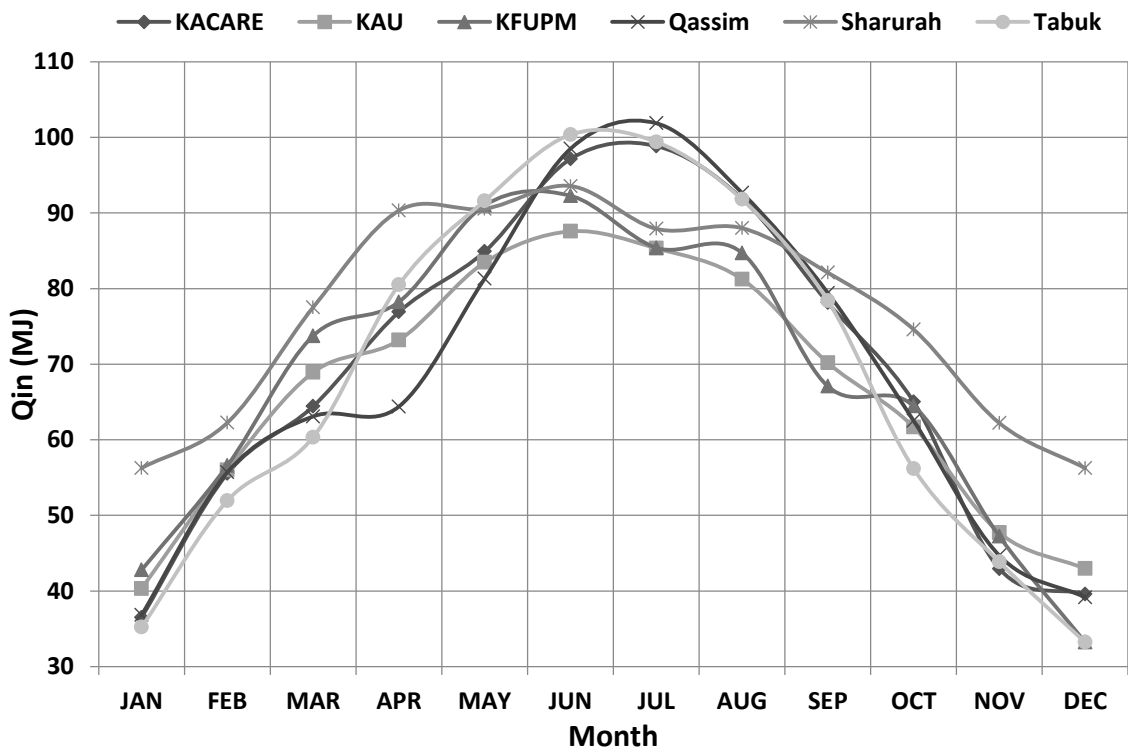


Figure 26: Heat input throughout the year at multiple locations.

Figure 26 shows the heat inputs to the system for each location. The graph only presents the results for the average flow case. This is in order to reduce redundancy since it was concluded previously in the report that the variation of the heat input amongst each of the four cases remains within a tolerance of 5 MJ. The average flow was chosen as its line in the comparative Figure lay centrally compared to all other cases. The Figure shows at first glance that the variations in solar radiation for each city changes significantly every month.

Taking the total radiation into account KACARE has the highest irradiation level in comparison to all other locations, followed by KFUPM and Sharurah being quite close to each other in terms of solar radiation levels. It is evident from the Figure that during colder months such as JAN through MAR and OCT through DEC, where the variations are considerably smaller in comparison to warmer months when the changes are significantly larger. The months of June, July and August show that Qassim, Tabuk and KACARE have significantly higher radiation in comparison to other locations. Sharurah notably has considerably higher radiation values during the colder months mentioned before, where Tabuk is shown to have the lowest during the same period of time.

The largest visible variance is shown in April where Sharurah and Qassim have the maximum and minimum heat gained values. It should be noted that the heat gained is directly proportional to the solar radiation availability since the system being tested only uses solar energy as a heat source. Therefore a high heat input value would generally suggest a relatively high solar radiation value. It should also be considered that the data

used in this comparison were monthly averaged data for the year 2014. Various weather conditions may also affect the readings in turn affecting the irradiation data. Therefore some of the effects shown in the Figure may well be due to significant changes in weather during certain months at given locations (for example, cloudy skies, rainy weather, dust storms etc.). This Figure can also be used as a reference to compare the operational hours of the systems as well as the total freshwater output. A higher heat input would suggest a relatively higher total freshwater output, a longer operational time as well as a higher storage tank temperature.

Table 9: Operating hours and daily total fresh water product (KACARE).

Month	Fresh water (liters per hour)				No. of operating hours				Total fresh water productivity per day			
	24 hour	Ideal Flow	Average Flow	Maximum Flow	24 hour	Ideal Flow	Average Flow	Maximum Flow	24 hour	Ideal Flow	Average Flow	Maximum Flow
JAN	3.0	3.4	5.6	9.3	23	22	15	11	69.2	74.3	84.2	102.8
FEB	3.0	3.4	5.6	9.3	23	23	16	11	69.2	77.7	89.9	102.8
MAR	3.0	3.4	5.6	9.3	24	24	17	13	72.2	81.1	95.5	121.5
APR	3.0	3.4	5.6	9.3	24	24	18	13	72.2	81.1	101.1	121.5
MAY	3.0	3.4	5.6	9.3	24	24	18	13	72.2	81.1	101.1	121.5
JUN	3.0	3.4	5.6	9.3	24	24	19	14	72.2	81.1	106.7	130.8
JUL	3.0	3.4	5.6	9.3	24	24	19	14	72.2	81.1	106.7	130.8
AUG	3.0	3.4	5.6	9.3	24	24	18	14	72.2	81.1	101.1	130.8
SEP	3.0	3.4	5.6	9.3	24	24	18	13	72.2	81.1	101.1	121.5
OCT	3.0	3.4	5.6	9.3	24	24	18	13	72.2	81.1	101.1	121.5
NOV	3.0	3.4	5.6	9.3	23	22	15	11	69.2	74.3	84.2	102.8
DEC	3.0	3.4	5.6	9.3	23	22	15	11	69.2	74.3	84.2	102.8

Table 10: Operating hours and daily total fresh water product (KAU).

Month	Fresh water (liters per hour)				No. of operating hours				Total fresh water productivity per day			
	24 hour	Ideal Flow	Average Flow	Maximum Flow	24 hour	Ideal Flow	Average Flow	Maximum Flow	24 hour	Ideal Flow	Average Flow	Maximum Flow
JAN	3.0	3.4	5.6	9.3	23	22	15	11	69.2	74.3	84.2	102.8
FEB	3.0	3.4	5.6	9.3	23	23	16	11	69.2	77.7	89.9	102.8
MAR	3.0	3.4	5.6	9.3	24	24	18	13	72.2	81.1	101.1	121.5
APR	3.0	3.4	5.6	9.3	24	24	18	13	72.2	81.1	101.1	121.5
MAY	3.0	3.4	5.6	9.3	24	24	18	13	72.2	81.1	101.1	121.5
JUN	3.0	3.4	5.6	9.3	24	24	18	13	72.2	81.1	101.1	121.5
JUL	3.0	3.4	5.6	9.3	24	24	18	13	72.2	81.1	101.1	121.5
AUG	3.0	3.4	5.6	9.3	24	24	18	13	72.2	81.1	101.1	121.5
SEP	3.0	3.4	5.6	9.3	24	24	18	13	72.2	81.1	101.1	121.5
OCT	3.0	3.4	5.6	9.3	24	24	17	13	72.2	81.1	95.5	121.5
NOV	3.0	3.4	5.6	9.3	23	23	16	11	69.2	77.7	89.9	102.8
DEC	3.0	3.4	5.6	9.3	23	22	15	11	69.2	74.3	84.2	102.8

Table 11: Operating hours and daily total fresh water product (KFUPM).

Month	Fresh water (liters per hour)				No. of operating hours				Total fresh water productivity per day			
	24 hour	Ideal Flow	Average Flow	Maximum Flow	24 hour	Ideal Flow	Average Flow	Maximum Flow	24 hour	Ideal Flow	Average Flow	Maximum Flow
JAN	3.0	3.4	5.6	9.3	22	21	15	10	66.2	71.0	84.2	93.5
FEB	3.0	3.4	5.6	9.3	23	23	16	12	69.2	77.7	89.9	112.2
MAR	3.0	3.4	5.6	9.3	23	23	17	12	69.2	77.7	95.5	112.2
APR	3.0	3.4	5.6	9.3	24	24	18	13	72.2	81.1	101.1	121.5
MAY	3.0	3.4	5.6	9.3	24	24	19	14	72.2	81.1	106.7	130.8
JUN	3.0	3.4	5.6	9.3	24	24	19	14	72.2	81.1	106.7	130.8
JUL	3.0	3.4	5.6	9.3	24	24	19	14	72.2	81.1	106.7	130.8
AUG	3.0	3.4	5.6	9.3	24	24	19	14	72.2	81.1	106.7	130.8
SEP	3.0	3.4	5.6	9.3	24	24	18	13	72.2	81.1	101.1	121.5
OCT	3.0	3.4	5.6	9.3	24	24	17	12	72.2	81.1	95.5	112.2
NOV	3.0	3.4	5.6	9.3	23	23	15	11	69.2	77.7	84.2	102.8
DEC	3.0	3.4	5.6	9.3	22	20	15	10	66.2	67.6	84.2	93.5

Table 12: Operating hours and daily total fresh water product (Qassim).

Month	Fresh water (liters per hour)				No. of operating hours				Total fresh water productivity per day			
	24 hour	Ideal Flow	Average Flow	Maximum Flow	24 hour	Ideal Flow	Average Flow	Maximum Flow	24 hour	Ideal Flow	Average Flow	Maximum Flow
JAN	3.0	3.4	5.6	9.3	22	20	14	9	66.2	67.6	78.6	84.1
FEB	3.0	3.4	5.6	9.3	23	23	16	11	69.2	77.7	89.9	102.8
MAR	3.0	3.4	5.6	9.3	23	23	16	12	69.2	77.7	89.9	112.2
APR	3.0	3.4	5.6	9.3	24	24	18	13	72.2	81.1	101.1	121.5
MAY	3.0	3.4	5.6	9.3	24	24	18	14	72.2	81.1	101.1	130.8
JUN	3.0	3.4	5.6	9.3	24	24	19	14	72.2	81.1	106.7	130.8
JUL	3.0	3.4	5.6	9.3	24	24	19	14	72.2	81.1	106.7	130.8
AUG	3.0	3.4	5.6	9.3	24	24	19	14	72.2	81.1	106.7	130.8
SEP	3.0	3.4	5.6	9.3	24	24	18	13	72.2	81.1	101.1	121.5
OCT	3.0	3.4	5.6	9.3	23	23	16	11	69.2	77.7	89.9	102.8
NOV	3.0	3.4	5.6	9.3	22	22	14	10	66.2	74.3	78.6	93.5
DEC	3.0	3.4	5.6	9.3	22	21	14	9	66.2	71.0	78.6	84.1

Table 13: Operating hours and daily total fresh water product (Sharurah).

Month	Fresh water (liters per hour)				No. of operating hours				Total fresh water productivity per day			
	24 hour	Ideal Flow	Average Flow	Maximum Flow	24 hour	Ideal Flow	Average Flow	Maximum Flow	24 hour	Ideal Flow	Average Flow	Maximum Flow
JAN	3.0	3.4	5.6	9.3	23	23	16	11	69.2	77.7	89.9	102.8
FEB	3.0	3.4	5.6	9.3	23	23	16	12	69.2	77.7	89.9	112.2
MAR	3.0	3.4	5.6	9.3	24	24	18	13	72.2	81.1	101.1	121.5
APR	3.0	3.4	5.6	9.3	24	24	18	13	72.2	81.1	101.1	121.5
MAY	3.0	3.4	5.6	9.3	24	24	18	13	72.2	81.1	101.1	121.5
JUN	3.0	3.4	5.6	9.3	24	24	19	13	72.2	81.1	106.7	121.5
JUL	3.0	3.4	5.6	9.3	24	24	18	13	72.2	81.1	101.1	121.5
AUG	3.0	3.4	5.6	9.3	24	24	18	13	72.2	81.1	101.1	121.5
SEP	3.0	3.4	5.6	9.3	24	24	18	13	72.2	81.1	101.1	121.5
OCT	3.0	3.4	5.6	9.3	24	24	18	13	72.2	81.1	101.1	121.5
NOV	3.0	3.4	5.6	9.3	23	23	16	12	69.2	77.7	89.9	112.2
DEC	3.0	3.4	5.6	9.3	23	23	16	11	69.2	77.7	89.9	102.8

Table 14: Operating hours and daily total fresh water product (Tabuk).

Month	Fresh water (liters per hour)				No. of operating hours				Total fresh water productivity per day			
	24 hour	Ideal Flow	Average Flow	Maximum Flow	24 hour	Ideal Flow	Average Flow	Maximum Flow	24 hour	Ideal Flow	Average Flow	Maximum Flow
JAN	3.0	3.4	5.6	9.3	22	21	15	10	66.2	71.0	84.2	93.5
FEB	3.0	3.4	5.6	9.3	23	23	16	11	69.2	77.7	89.9	102.8
MAR	3.0	3.4	5.6	9.3	23	24	16	11	69.2	81.1	89.9	102.8
APR	3.0	3.4	5.6	9.3	24	24	18	13	72.2	81.1	101.1	121.5
MAY	3.0	3.4	5.6	9.3	24	24	18	13	72.2	81.1	101.1	121.5
JUN	3.0	3.4	5.6	9.3	24	24	19	14	72.2	81.1	106.7	130.8
JUL	3.0	3.4	5.6	9.3	24	24	18	13	72.2	81.1	101.1	121.5
AUG	3.0	3.4	5.6	9.3	24	24	18	13	72.2	81.1	101.1	121.5
SEP	3.0	3.4	5.6	9.3	24	24	18	13	72.2	81.1	101.1	121.5
OCT	3.0	3.4	5.6	9.3	24	24	17	12	72.2	81.1	95.5	112.2
NOV	3.0	3.4	5.6	9.3	23	22	15	11	69.2	74.3	84.2	102.8
DEC	3.0	3.4	5.6	9.3	23	21	15	9	69.2	71.0	84.2	84.1

Tables 9 through 14 present results from all four cases for each of the locations mentioned above. The Tables illustrate that amount of freshwater produced for each hour under each case along with the number of operational hours. These two parameters were then used to calculate the total productivity for the average day of the month for a complete year, also shown in the Tables. The main parameter that varies among the different locations is the number of operating hours. The product per hour was not expected to change due to reasons discussed previously within the report. The operational hours is related to the variables of changing the location are the ambient temperature and the availability of solar radiation. Although the effects of ambient temperature are quite low since it only relates to the losses of the system where the system is assumed to be well insulated and the storage tank standby losses are considerably low.

The change in the number of hours of operation also relate to the total daily productivity. The higher the total the more heat added to the system. This also means a greater availability of solar energy. Longer hours of operation would be expected with locations that have a higher availability of irradiation, which would also lead to a greater system output.

Table 15: Annual Productivity for all locations and all cases.

Location	Annual Productivity (L)			
	24 hour	Ideal Flow	Average Flow	Maximum Flow
KACARE	23960.5	26684.6	32704.9	39910.4
KAU	23960.5	26785.9	32530.8	39050.6
KFUPM	23770.9	26569.7	32879.0	39583.3
Qassim	23587.3	26262.2	32008.5	38452.4
Sharurah	23960.5	26894.1	33053.1	39592.6
Tabuk	23773.9	26576.4	32182.6	38153.3

The total annual production for each case at each specified location is shown in Table 15. As explained previously the maximum flow rate case is expected to have the highest productivity also shown in this Table. The change in the 24 hour and ideal flow cases is quite low or sometimes insignificant as the change in the number of hours of operation is not possible. The greatest difference therefore is shown in the average flow and maximum flow cases. However the number of operational hours for each of these cases vary and therefore it is evident that when considering the maximum flow case KACARE has the highest productivity followed by Sharurah, KFUPM, KAU, Qassim and Tabuk respectively. In the case of the average flow the highest productivity is shown to be at

Sharurah followed by KFUPM, KACARE, KAU, Tabuk and Qassim in order. The differences in the two cases are mainly due to the amount of heat gained at a given hour, where a controlled flow rate would gain slightly less heat but also loose considerably lesser heat in order to produce fresh water. In the case of the maximum flow rate there will be a greater heat gain at a given hour but also loose energy just as instantly with the production of freshwater at each hour.

Table 16: Maximum Tank Temperatures for KACARE.

Month	Maximum Storage Temperature (K)			
	24 hour	Ideal Flow	Average Flow	Maximum Flow
JAN	344.4	343.8	341.3	338.7
FEB	349.5	348.6	344.8	341.1
MAR	351.4	350.4	345.9	341.8
APR	353.6	352.4	347.3	342.6
MAY	354.9	353.6	348	343.1
JUN	357.4	356	349.7	344.2
JUL	357.9	355.6	350.1	344.4
AUG	356.8	355.4	349.4	344
SEP	354.1	352.9	347.7	342.9
OCT	351.7	350.6	346.2	341.9
NOV	346.1	345.4	342.4	339.5
DEC	345.3	344.7	341.9	339.2

Table 17: Maximum Tank Temperatures for KAU.

Month	Maximum Storage Temperature (K)			
	24 hour	Ideal Flow	Average Flow	Maximum Flow
JAN	345.2	344.6	341.8	339
FEB	349.5	348.6	344.7	341
MAR	352.4	351.3	346.6	342.2
APR	352.7	351.6	346.7	342.2
MAY	354.8	353.5	348	343.1
JUN	355.5	354.2	348.4	343.3
JUL	355	353.7	348.1	343.1
AUG	354.4	353.1	347.8	342.9
SEP	352.2	351.1	346.4	342
OCT	350.7	349.7	345.5	341.5
NOV	347.2	346.4	343.1	339.9
DEC	346	345.3	342.3	339.4

Table 18: Maximum Tank Temperatures for KFUPM.

Month	Maximum Storage Temperature (K)			
	24 hour	Ideal Flow	Average Flow	Maximum Flow
JAN	345.9	345.2	342.8	339.8
FEB	349.8	348.9	344.7	341.2
MAR	353.2	352.1	347.1	342.5
APR	354.3	353.1	347.6	342.8
MAY	356.4	355.1	349	343.7
JUN	356.7	355.3	349.2	343.8
JUL	354.3	353.1	347.5	342.7
AUG	354.7	353.4	347.7	342.8
SEP	351.5	350.4	345.7	341.6
OCT	351.7	350.7	346.1	341.9
NOV	347.5	346.6	343.4	340.2
DEC	344.1	343.5	341.1	338.8

Table 19: Maximum Tank Temperatures for Qassim.

Month	Maximum Storage Temperature (K)			
	24 hour	Ideal Flow	Average Flow	Maximum Flow
JAN	345.1	344.5	342.1	339.4
FEB	350.2	349.3	345.4	341.6
MAR	351.2	350.2	345.9	341.7
APR	350	349.7	344.7	340.9
MAY	352.8	351.6	346.5	342
JUN	355.9	354.5	348.5	343.3
JUL	356.9	355.4	349.1	343.7
AUG	355.9	354.6	348.6	343.4
SEP	354.3	353	347.7	342.9
OCT	351.5	350.5	346.1	342
NOV	347.4	346.6	343.6	340.4
DEC	346.3	345.3	342.7	339.8

Table 20: Maximum Tank Temperatures for Sharurah.

Month	Maximum Storage Temperature (K)			
	24 hour	Ideal Flow	Average Flow	Maximum Flow
JAN	350.7	349.7	345	341.2
FEB	352	351	346.4	341.8
MAR	354.9	353.7	348.3	343.4
APR	357	355.6	349.7	344.2
MAY	356.1	354.8	349	343.7
JUN	356.4	355.1	349.2	343.8
JUL	354.9	353.6	348.1	343.1
AUG	355.4	354.1	348.5	343.4
SEP	354.3	353.5	348.2	343.2
OCT	354.1	352.9	347.8	343
NOV	351.7	350.7	346.3	342
DEC	350.9	349.9	345.7	341.7

Table 21: Maximum Tank Temperatures for Tabuk.

Month	Maximum Storage Temperature (K)			
	24 hour	Ideal Flow	Average Flow	Maximum Flow
JAN	344.2	343.7	341.2	338.7
FEB	348.6	347.8	344.2	340.7
MAR	350.5	349.9	345.3	341.4
APR	354.6	353.2	348	343.1
MAY	356.6	354.8	348.9	343.8
JUN	358.1	355.9	349.7	344.1
JUL	358	355.6	349.5	344
AUG	356.8	354.4	348.7	343.6
SEP	354.4	352.6	347.5	342.8
OCT	349.4	348.5	344.6	340.9
NOV	347.1	345.8	343.1	340
DEC	344.5	343.1	341.4	338.5

Another significant change can be seen by studying the maximum storage tank temperature for each case at each of the locations. The maximum tank temperatures are shown in Tables 16 through 21. The temperature increases with the increase in the availability of solar energy as more useful heat gained. The trend of the maximum tank temperature follows a similar trend to that of the heat input shown earlier in this section of the report.

When studying the different months it is evident that the summer months have a higher temperature as expected within the middle of the year, where the months of June or July have the highest recorded temperature for all cases and all locations. This is mainly due to all chosen locations being situated above the equator. The lowest temperatures are

recorded in the winter months where the day is shorter and solar intensity is significantly lower compared to the rest of the year, namely the months of January and December. The highest recorded temperature for the 24 hour case was 358.1°K at Tabuk, for the Ideal case it was at 355.9°K for the same location, for the Average flow case both Tabuk and KACARE and for the maximum flow case a temperature of 344.4°K was recorded at KACARE.

This proves that the change in neither the freshwater produced or the tank temperatures are directly proportional to the availability of solar energy alone, but still however show an increase with the increase of irradiation.

The tank temperature variation throughout the 4 main seasonal months March, June September and December are shown in Figures 27 through 30 for all locations. Each Figure consists of four parts where it represents the four different months for a specific case. Similar conclusions on the temperature variation for the different cases and the four months as discussed previously may be drawn through these Figures, where the summer months with a higher radiation value represents a wider curve suggesting longer time to reach the cut off temperature at 333°K also the lower flow rate cases reaching higher storage tank temperatures.

Considering the effects due to the geographical location it is evident that the seasonal changes have an impact on which location maintains a higher temperature where longer hours of productivity may be achieved. These changes are mainly due to the variance in ambient temperatures at each location and the variation of solar radiation availability. It is

evident that in all four cases for the summer month of June, Tabuk generally has higher temperature values whereas during winter, in December the higher temperatures are maintained by the system simulated in Sharurah. Considering the spring and Autumn seasons related to the months of March and September the system located in Sharurah still maintains the highest recorded temperatures suggesting that when annual productivity is considered, on average for all four cases this systems performs best in terms of fresh water produce and the number of operating hours.

A major advantage with the proposed system is that under extreme weather conditions such snowy winter in Tabuk for example the freezing of water may be prevented through the use of a glycol mixture or antifreeze in the collector loop of the system since no direct mixing is present in the system, also due to the use of heat exchangers in the storage tank and the heating element of the HDH system.

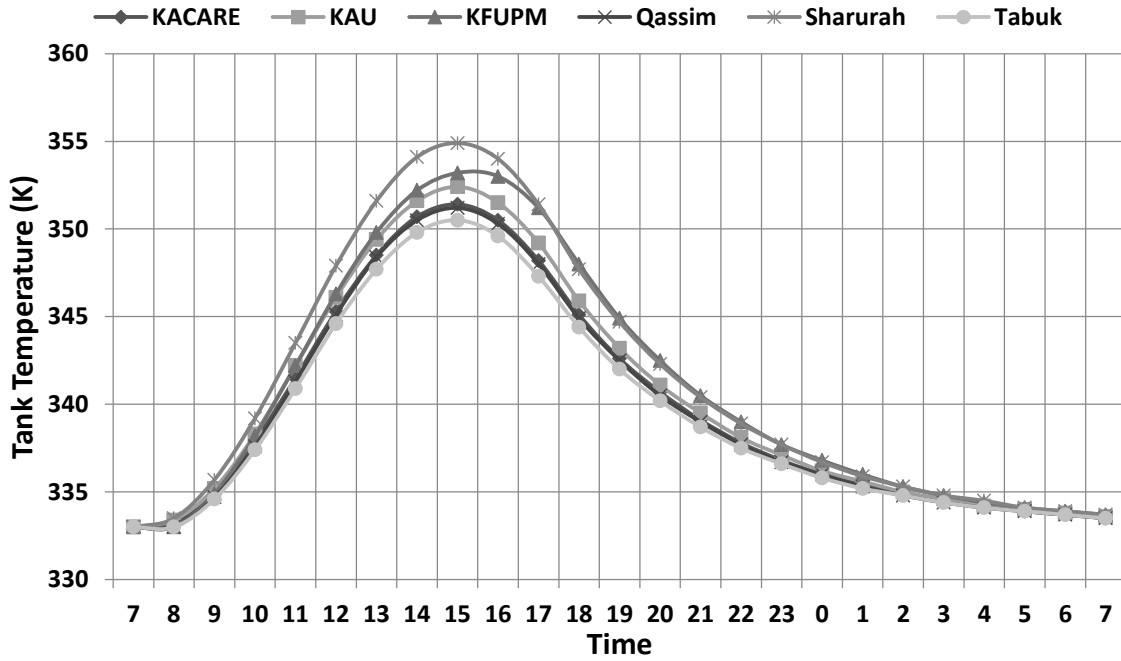


Figure 27a: Storage Tank Temperature variation for the 24 hour case (March).

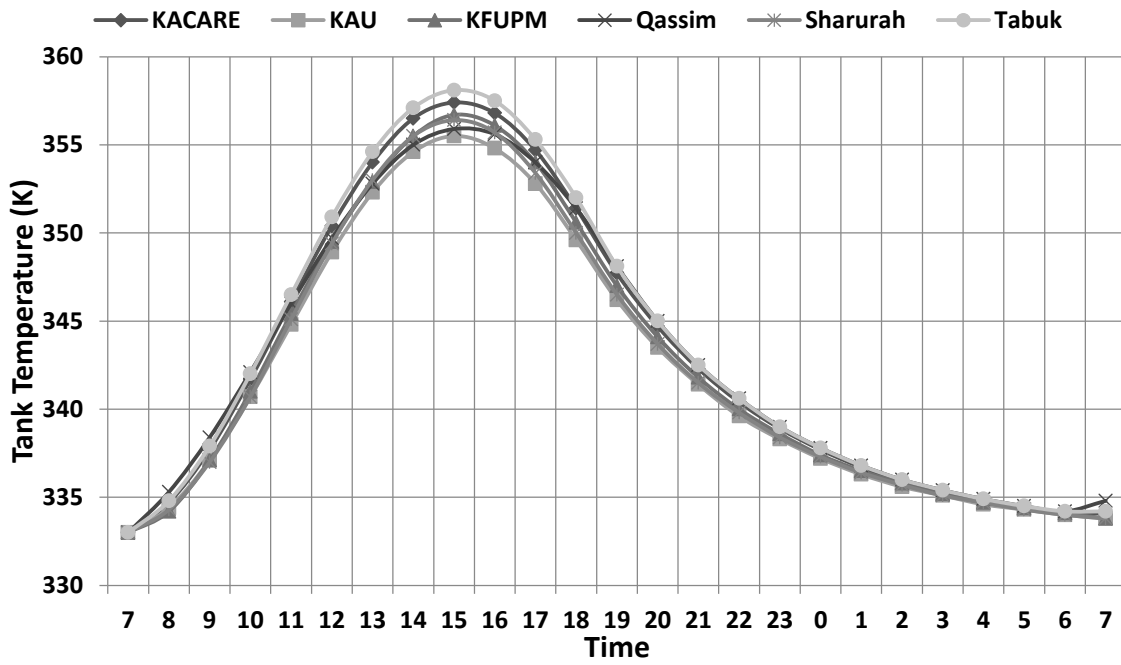


Figure 27b: Storage Tank Temperature variation for the 24 hour case (June).

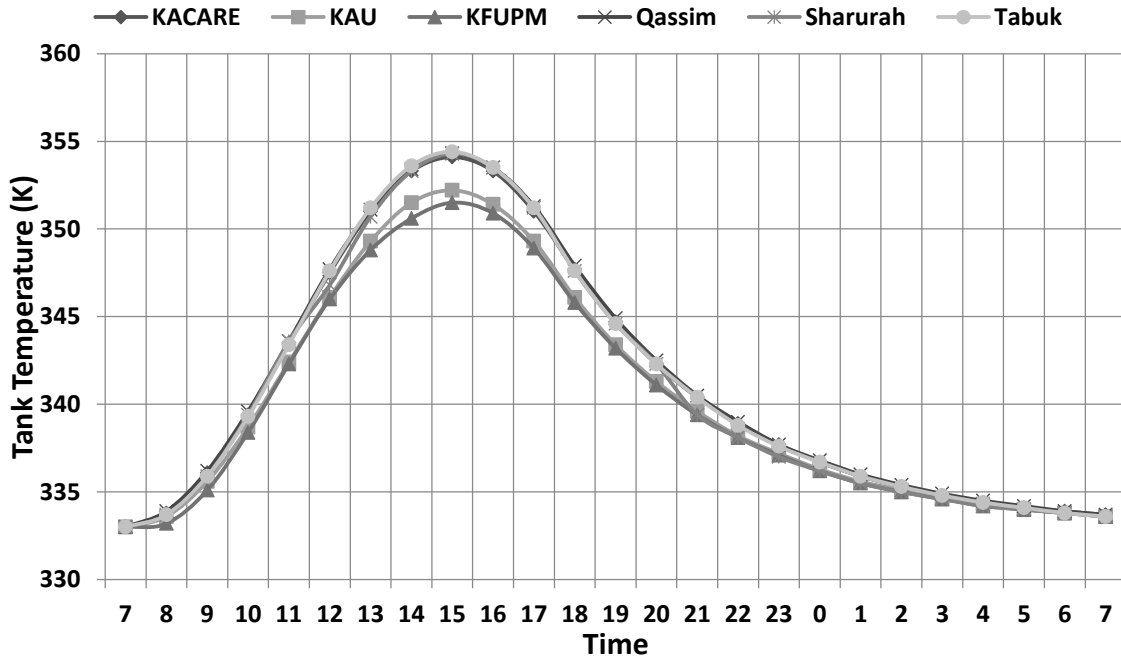


Figure 27c: Storage Tank Temperature variation for the 24 hour case (September).

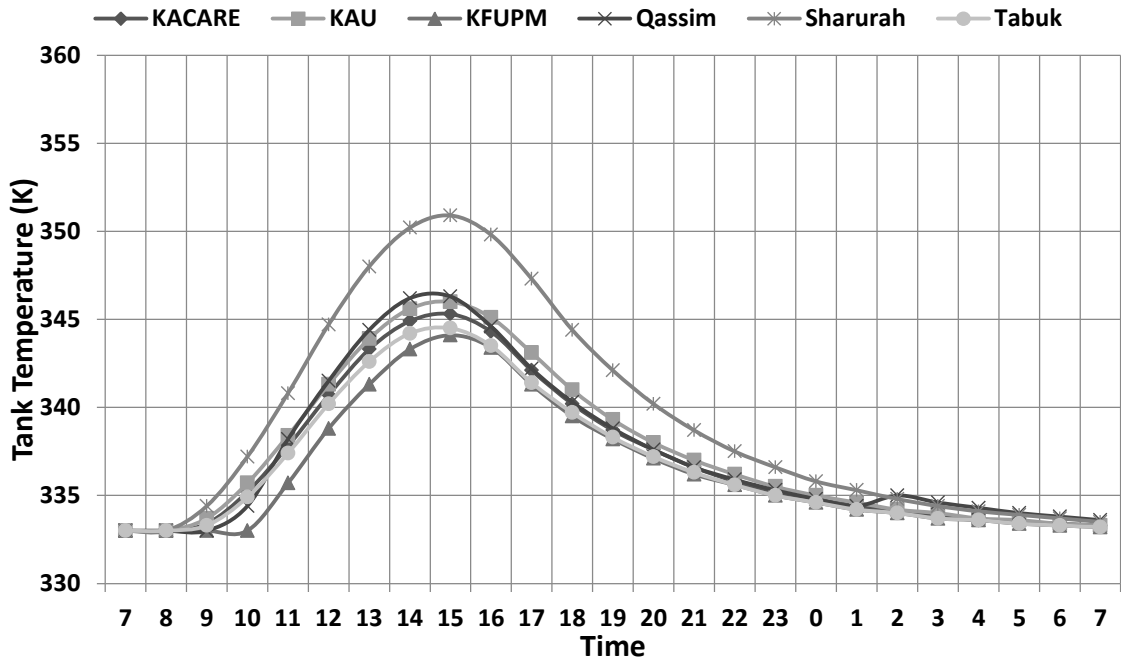


Figure 27d: Storage Tank Temperature variation for the 24 hour case (December).

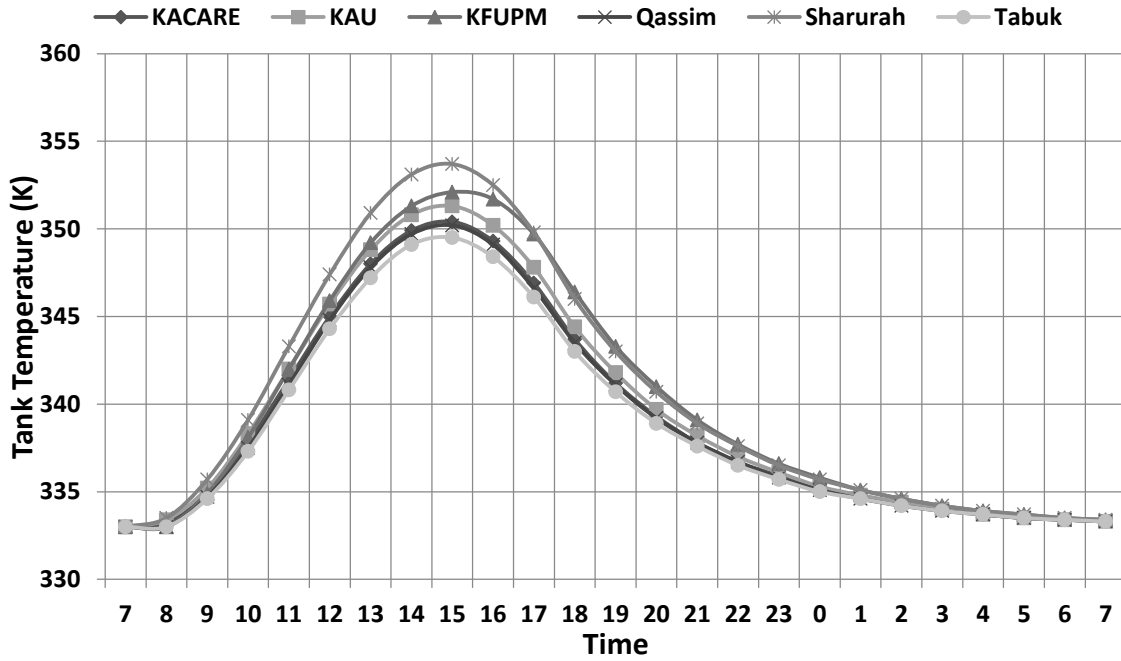


Figure 28a: Storage Tank Temperature variation for the Ideal Flow case (March).

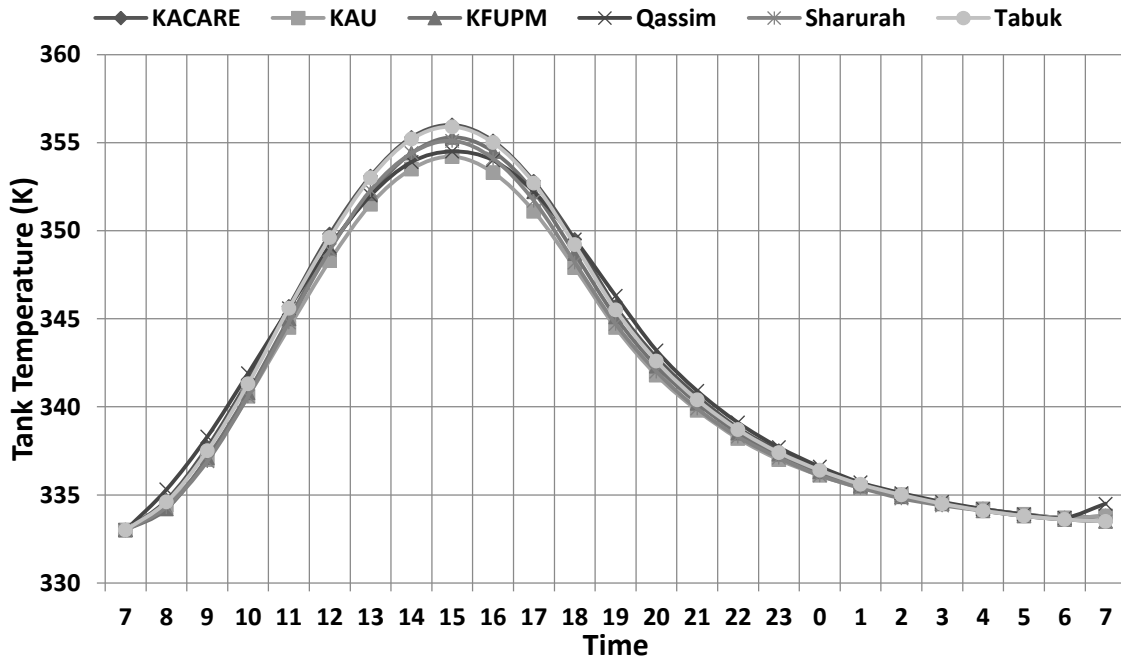


Figure 28b: Storage Tank Temperature variation for the Ideal Flow case (June).

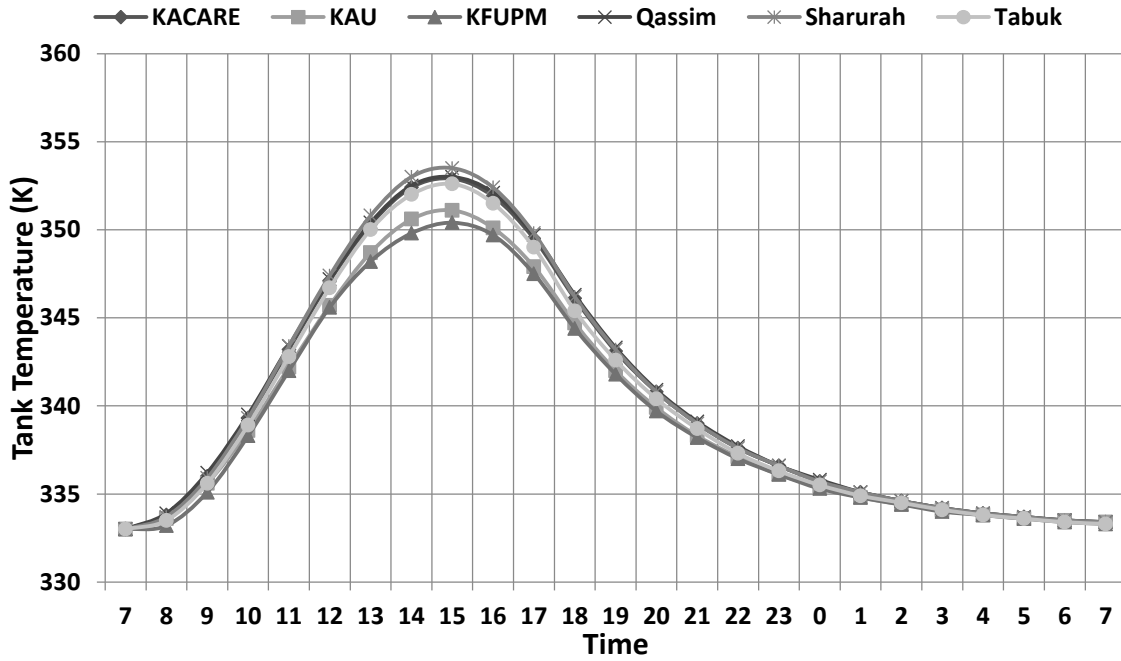


Figure 28c: Storage Tank Temperature variation for the Ideal Flow case (September).

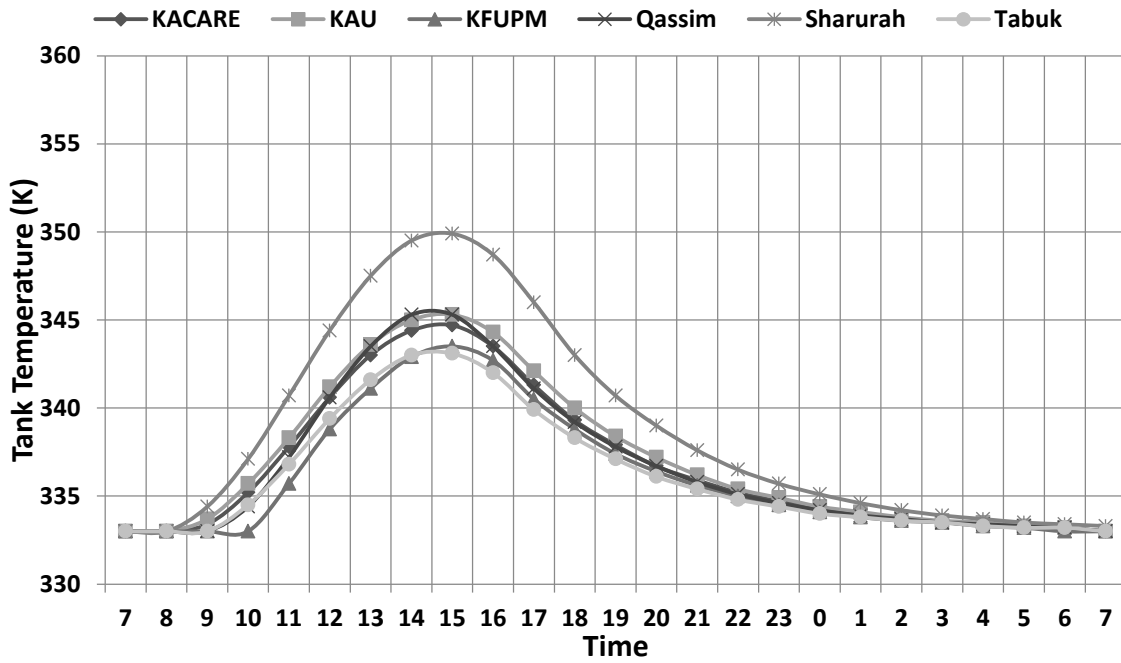


Figure 28d: Storage Tank Temperature variation for the Ideal Flow case (December).

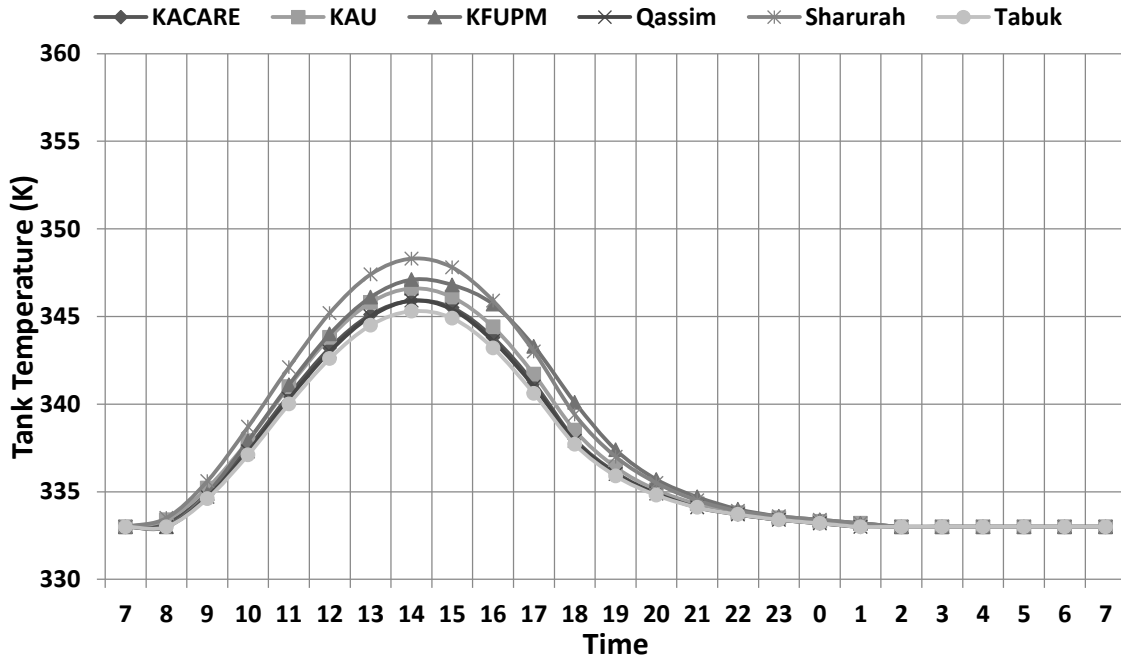


Figure 29a: Storage Tank Temperature variation for the Average Flow case (March).

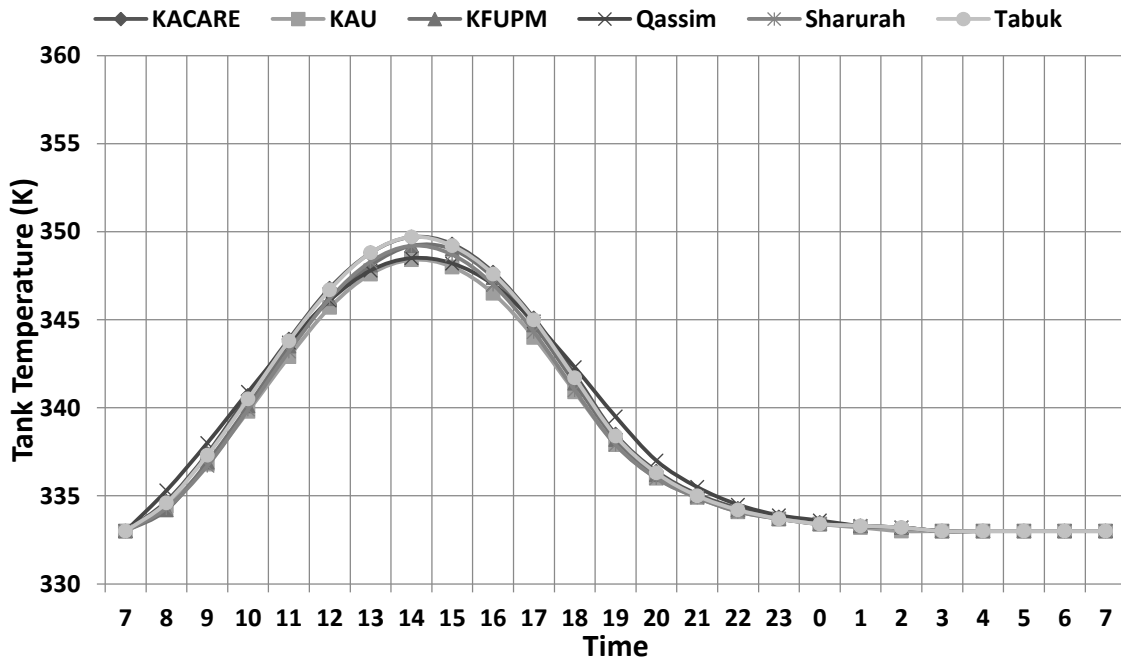


Figure 29b: Storage Tank Temperature variation for the Average Flow case (June).

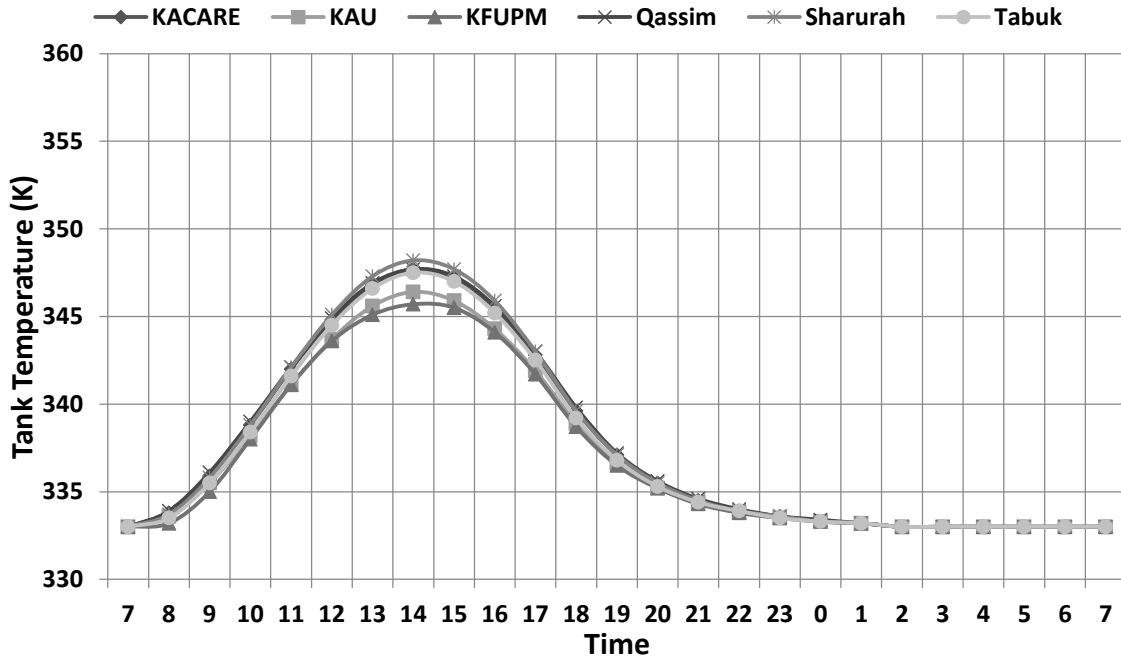


Figure 29c: Storage Tank Temperature variation for the Average Flow case (September).

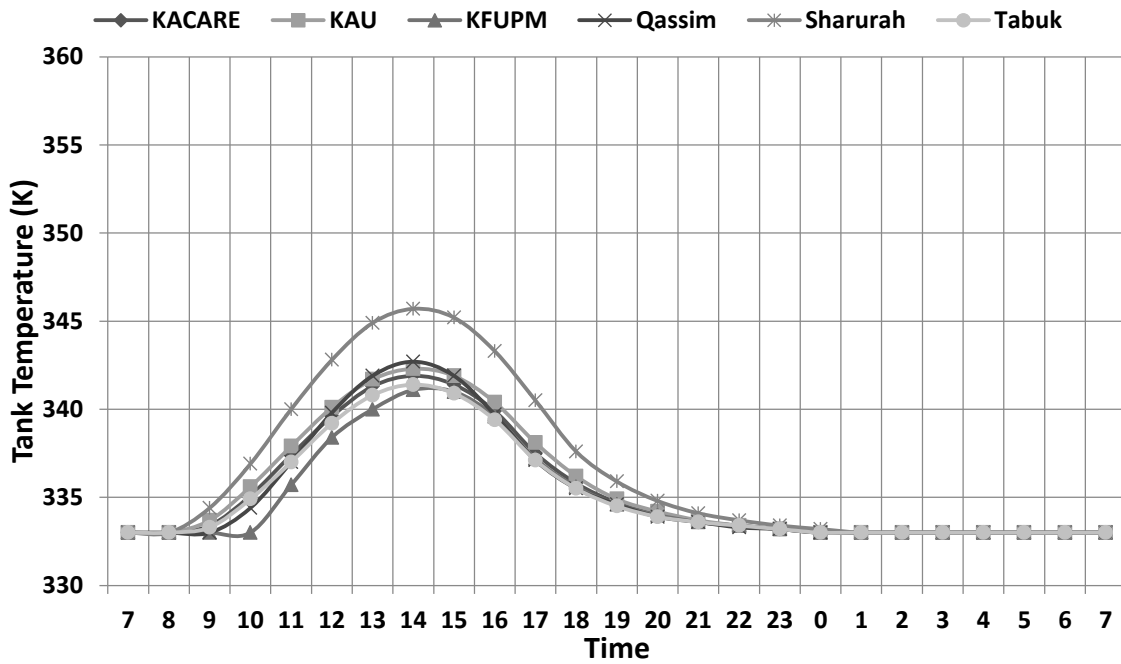


Figure 29d: Storage Tank Temperature variation for the Average Flow case (December).

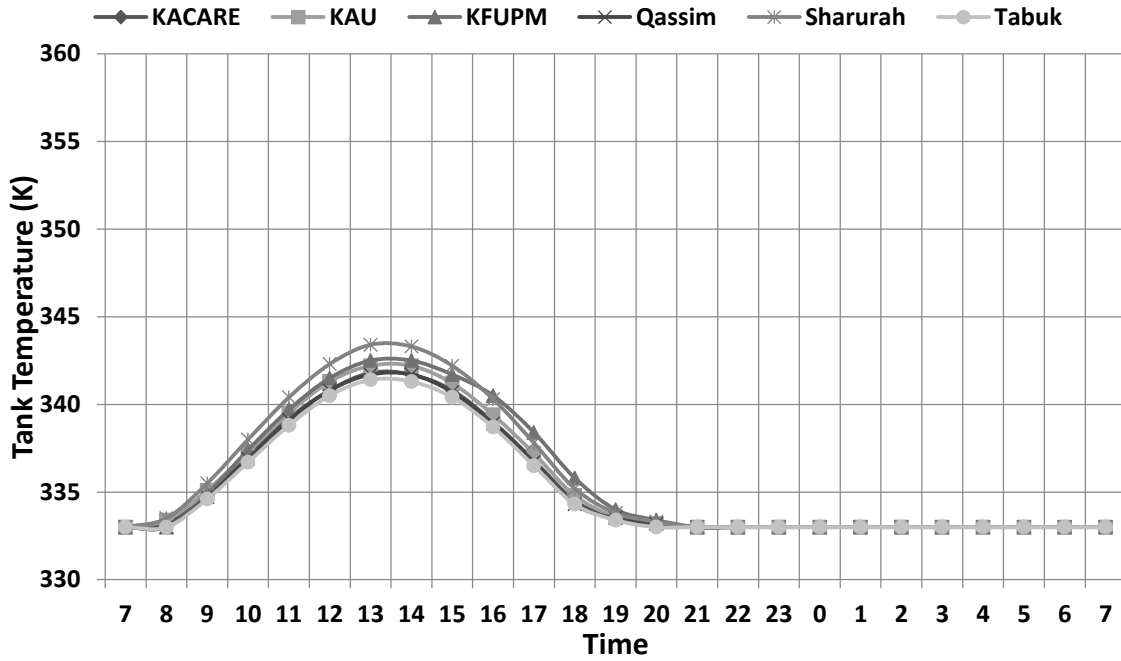


Figure 30a: Storage Tank Temperature variation for the Max Flow case (March).

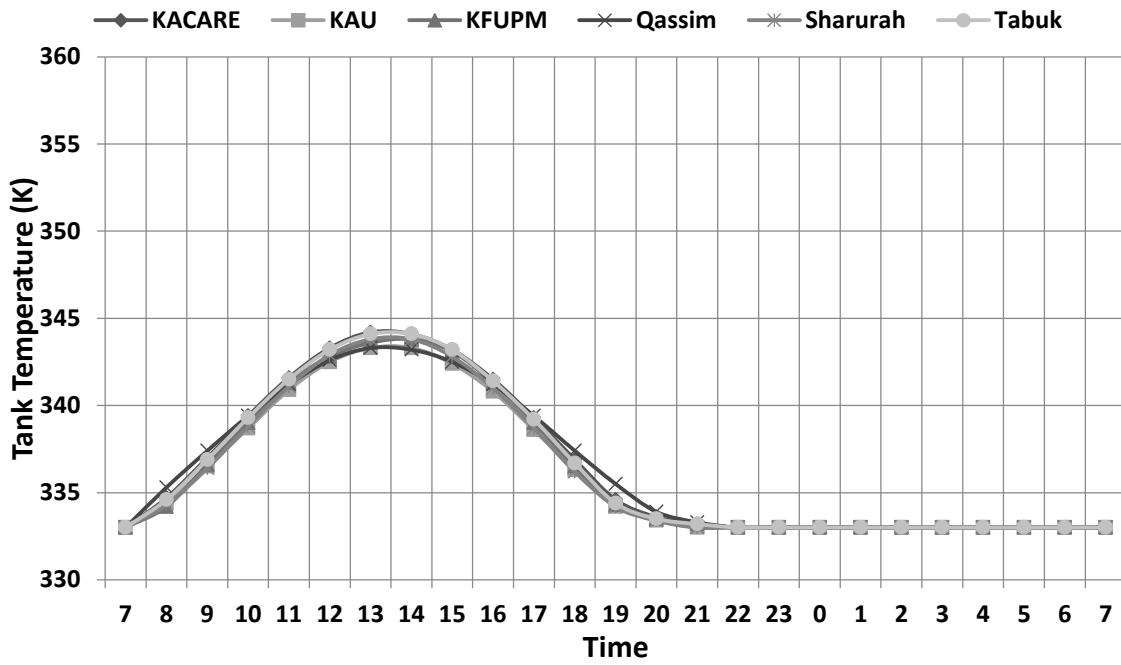


Figure 30b: Storage Tank Temperature variation for the Max Flow case (June).

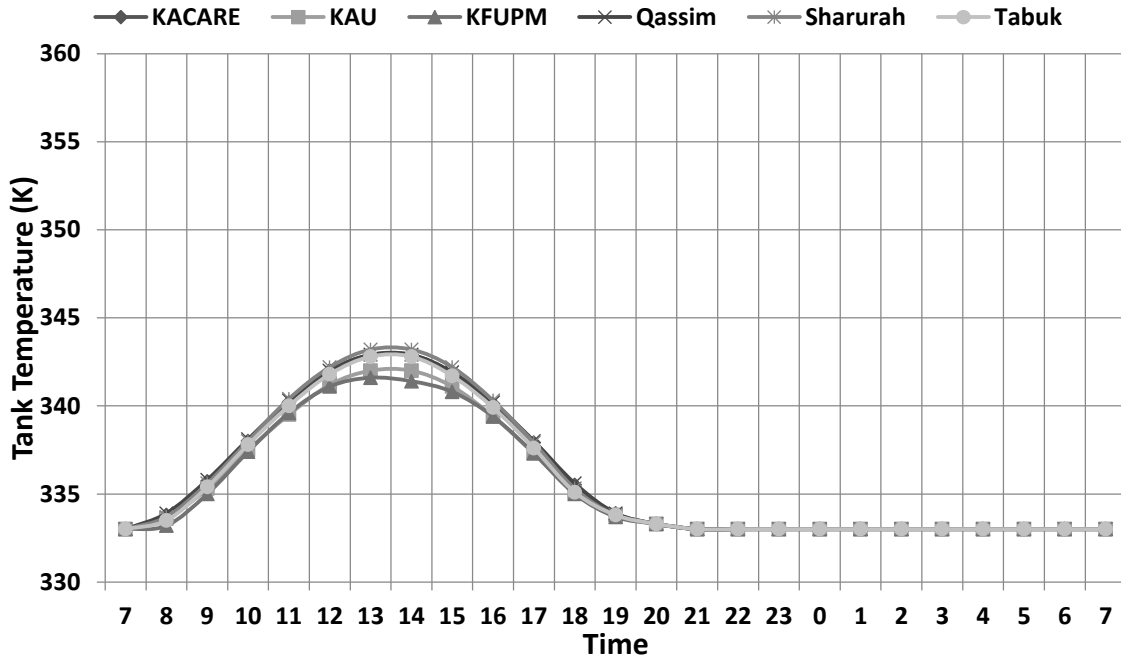


Figure 30c: Storage Tank Temperature variation for the Max Flow case (September).

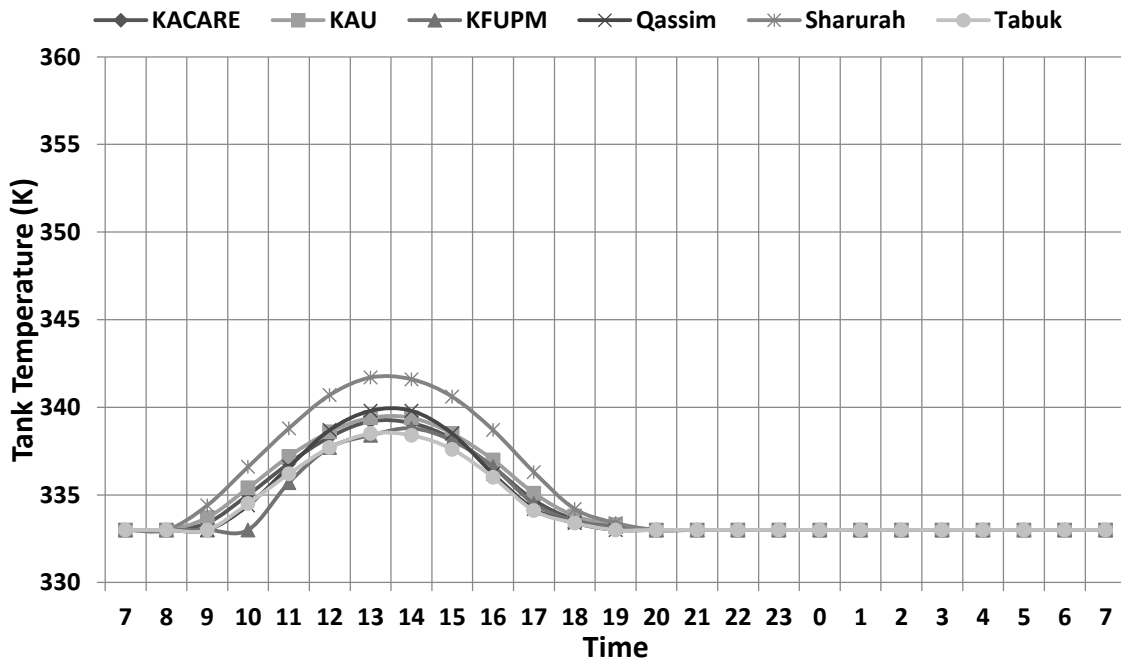


Figure 30d: Storage Tank Temperature variation for the Max Flow case (December).

CHAPTER 5

CONCLUSIONS

The study considers the use of thermal storage along with an HDH system that uses evacuated tube collectors as a water heater; in addition to a two tank storage system that controls the heat output to a required temperature, allowing the system to use less energy while maintaining a prolonged operational time. The following are the key conclusions:

1. The variations in freshwater production rates were evident depending on the month and season, where the output was notably greater in summer months and significantly lower in winter months.
2. The product output was considerably uneven forcing a need to store the extra fresh water, and the operational time was constrained by the number of day light hours.
3. The flow rate of water across the storage tank controlled the heat input to the HDH system, which accordingly adjusted the flow rate of seawater through the HDH component.
4. Thereby operating hours of the storage linked solar HDH system could be varied from 9 hours to 24 hours, where the longer hours would produce less water with a longer operational time and the shorter number of operating hours produced more freshwater.

5. Higher flow rates means faster heat addition and removal, whereas a lower flow rate would store slightly less heat but uses less heat in the production of fresh water, and thereby increasing the operational time.
6. The total daily output from the direct system was at an average of about 40 liters a day, whereas with storage it varies from 70 liters to 130 liters per day using the same number of evacuated tube collectors.
7. Higher storage tank temperatures were reached with lower flow rates and considerably lower temperatures were reached with higher flow rates. These results are mainly due to the dependency on the heat removal factor that changed with the change in the storage tank's flow rate.
8. The location dependency was also studied, where the system had longer operational hours for locations with higher solar radiation intensity or longer hours of daylight and a lower productivity for shorter days or lower irradiation availability.
9. A cost analysis considering the capital costs for the proposed system with an expected lifetime of 20 years showed that the cost of fresh water produced, would vary from \$15 to \$24 per cubic meter.

In light of the results discussed in this report it would be recommended to use the average flow case in practice, due to its high productivity and the averaged 16 hours of operation. Since the system will not be operating for prolonged hours, system components such as pumps and fans will produce a longer operational life that also leads to electrical energy savings. Further improvement of the model presented in this study would include an

analysis for locations south of the equator while considering a change in the storage size rather than the standard 75 liters per square meter of the collector area. Various other types of collectors may also be considered to study the system performance, depending on the location and the availability of solar radiation.

REFERENCES

- [1] T. E.-D. Hisham and M. E. Hisham, *Fundamentals of Salt Water Desalination*. Elsevier B.V., 2002.
- [2] V. Patrick, B. Hightowe, and M. Michael, *Desalination*. Hoboken, NJ, USA: John Wiley & Sons, Inc., 2014.
- [3] J. A. Duffie and W. A. Beckman, *Solar Engineering of Thermal Processes*, 4th ed. John Wiley & Sons, 2013.
- [4] M. Webster, “Desalinate,” 2014. [Online]. Available: <http://www.merriam-webster.com/dictionary/desalinate>. [Accessed: 05-Nov-2014].
- [5] A. Hassabou, *Experimental and Numerical Analysis of a PCM-Supported Humidification-Dehumidification Solar Desalination System*. 2011.
- [6] Global Water Intelligence, “Desalination industry enjoys growth spurt as scarcity starts to bite,” 2014. [Online]. Available: <http://www.globalwaterintel.com/desalination-industry-enjoys-growth-spurt-scarcity-starts-bite/>.
- [7] H. Ettouney, “Seawater Desalination,” 2009.
- [8] G. P. Narayan, M. H. Sharqawy, E. K. Summers, J. H. Lienhard, S. M. Zubair, and M. a. Antar, “The potential of solar-driven humidification–dehumidification desalination for small-scale decentralized water production,” *Renew. Sustain. Energy Rev.*, vol. 14, no. 4, pp. 1187–1201, May 2010.
- [9] R. Tripathi and G. Tiwari, “Effect of water depth on internal heat and mass transfer for active solar distillation,” *Desalination*, vol. 173, pp. 187–200, 2005.
- [10] F. a. Al-Sulaiman, M. I. Zubair, M. Atif, P. Gandhidasan, S. a. Al-Dini, and M. a. Antar, “Humidification dehumidification desalination system using parabolic trough solar air collector,” *Appl. Therm. Eng.*, vol. 75, pp. 809–816, Jan. 2015.
- [11] H. Ettouney, “Design and analysis of humidification dehumidification desalination

- process,” *Desalination*, vol. 183, no. 1–3, pp. 341–352, Nov. 2005.
- [12] J. Wang, N. Gao, Y. Deng, and Y. Li, “Solar power-driven humidification–dehumidification (HDH) process for desalination of brackish water,” *Desalination*, vol. 305, pp. 17–23, Nov. 2012.
- [13] M. T. Chaibi and A. M. El-Nashar, “A Review of Solar Thermal Energy Technologies for Water Desalination,” in *Solar Thermal Processes*, 2009, pp. 131–163.
- [14] I. Budihardjo and G. L. Morrison, “Performance of water-in-glass evacuated tube solar water heaters,” *Sol. Energy*, vol. 83, no. 1, pp. 49–56, 2009.
- [15] Y. Kim and T. Seo, “Thermal performances comparisons of the glass evacuated tube solar collectors with shapes of absorber tube,” *Renew. Energy*, vol. 32, no. 5, pp. 772–795, 2007.
- [16] K. C. Ng, C. Yap, and T. H. Khor, “Outdoor testing of evacuated-tube heat-pipe solar collectors,” *Proc. Inst. Mech. Eng. Part E J. Process Mech. Eng.*, vol. 214, no. 1, pp. 23–30, 2000.
- [17] F. Jafarkazemi and H. Abdi, “Evacuated tube solar heat pipe collector model and associated tests,” *J. Renew. Sustain. Energy*, vol. 4, no. 2, p. 023101, 2012.
- [18] H. Jafari Mosleh, S. Jahangiri Mamouri, M. B. Shafii, and A. Hakim Sima, “A new desalination system using a combination of heat pipe, evacuated tube and parabolic trough collector,” *Energy Convers. Manag.*, vol. 99, pp. 141–150, 2015.
- [19] C. Yildirim and I. Solmuş, “A parametric study on a humidification–dehumidification (HDH) desalination unit powered by solar air and water heaters,” *Energy Convers. Manag.*, vol. 86, pp. 568–575, 2014.
- [20] H. Müller-Holst, M. Engelhardt, and W. Schölkopf, “Small-scale thermal seawater desalination simulation and optimization of system design,” *Desalination*, vol. 122, pp. 255–262, 1999.
- [21] A. A. Shabaneh, P. Gandhidasan, M. A. Antar, and H. Baig, “Simulation of hdh

desalination system using tilted , two-pass solar air heater,” in *Fifteenth International Water Technology Conference*, 2011.

- [22] E. Summers, M. Antar, and J. L. V, “Design and optimization of an air heating solar collector with integrated phase change material energy storage for use in humidification–dehumidification desalination,” *Sol. Energy*, vol. 86, no. 11, pp. 3417–3429, Nov. 2012.
- [23] S. Xu, X. Ling, and H. Peng, “Experimental of New Thermal Storage in a Desalination System,” *Appl. Mech. Mater.*, vol. 143–144, pp. 531–535, Dec. 2011.
- [24] H. Muller-Holst, M. Engelhardt, M. Herve, and W. Schijlkopf, “Solarthermal seawater desalination systems for decentralised use,” *Renew. Energy*, vol. 14, pp. 311–318, 1998.
- [25] O. Miyatake, Y. Koito, K. Tagawa, and Y. Maruta, “Transient characteristics and performance of a novel desalination system based on heat storage and spray flashing,” *Desalination*, vol. 137, no. 1–3, pp. 157–166, May 2001.
- [26] M. H. Sharqawy, M. a. Antar, S. M. Zubair, and A. M. Elbashir, “Optimum thermal design of humidification dehumidification desalination systems,” *Desalination*, vol. 349, pp. 10–21, Sep. 2014.
- [27] Apricus, “Product Catalog 2012 Sustainable Hot Water Solutions,” 2012.
- [28] G. P. Narayan, M. H. Sharqawy, J. H. Lienhard V, and S. M. Zubair, “Thermodynamic analysis of humidification dehumidification desalination cycles,” *Desalin. Water Treat.*, vol. 16, no. 1–3, pp. 339–353, Apr. 2010.

APPENDIX

Evacuated Tube Manufacturer	Model	Gross area per collector (m ²)	Capacity (kW)	Cost per unit	capacity per dollar	Capacity/Gross Area
Apricus	Arpicus AP-30	4.05	2.66	\$2,027	0.00131	0.65679
Calpak	16 VTN	2.86	1.83	\$1,430	0.00128	0.63986
Ritter Solar	CPC 30 Star Azzurro	3.30	2.11	\$1,651	0.00128	0.639394
Calpak	6 VTN	1.06	0.67	\$530	0.00126	0.632075
Oventrop	OV 5-8 AS/AB	2.03	1.28	\$1,014	0.00126	0.630542
Ritter Solar	CPC 14 Star azzurro	2.61	1.63	\$1,305	0.00125	0.624521
Beijing Sunda Solar Energy Technology	Seido 10-20 AS/AB	3.39	2.11	\$1,697	0.00124	0.622419
Oventrop	OV 10-20 AS/AB	3.39	2.11	\$1,697	0.00124	0.622419
Oventrop	OV 5-16 AS/AB	4.10	2.54	\$2,049	0.00124	0.619512
Beijing Sunda Solar Energy Technology	Seido 10-10 AS/AB	1.68	1.04	\$840	0.00124	0.619048
Ritter Solar	CPC 12 INOX	2.28	1.41	\$1,140	0.00124	0.618421
Shangdong Linuo Paradigma	CPC 1518	3.41	2.10	\$1,705	0.00123	0.615836
Thermomax	Solamax AST20	2.85	1.75	\$1,425	0.00123	0.614035
Shangdong Linuo Paradigma	CPC 1512	2.28	1.40	\$1,140	0.00123	0.614035
Thermomax	Solamax AST80	11.41	7.00	\$5,704	0.00123	0.613497
Thermomax	Solamax AST70	9.98	6.12	\$4,989	0.00123	0.613226
Viessmann	Vitosol 300-T, SP3 3m ²	4.29	2.63	\$2,144	0.00123	0.613054
Apricus	Arpicus AP-22	2.98	1.83	\$1,492	0.00123	0.614094
Thermomax	Solamax AST50	7.13	4.37	\$3,565	0.00123	0.612903
Apricus	Arpicus AP-20	2.71	1.66	\$1,355	0.00123	0.612546
Thermomax	Solamax AST30	4.28	2.62	\$2,140	0.00122	0.61215
Apricus	Arpicus AP-10	1.34	0.82	\$671	0.00122	0.61194
Shangdong Linuo Paradigma	CPC 1506	1.15	0.70	\$575	0.00122	0.608696
Viessmann	Vitosol 300-T, SP3 2m ²	2.88	1.75	\$1,439	0.00122	0.607639
G.S.	EOS Solar EOS-S30	4.65	2.82	\$2,323	0.00121	0.606452

American Solar Works	ASW52B Stretch	3.91	2.37	\$1,953	0.00121	0.606138
G.S.	EOS Solar EOS-S20	3.09	1.87	\$1,544	0.00121	0.605178
Solar Panels Plus	SPP-30	4.81	2.91	\$2,405	0.00121	0.60499
Solar Panels Plus	SPP-25	4.00	2.42	\$2,001	0.00121	0.605
American Solar Works	ASW52B	2.86	1.73	\$1,432	0.00121	0.604895
Ritter Solar	CPC 16W INOX	3.52	2.12	\$1,761	0.00120	0.602273
G.S.	EOS Solar EOS-S10	1.58	0.92	\$792	0.00116	0.582278
American Solar Works	ASW-58A	3.52	2.01	\$1,759	0.00114	0.571023
Thermomax	TMO 600	2.76	1.51	\$1,381	0.00109	0.547101
Thermomax	MS 30 - TMO 500	4.16	2.24	\$2,081	0.00108	0.538462
Thermomax	MS 20 - TMO 500	2.78	1.49	\$1,390	0.00107	0.535971
Thermomax	Solarmax 20 - TDS 300	2.85	1.51	\$1,426	0.00106	0.529825
Thermomax	Solarmax 30 - TDS 300	4.28	2.26	\$2,139	0.00106	0.528037
Viessmann	VitoSol 300	2.93	1.53	\$1,465	0.00104	0.522184
Viessmann	VitoSol 200 D20	2.90	1.51	\$1,449	0.00104	0.52069
SunComfort	DS-24-58-1800	3.92	2.03	\$1,961	0.00104	0.517857
Thermo Technologies	Mazdon TMA-600-30	4.58	2.37	\$2,291	0.00103	0.517467
Thermo Technologies	Mazdon TMA-600-20	3.06	1.58	\$1,530	0.00103	0.51634
Thermo Technologies	Mazdon TMA-600-80	12.22	6.31	\$6,111	0.00103	0.516367
Thermo Technologies	Mazdon TMA-600-70	10.70	5.52	\$5,351	0.00103	0.515888
Thermo Technologies	Mazdon TMA-600-50	7.64	3.94	\$3,821	0.00103	0.515707
Thermomax	Mazdon 30 - TMA 600S	4.47	2.25	\$2,233	0.00101	0.503356
Apricus	AP-30C (USA only)	4.16	2.09	\$2,079	0.00101	0.502404
Thermomax	Mazdon 20 - TMA 600S	3.03	1.50	\$1,516	0.00099	0.49505
Oventrop	OV 10-10 AS/AB	1.68	0.82	\$840	0.00098	0.488095
Apricus	AP-20	2.69	1.30	\$1,343	0.00097	0.483271
Apricus	AP-10	1.34	0.65	\$672	0.00097	0.485075
Apricus	AP-30	4.16	1.95	\$2,079	0.00094	0.46875
Jiangsu Sunrain Solar Energy	DMG 100-10	2.77	1.28	\$1,385	0.00092	0.462094

Jiangsu Sunrain Solar Energy	DMG 100-8	2.21	1.02	\$1,105	0.00092	0.461538
Beijing Sunda Solar Energy Technology	Seido 10-20	3.42	1.58	\$1,712	0.00092	0.461988
Jiangsu Sunrain Solar Energy	DMG 100-12	3.32	1.53	\$1,660	0.00092	0.460843
Jiangsu Sunrain Solar Energy	DMG 100-16	4.44	2.04	\$2,220	0.00092	0.459459
Zhejiang Shentai Solar Energy	SR 10	1.59	0.70	\$795	0.00088	0.440252
Viessmann	VitoSol 250	1.66	0.71	\$831	0.00085	0.427711
Solar Collector	SCM15-58/1800	2.32	0.99	\$1,162	0.00085	0.426724
Solar Collector	SCM20-58/1800	3.12	1.32	\$1,558	0.00085	0.423077
Zhejiang Shentai Solar Energy	SCM 20	3.10	1.31	\$1,552	0.00084	0.422581
Solar Collector	SCM30L-58/1800	4.69	1.98	\$2,346	0.00084	0.422175
SunComfort	DS-30-58-1800	4.73	1.98	\$2,363	0.00084	0.418605
Ritter Solar	OEM21	2.36	0.99	\$1,182	0.00084	0.419492
Jiangsu Sunrain Solar Energy	TZ58/1800-10R	1.71	0.70	\$855	0.00082	0.409357
SunMaxx Solar	ThermoPower-VHP10	1.69	0.69	\$846	0.00082	0.408284
Calpak	20 VT	2.35	0.95	\$1,175	0.00081	0.404255
Zhejiang Shentai Solar Energy	SCM 12	1.94	0.78	\$970	0.00080	0.402062
Jiangsu Sunrain Solar Energy	TZ58/1800-15R	2.59	1.04	\$1,295	0.00080	0.401544
SunMaxx Solar	ThermoPower-VHP20	3.44	1.38	\$1,721	0.00080	0.401163
Jiangsu Sunrain Solar Energy	TZ58/1800-30R2	4.86	1.95	\$2,432	0.00080	0.401235
Shangdong Linuo Paradigma	U 1521	2.32	0.93	\$1,160	0.00080	0.400862
SunMaxx Solar	ThermoPower-VHP25	4.32	1.73	\$2,158	0.00080	0.400463
Jiangsu Sunrain Solar Energy	TZ58/1800-20R	3.48	1.39	\$1,740	0.00080	0.399425
Jiangsu Sunrain Solar Energy	TZ 58/1800-12R	1.95	0.78	\$977	0.00080	0.4
Jiangsu Sunrain Solar Energy	TZ 58/1800-24R	3.91	1.56	\$1,954	0.00080	0.398977
Jiangsu Sunrain Solar Energy	TZ 58/1800-14R	2.28	0.91	\$1,140	0.00080	0.399123
Jiangsu Sunrain Solar Energy	TZ 58/1800-28R	4.56	1.82	\$2,280	0.00080	0.399123
Jiangsu Sunrain Solar Energy	TZ58/1800-25R	4.36	1.74	\$2,180	0.00080	0.399083
Jiangsu Sunrain Solar Energy	TZ 58/1800-18R	2.93	1.17	\$1,466	0.00080	0.399317

Jiangsu Sunrain Solar Energy	TZ58/1800-30R	5.24	2.09	\$2,620	0.00080	0.398855
SunMaxx Solar	ThermoPower-VHP30	5.19	2.07	\$2,595	0.00080	0.398844
SunComfort	DS-10-58-1800	1.66	0.66	\$829	0.00080	0.39759
Jiangsu Sunrain Solar Energy	TZ58/1800-25R2	4.08	1.62	\$2,041	0.00079	0.397059
Jiangsu Sunrain Solar Energy	TZ58/1800-20R2	3.30	1.30	\$1,651	0.00079	0.393939
Advanced Thermal Solar	ATS-30	5.06	1.98	\$2,528	0.00078	0.391304
Jiangsu Sunrain Solar Energy	TZ58/1800-15R2	2.52	0.97	\$1,261	0.00077	0.384921
Advanced Thermal Solar	ATS-20	3.43	1.32	\$1,716	0.00077	0.38484
Jiangsu Sunrain Solar Energy	TZ58/1800-10R2	1.74	0.65	\$870	0.00075	0.373563
Advanced Thermal Solar	ATS-10	1.81	0.66	\$904	0.00073	0.364641
Himin Solar Energy Group	HUJ 16/2.1	3.47	1.23	\$1,735	0.00071	0.354467
Himin Solar Energy Group	HUJ 16/1.8	3.02	1.06	\$1,510	0.00070	0.350993
Apricus	FSCB-20-SS	2.50	0.87	\$1,250	0.00070	0.348
Himin Solar Energy Group	HUJ 16/1.6	2.71	0.94	\$1,355	0.00069	0.346863
Himin Solar Energy Group	HUJ 12/2.1	2.67	0.92	\$1,335	0.00069	0.344569
Himin Solar Energy Group	HUJ 12/1.8	2.32	0.79	\$1,160	0.00068	0.340517
Himin Solar Energy Group	HUJ 12/1.6	2.09	0.70	\$1,043	0.00067	0.334928

VITAE

Name : { Mohamed Ifras Zubair }

Nationality : { Sri Lankan }

Date of Birth : { 12/12/1990 }

Email : { mizubairs@gmail.com }

Address : { Kurugama Estate, Muruthalawa, Kandy. Sri Lanka }

Academic Background : *BEng (hons)* in Mechanical Engineering; June 2012
Kingston University
London, United Kingdom

MSc in Thermofluid Sciences
(Mechanical Engineering); December 2015
King Fahd University of Petroleum & Minerals (KFUPM)
Dhahran, Saudi Arabia

Research Interests : Solar Energy Applications, Renewable & Sustainable
Energy Sources